Fall 2007

Effects of combined exposure to ethanol and ionizing radiation on the antioxidant status of in vitro and in vivo models

Joshua Ogony

Department: Chemistry

EFFECTS OF COMBINED EXPOSURE TO ETHANOL AND IONIZING RADIATION ON THE ANTIOXIDANT STATUS OF *IN VITRO* AND *IN VIVO* MODELS

by

JOSHUA OGONY

A DISSERTATION

Presented to the Faculty of the Graduate School of the

UNIVERSITY OF MISSOURI-ROLLA

In Partial Fulfillment of the Requirements for the Degree

DOCTOR OF PHILOSOPHY

In

CHEMISTRY

2007

Nuran Ercal , Advisor	**Ekkehard Sinn**
Yinfa Ma	**V. Prakash Reddy**

Yue-Wern Huang

ABSTRACT

Ethanol and ionizing radiation exposure are independently known to cause tissue damage through various mechanisms. Non-enzymatic and enzymatic metabolism of ethanol, the latter via the cytochrome P_{450} 2E1-dependent pathway, produces free radicals which deplete cellular glutathione (GSH). Ionizing radiation exposure has been shown to induce lipid peroxidation, DNA damage, protein oxidation, and GSH depletion, as well. It was postulated that initial exposure to ethanol, followed by ionizing radiation, would result in heightened oxidative stress. The *in vitro* model used in this investigation was HepG2 cells (human hepatocellular liver carcinoma cell line), while the *in vivo* model was CD-1 mice. The antioxidant status of the models was evaluated by an array of techniques. Levels of reduced glutathione, oxidized glutathione (GSSG), cysteine (CYS), and malondialdehyde (MDA) were measured by the HPLC method. Activities of antioxidant enzymes, catalase, and glutathione reductase (GR) were determined enzymatically. Apoptosis was evaluated by the caspase 3 assay and fluorescence microscopy. Our data showed that, in both of the models, combined treatment resulted in the lowest levels of GSH, and the highest MDA and GSSG levels compared with the control and single agent exposure. The catalase activity was significantly lower in the combined exposure groups, when compared to the single agent exposure groups, and the glutathione reductase activity was highest in the combined exposure groups and lowest in the control. These findings suggest that a combination of ethanol and ionizing radiation produces deleterious effects *in vitro* and *in vivo* through augmented oxidative stress.

ACKNOWLEDGMENTS

My sincere thanks and appreciation are due to my advisor, Dr. Nuran Ercal, M.D., Ph.D., for her support and very valuable insights, foresight, constant encouragement, and wisdom, without which this dissertation would not have been possible.

Thanks are due to the members of my Ph.D. Committee: Ekkehard Sinn, Ph.D., Yinfa Ma, Ph.D., V. Prakash Reddy, Ph.D., and Yue-Wern Huang, Ph.D., for their help, encouragement, and guidance during my studies. I would also like to thank Dr. Richard Matthews for his support and helpful insights. I thank Dr. Helen Anni for providing me with HepG2 cells, which were used for the *in vitro* part of this investigation, and for her invaluable help throughout my studies; Dr. Viswanathan Subbaratnam from the Department of Radiation Oncology at the Phelps County Regional Medical Center for his help with irradiation procedures; Barbara Harris for editing the manuscript; and all of my previous and present lab group members for their constant support and encouragement.

My sincere gratitude goes to my wife, Isabell Were, for her love, constant encouragement, support, and inspiration; and to my sons, Steve Were and Ethan T. Were, and my daughter, Dawn R. Were, for their unfailing love, patience, and inspiration to work hard. My deepest appreciation and gratitude also goes to my parents, Nashon and Prisca Ogony, for their love, inspiration, and spiritual guidance; to my brother Enos for supporting and believing in me; and to all of my family members for their love, support, encouragement, and inspiration throughout my studies; and above all, to God who, by his grace, enabled me to accomplish this work.

TABLE OF CONTENTS

Page

LIST OF ILLUSTRATIONS

LIST OF TABLES

1. INTRODUCTION

Ethanol and ionizing radiation exposure are known to independently cause tissue damage through various mechanisms. Non-enzymatic and enzymatic metabolism of ethanol, the latter via the cytochrome P_{450} 2E1-dependent pathway, produces free radicals which deplete cellular glutathione (GSH). Acetaldehyde, an ethanol metabolite, has been documented to form adducts with proteins, that can induce an immune response in the liver, resulting in liver diseases such as hepatitis and cirrhosis. The metabolism of ethanol by the enzymes alcohol dehydrogenase and acetaldehyde dehydrogenase produce NADH, increasing the $NADH/NAD^+$ ratio. High $NADH/NAD^+$ hinders the oxidation of fatty acids, leading to fat accumulation in the liver, resulting in fatty liver disease. Ionizing radiation exposure has been shown to induce lipid peroxidation, DNA damage, protein oxidation, and GSH depletion. The damaging effects of ionizing radiation are mainly due to secondary radicals formed from radiolysis of water molecules in the cells. In spite of the dangers posed by ethanol and ionizing radiation exposure, the number of people exposed to these agents has continued to be on the rise as a result of increased use of radiation therapy in cancer treatment. Unfortunately, the habit of chronic alcohol consumption normally precedes tumor diagnosis in many individuals, and since ethanol consumption can be addictive, breaking the habit becomes extremely difficult, even when the health risks involved are obvious. Combined exposure studies would generate data that can elucidate on the dangers associated with heavy ethanol consumption, and educate the public before the consequences of their actions become irreversible.

1.1. REVIEW OF LITERATUTE

1.1.1 Ethanol Consumption and Metabolism. Consumption of alcoholic beverages, containing varying percentages of ethanol, is widespread in every human society across the globe. In almost every human culture, social events, such as celebrations (St Pat's Day, Independence Day), anniversaries, and parties are always punctuated with servings of alcoholic beverages as a part of the menu. Consumption of ethanol is documented as early as 8000 B.C [1]. In industrialized countries, alcoholic beverages are a part of the daily meals, while in developing countries, alcohol drinking is more often for pleasure and relaxation. The ethanol content of different beers, distilled spirits and wines varies a great deal. Low to moderate drinking of alcohol has been reported to have some inherent advantages such as cardioprotection, especially against coronary heart disease and ischemia-reperfusion injury [2], and provision of calories [3]. However, alcohol drinking can lead to alcoholism; a condition characterized by craving for alcohol and continued drinking in spite of alcohol-related problems, preoccupation with drug alcohol, and distortion in thinking, especially denial. In this condition, the alcohol addicts chronically take large amounts of alcoholic drinks and this leads to a number of medical conditions that are discussed later in the text.

There are great economic losses in terms of health care, reduced or lost productivity, destruction of property through accidents, and an increased crime rate which can be directly attributed to alcohol drinking. Between the years of 1985 and 1990, the economic cost of alcohol-related problems rose by 40% to $98.6 billion [4]. It has been estimated that 100,000 people die annually in the United States from drinking and related causes, making it the third leading cause of preventable mortality in the United

States [5]. Enzymatic pathways of ethanol metabolism produce two byproducts, namely acetaldehyde and NADH, which have adverse effects on the liver [6]. High concentrations of NADH in the liver inhibit the oxidation of fatty acids leading to their accumulation in the liver tissues. This results in a condition known as “fatty liver”. Acetaldehyde is known to react with many functional groups in proteins, thus impairing their function and leading to tissue damage [7]. Free radicals are also produced during both enzymatic and non-enzymatic ethanol metabolism, causing oxidative stress [6].

Ethanol is highly soluble in water due to the hydrogen bonds it forms with water molecules. When ethanol is consumed, it easily crosses the cell membrane, enters the circulatory system, and is transported to various tissues and organs of the body such as the liver, the kidney and the brain. Ethanol crosses the blood brain barrier causing lipid peroxidation in the brain tissues [8]. This is because the brain is rich in polyunsaturated fatty acid side chains and is low in antioxidants [9]. The enzymatic pathway of ethanol metabolism through cytochrome P 4502E1 generates acetaldehyde and acetate and, in the process oxidizes, NADPH to NADP+. Because this pathway uses oxygen, it generates free radicals which cause tissue damage in the liver, leading to alcoholic hepatitis and cirrhosis [10]. This pathway also consumes NADPH which is used to reduce GSSG to GSH. This leads to a drop in GSH level, resulting in oxidative stress [11]. Catalase and alcohol dehydrogenase pathways of ethanol metabolism produce acetaldehyde. Acetaldehyde reacts with the protein’s various functional groups impairing their functions. The primary targets include erythrocyte membrane proteins, hemoglobin, albumin, tubulin, lipoproteins, and collagens [12].

Accumulation of NADH from ethanol metabolism inhibits the oxidation of fatty acids leading to a condition known as fatty liver. The free radicals produced during ethanol metabolism include: hydroxyethyl radical, super oxide radical, peroxy radical, and a host of other radicals.

Ethanol is metabolized through enzymatic and non-enzymatic free radical pathways. The enzyme alcohol dehydrogenase catalyzes the oxidation of ethanol to acetaldehyde. This reaction takes place in the cytoplasm of the liver cells in the presence of NAD+. NADH is produced in the process. Acetaldehyde defuses into the mitochondria where aldehyde dehydrogenase enzyme catalyzes its metabolism to ethanoic acid and more NADH is produced [13]. Accumulation of NADH in the liver has been proved to be responsible for the fatty liver disease. Other enzymes involved in ethanol metabolism include catalase and cytochrome P-4502E1.

The first step of ethanol metabolism through enzymatic pathways involves oxidation of ethanol to acetaldehyde.

Alcohol Dehydrogenase:

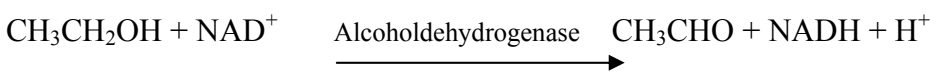

Aldehyde Dehydrogenase:

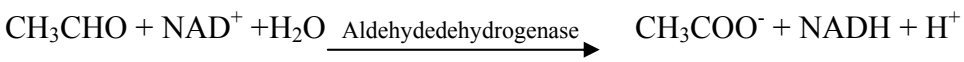

Catalase**:**

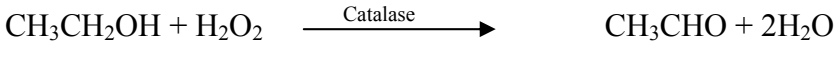

Cytochrome P-4502E1:

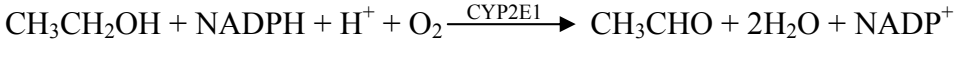

Non-enzymatic free radical pathway of ethanol metabolism takes place when a hydroxyl radical abstracts a hydrogen atom from ethanol producing α- hydroxyethyl radical as follows:

$CH_3CH_2OH + {}^{\bullet}OH \longrightarrow CH_3C^{\bullet}HOH + H_2O$

Hypervalent iron complexes may also catalyze this reaction without apparent involvement of hydroxyl radical [14, 15].

The hydroxyethyl radical produced reacts with oxygen to form a peroxy radical intermediate, which rearranges to release acetaldehyde and a super oxide radical as follows:

$CH_3C^{\bullet}HOH + O_2 \longrightarrow CH_3C(OO^{\bullet})HOH$

$CH_3C(OO^{\bullet})HOH \longrightarrow CH_3CHO + O_2^{\bullet -} + H^+$

1.1.2. The Mechanism of Ethanol-Induced Oxidative Stress. The mechanism by which ethanol induces oxidative stress has been the subject of investigation by many leading scientists. Several mechanisms have been suggested to play an important role in how ethanol induces oxidative stress. Some of the suggested mechanisms include: redox state change (decrease in the NAD+/NADH ratio) as a result of metabolism of ethanol by alcohol dehydrogenase and aldehyde dehydrogenase; acetaldehyde, mitochondrial damage leading to less ATP production; Kupffer cell activation by endotoxin; membrane effects; induction of CYP2E1 by ethanol; ethanol mobilization of iron resulting in enhanced levels of low molecular weight non-heme iron; effect on antioxidant enzymes (particularly cytosolic and mitochondrial glutathione levels); one-electron oxidation of ethanol to 1-hydroxyethyl radical; and conversion of xanthine dehydrogenase to the xanthine oxidase form. These pathways are interrelated and contribute to ethanol-induced

oxidative stress. The CYP2E1 pathway of ethanol- induced oxidative stress has the consensus of many investigators as the major pathway by which ethanol induces oxidative stress.

At high concentrations of ethanol and chronic ethanol consumption, alcohol dehydrogenase alone is not sufficient to metabolize all the ethanol. Under these circumstances, CYP2E1 becomes involved in ethanol oxidation [16]. CYP2E1 is mainly present in the liver; however, small quantities are present in other tissues such as the brain, kidney, and gastro-intestinal tract [17]. It has the ability to oxidize ethanol to generate reactive oxidation products such as acetaldehyde and the 1-hydroxyethyl radical. Additionally, it can activate various agents such as carbon tetrachloride, acetaminophen, benzene, halothane, halogenated alkanes, and alcohol to reactive products and generate reactive oxygen species. Ethanol increases levels of CYP2E1 by a posttranscriptional mechanism that leads to its stabilization against degradation. The catalytic cycle of CYP2E1, a loosely coupled enzyme, generates reactive oxygen species such as super oxide radical and hydrogen peroxide. The iron level is normally increased after ethanol treatment and enhances the production of more powerful oxidants such as hydroxyl radical, ferryl species, and 1-hydroxyethyl radical. Toxicity of these reactive oxygen species is due to protein oxidation and enzyme inactivation and damage to the cell membrane through lipid peroxidation, and production of reactive lipid aldehydes such as malondialdehyde and 4-hydroxynonenal. Damage to mitochondrial membrane by the ROS leads to a decrease in the membrane potential and alters the membrane permeability. This causes apoptosis to occur due to the release of proapoptotic factors.

1.1.3. Evidence from Previous Research. There is strong evidence from research suggesting that ethanol induces developmental toxicity in organisms. Investigation conducted by Reimers et al. [18], using zebrafish exposed to ethanol and acetaldehyde established a number of developmental malfunctions such as pericardial edema, yolk sac edema, axial malformations, delayed development and axial blistering. Reduced exposure to ethanol and acetaldehyde led to a proportional decrease in the effects.

Studies conducted by Gohlke et al. [19] using rat models, investigated ethanol-induced neocortical neuronal cell death during the synaptogenesis period. This study suggested that ethanol induces inhibition of proliferation during neurogenesis, and apoptosis. Sakuta et al. [20] have studied the relationship between heavy alcohol intake and homocysteine levels in type 2 diabetes. They found elevated levels of homocysteine in heavy alcohol drinking diabetic patients. Homocysteine is pro-oxidant [21], oxidizing low-density lipoproteins, thus enhancing the atherosclerosis process.

Ethanol consumption has been implicated in deaths due to acute ethanol poisoning [22]. Jones et al. conducted a study in which they compared the blood-ethanol concentration in deaths attributed to acute alcohol poisoning and chronic alcoholism. Alcoholic ketoacidosis was suggested as a more probable cause of death since more death cases had very high concentrations of acetone in the blood.

Research conducted by Agnieszka et al. [23] relates alcoholic liver cirrhosis and apoptosis of blood mononuclear cells. The result of their study showed that peripheral blood mononuclear cells (PBMCs), isolated from the blood of patients with alcoholic cirrhosis, showed accelerated spontaneous apoptosis after a 24-hr incubation period in *in vitro* compared to the PBMCs from the blood of healthy patient.

Besides the production of free radicals and the reactive oxygen species from ethanol metabolism, ethanol has been shown to increase the levels of bacterial protein called endotoxin in the blood and the liver [24]. The presence of endotoxin in the blood and the liver activates the immune cells called Kupffer cells in the liver to produce TNF-α, which in turn, activate another type of cells (stellate cells) in the liver to produce transforming growth factor beta (TGF-β), and collagen, which promotes scar tissue formation (fibrosis). The release of other types of cytokines such as interleukin-8 (IL-8) is also induced by TNF-α. This leads to the attraction of the inflammatory cells from the blood stream to the liver, causing inflammation of the liver. The acetaldehyde produced during enzymatic metabolism of ethanol, forms adduct with proteins, lipids, and the DNA molecules. The presence of these adducts in the blood stream also lead to the activation of certain immune cells such as IL-1, IL-2 and TNF-α. The activation of these immune cells leads to the attraction of inflammatory cells to the liver, resulting in inflammation, fibrosis, and organ damage. A summary of all the pathways by which ethanol metabolism induces the production of reactive oxygen species, and activates the diverse pathways which lead to apoptosis and organ damage is illustrated in Figure 1.1. It is apparent that there are numerous pathways by which ethanol can cause tissue damage and the onset of disease. There seems to be endless pathological conditions that ethanol consumption can initiate. The on going research on ethanol and its effects on the biological systems has uncovered very essential mechanisms by which ethanol induces damage to tissues, and created un awareness on potential dangers that heavy alcohol drinking can potentiate.

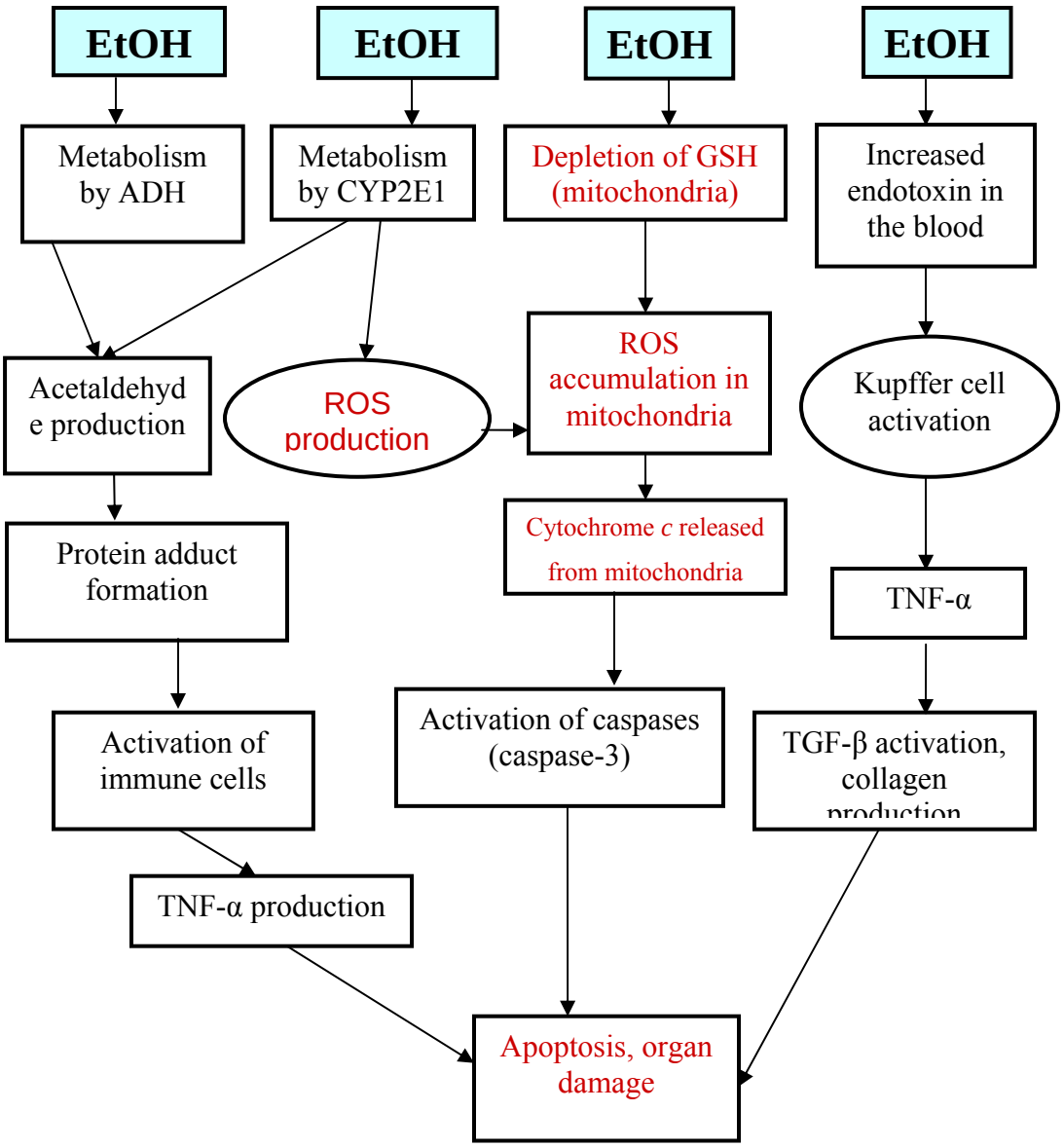

Figure 1.1. Pathways through which ethanol induces apoptosis and tissue damage [24].

1.1.4. Ionizing Radiation. Ionizing radiation is high-energy radiation capable of producing ionization on the atoms of the molecules it comes into contact with. The atom

becomes ionized when the radiation energy it absorbs is equal to or greater than the ionization energy of that atom, which results in an electron being ejected from the atom (illustrated in Figure 1.2). Alternatively, the energy absorbed may not be sufficient to eject an electron from an atom, resulting in excitation of an electron(s) (illustrated in Figure 1.3). Ionizing radiation is characterized by localized release of large amounts of energy [25].

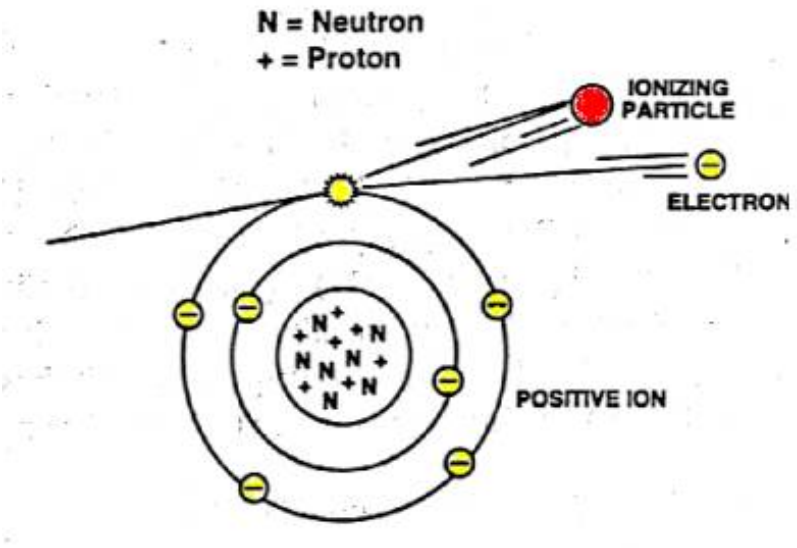

Figure 1.2. Ionization of an atom by ionizing radiation.
(www.fas.org/.../usa/doctrine/dod/fm8-9/1ch2.htm)

The radiations capable of producing such an effect on the atoms of the target molecules in the biological systems are called ionizing radiation. The particulate radiations (have high linear energy transfer) that travel short distances and release all of

their energies on their paths are the most ionizing. Alpha particles and neutrons are examples of highly ionizing radiations.

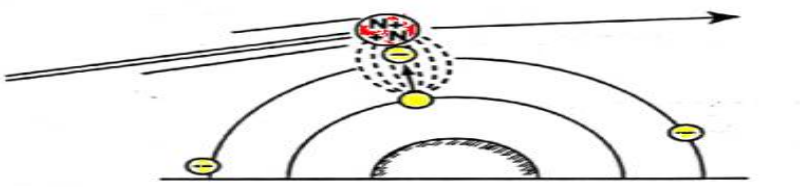

Figure 1.3. Excitation of an atom by ionizing radiation.
(www.fas.org/.../usa/doctrine/dod/fm8-9/1ch2.htm)

This type of effect is caused by low linear energy transfer radiations such as X-rays and γ-rays. The excited molecules produce secondary radicals, which in turn cause damage to the biological targets.

1.1.5. Types of Ionizing Radiation. Ionizing radiation is classified as electromagnetic radiation, such as X-rays and γ-rays, and particulate radiations has forms such as α-particle and β-particles, neutrons and protons. X-rays are electromagnetic radiation of short wavelengths produced when high-speed electrons strike a solid target, while γ-rays are electromagnetic radiation produced by decomposition of unstable radionuclide. X-rays and γ-rays are low linear energy transfer radiation and produce most of their effects in the biological systems by indirect action, while particulate radiations (α-particles, neutrons, protons) are high linear energy transfer radiations and produce

their effects by direct action. Linear energy transfer (LET) is the number of ionizations which radiation causes per unit distance as it passes through the cells. The damaging effects of ionizing radiation are consequences of both direct and indirect actions. It has been estimated that 60%-70% of radiation-induced tissue damage is due to free radicals, particularly the hydroxyl radical ($^{\bullet}OH$) [26]. The DNA molecule is the most critical target of ionizing radiation, and suffers extensive oxidative damage by both direct and indirect mechanisms of exposure [27]. A segment of the DNA molecule is shown in Figure 1.4.

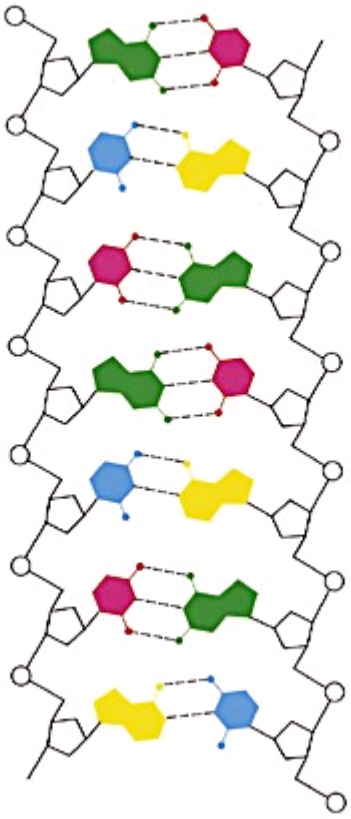

Figure 1.4. A segment of the DNA molecule.
(http://web.umr.edu/~nercal/chem 361 lecture)

The DNA suffers single and double strand breaks, and base modifications due to direct and indirect actions of radiation. Radiolysis of water produces $^{\bullet}OH$, which has been shown to produce the most damage to the DNA molecules [28].

1.1.6. Direct Action of Radiation. The direct action of radiation on biological systems is caused mostly by particulate radiation when the particles have sufficient kinetic energy to disrupt the atomic structure of the atoms of the absorbing molecule, resulting in chemical and biological changes. The alpha particles and neutrons are high LET radiations and produce their effects on biological systems by direct action.

1.1.7. Indirect Action of Radiation. The indirect action of radiation is caused by electromagnetic radiations: X-rays and γ-rays, which do not produce biological changes themselves, but induce the production of free radicals, which mediate the radiation damage. When these radiations are absorbed by cells, the water in the cells becomes charged due to loss of the electron.

$$H_2O \rightarrow H_2O^+ + e^-$$

The water molecule loses an electron as a result of the interaction with electromagnetic radiation to form a water radical cation, which is a strong acid. The water radical cation donates a proton to water, forming the hydronium ion and the hydroxyl radical.

$$H_2O^+ + H_2O \rightarrow H_3O^+ + {}^{\bullet}OH$$

The hydroxyl radicals formed can react with biological targets such as DNA, proteins, lipids, and other molecules and structures in the cells, or recombine to form hydrogen peroxide

$$^{\bullet}OH + {}^{\bullet}OH \rightarrow H_2O_2$$

The energy absorbed may, alternatively, cause radiolysis of water molecules to form the hydrogen and hydroxyl radicals.

$$H\text{-}O\text{-}H \xrightarrow{\text{radiolysis}} {}^{\bullet}OH + H^{\bullet}$$

The $^{\bullet}OH$ radical formed by radiolysis of water molecules has been reported to damage 60%-70% of the DNA molecules. The interaction of free radicals with DNA bases and sugars produces the most significant damage to DNA, which includes: oxidized bases, DNA-DNA strand adducts, DNA single and double strand breaks, DNA-protein cross-links, and various forms of aberrations [29]. Guanine is the DNA base that is most susceptible to attack by free radical, forming 8-hydroxyguanine [30-31]. The attack on the sugar moieties leads to cleavage of the sugar-phosphate backbone of DNA resulting in strand breaks. The free radicals also attack proteins and lipids, resulting in protein oxidation and lipid peroxidation [32].

1.2. EFFECTS OF FREE RADICALS ON BIOLOGICAL SYSTEMS

The free radicals produced by ethanol and ionizing radiation produce major biological changes, which can be classified as DNA damage, lipid peroxidation, and protein oxidation [33].

1.2.1. DNA Damage. The DNA molecule has many specific sites that are prone to attack (hot spots) by the ROS, as shown in Figure 1.5. The attacks can occur on the DNA bases or the sugar-phosphate backbone, resulting in DNA double and single strand breaks, and numerous base and sugar modifications.

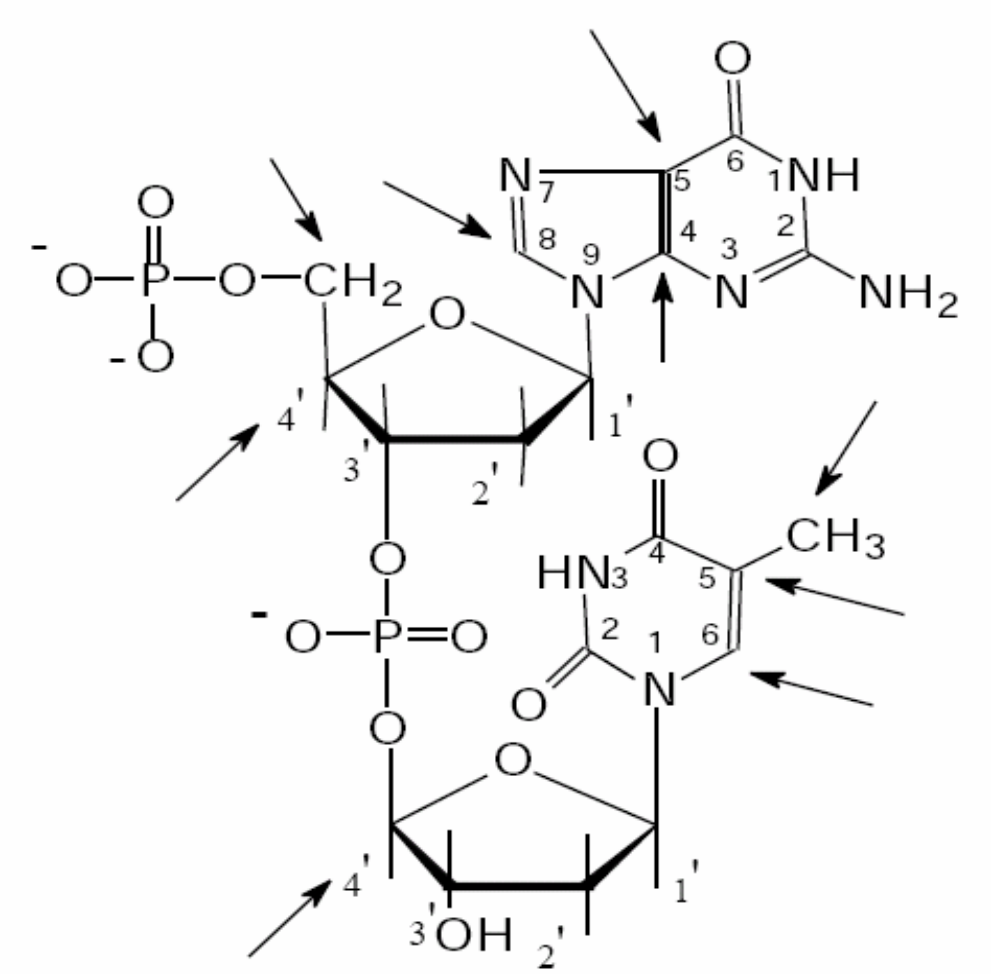

Figure 1.5. Hot spots for free radical attack on the DNA molecule.
(Freya Q. Schafer, PhD. Oxidative DNA damage. Sunrise Free Radical school, 1997)

The attack on the DNA molecule by the •OH radical can fall in to three categories, namely, hydrogen abstraction, addition, and electron transfer [34]. These reactions have the potential of causing damage to all of the four bases and the deoxyribose sugar.

The •OH radical reacts with the bases in the DNA molecule by addition. In pyrimidines, such as thymine, the •OH radical adds to the C5-C6 double bond, forming base radicals, of which 5-hydroxy-6-yl radicals have reducing properties, while the 6-

hydroxy-5-yl radicals are oxidizing [35]. The free radical can also abstract a hydrogen from the methyl group of thymine, resulting in radical formation. The reactions of the •OH radicals with the pyrimidines are shown in Figure 1.6.

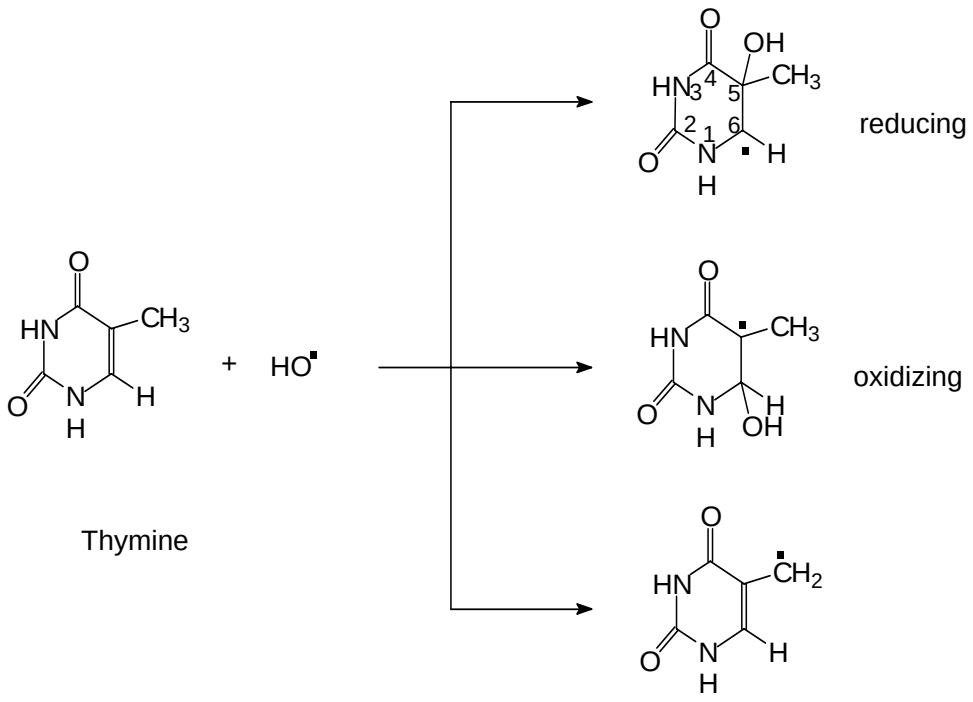

Figure 1.6. Hydroxyl radical attack on thymine.
(Adapted from: von Sontag C. (1987). The chemical basis of radiation biology, Taylo & Francis London, NY)

The •OH radical reacts with purines by adding to C4, C5, and C8 positions resulting in equal amounts of oxidizing and reducing adduct radicals [36]. The C4-OH

and C5-OH radicals dehydrate and are converted to oxidizing radicals [37]. These reactions are shown in Figure 1.7

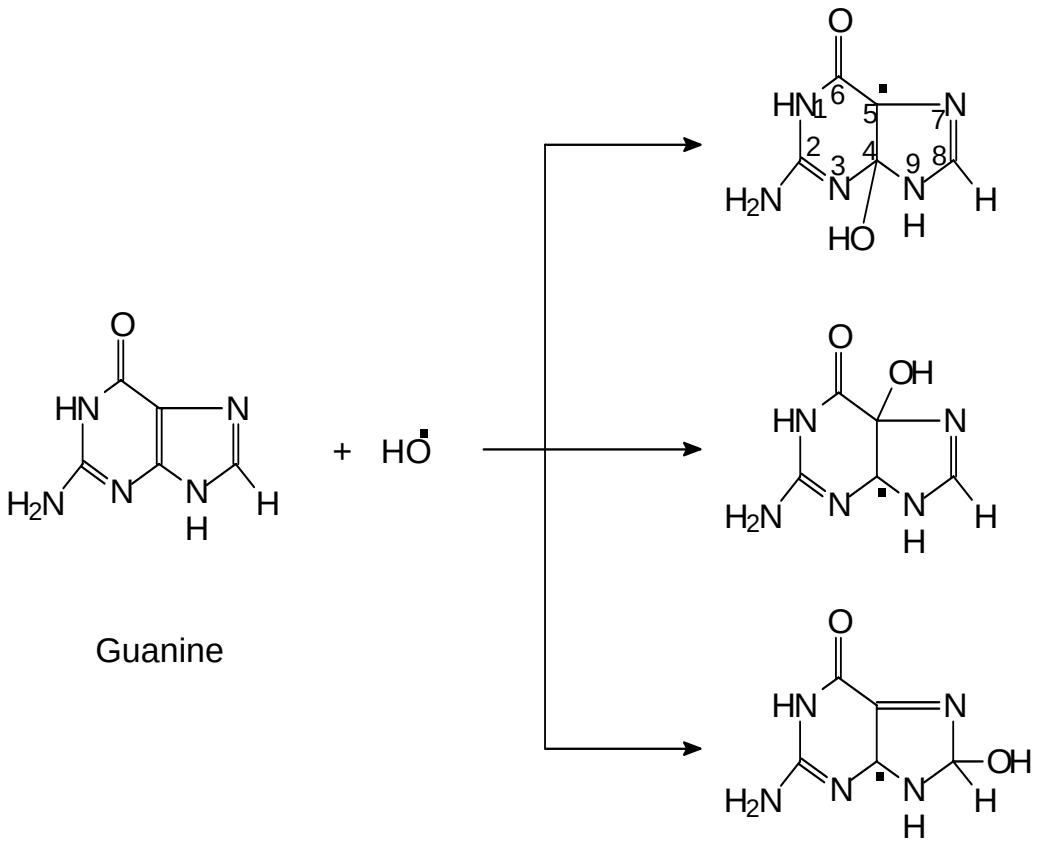

Figure 1.7. Hydroxyl radical attack on guanine (purine).
(Adapted from: von Sontag C. (1987). The chemical basis of radiation biology, Taylo & Francis London, NY)

A wide range of oxidized DNA base products are shown in Figure 1.8. These modifications have been suspected to be responsible for various types of mutations and tumor development, and many disease conditions.

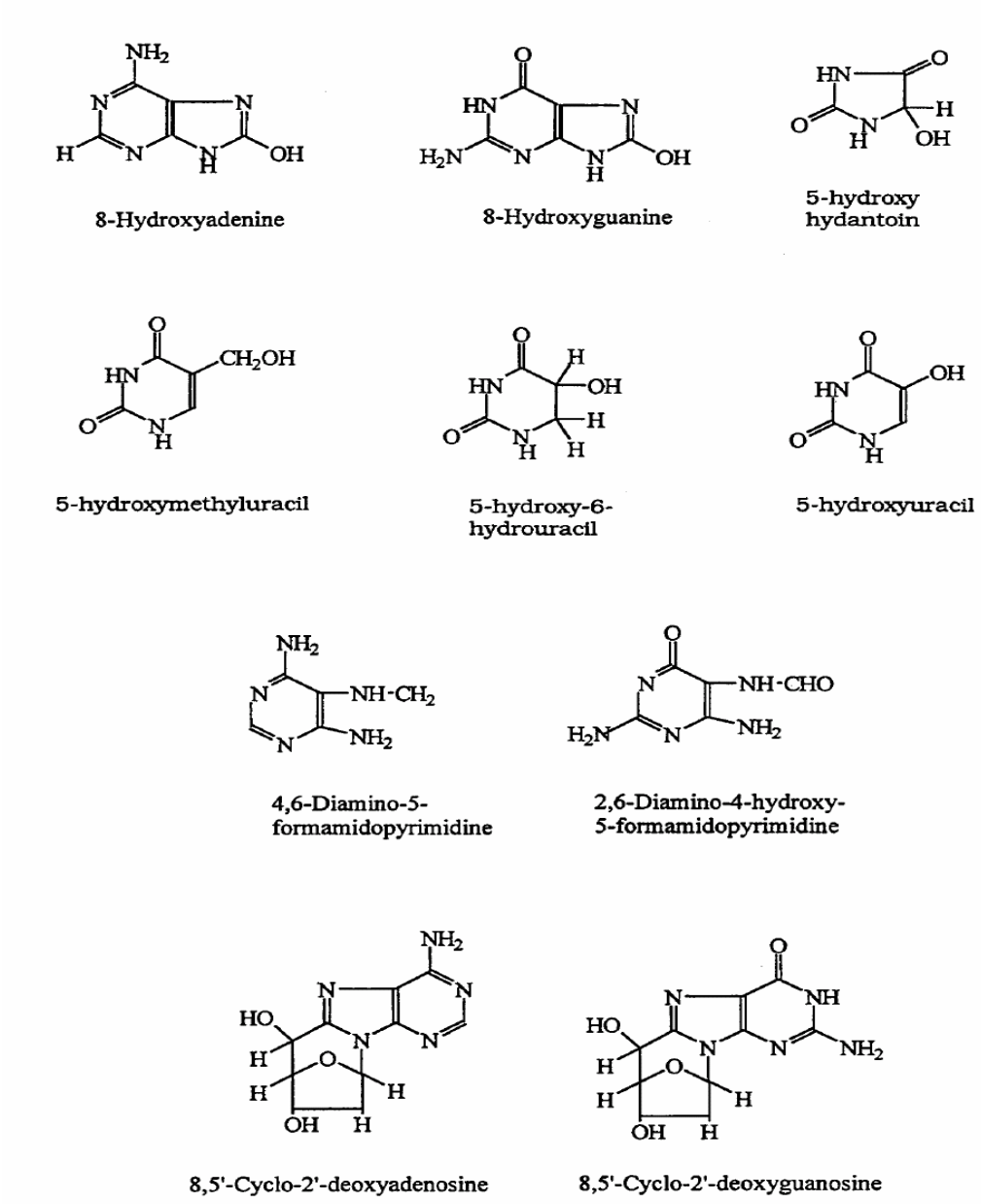

Figure 1.8. Base products of oxidative damage to DNA [38].
(Adapted from Dizdaroglu M. (1992). Free. Radic. Biol. Med.)

Attack by the $^{\bullet}OH$ radical on the deoxyribose sugar leads to an abstraction of hydrogen (possible in all the five carbons of the ribose sugar), and subsequent formation

of carbon-centered radicals. The carbon centered radicals can react with oxygen to form peroxyl radicals. Additionally, the radicals can react with each other forming non-radicals [39]. The C4' –centered radical can undergo β cleavage under anaerobic conditions, resulting in DNA strand breakages and the release of an intact base and altered sugars [40]. The sugar lactone, and an intact base are formed when the C1'-centered radical is oxidized [41]. The oxidation of sugar phosphate backbone is shown in Figures 1.9 and 1.10.

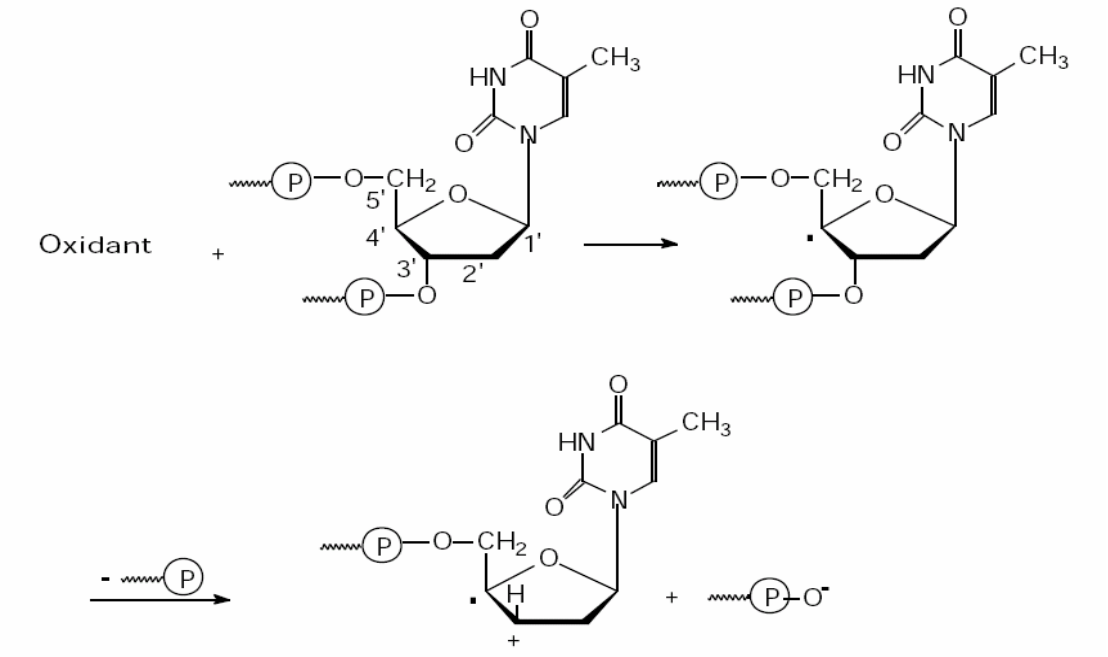

Figure 1.9. Attack of free radicals on the sugar phosphate backbone.
(Adapted from: von Sontag C. (1987). The chemical basis of radiation biology, Taylo & Francis London, NY)

These types of attacks result in single and double strand DNA breakages. The single strand breaks are normally easily repaired by the DNA repair enzymes. However,

the double strand breakages are very difficult to repair, and usually result in apoptosis, mutagenesis, and carcinogenesis [42].

The oxidation of sugar phosphate backbone is shown in Figures 1.9 and 1.10.

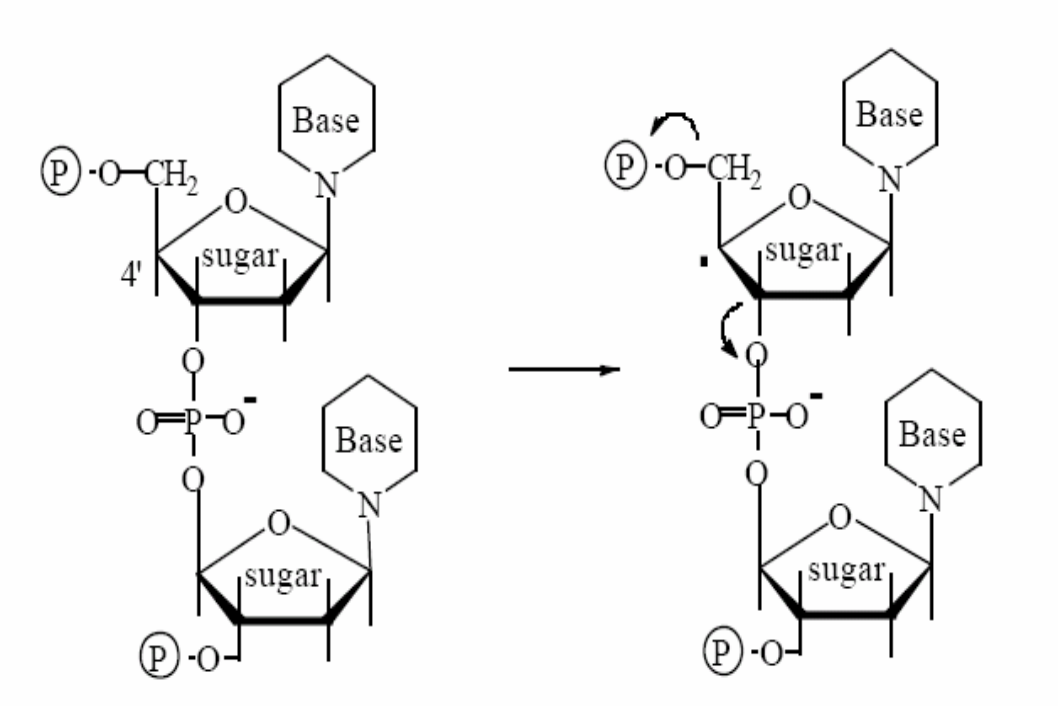

Figure 1.10. Attack on the deoxyribose.
(Adapted from: von Sontag C. (1987). The chemical basis of radiation biology, Taylo & Francis London, NY)

The modified bases can react with proteins, forming DNA-protein cross-links, shown in Figure 1.11 [43]. These in turn can trigger other signal transduction pathways.

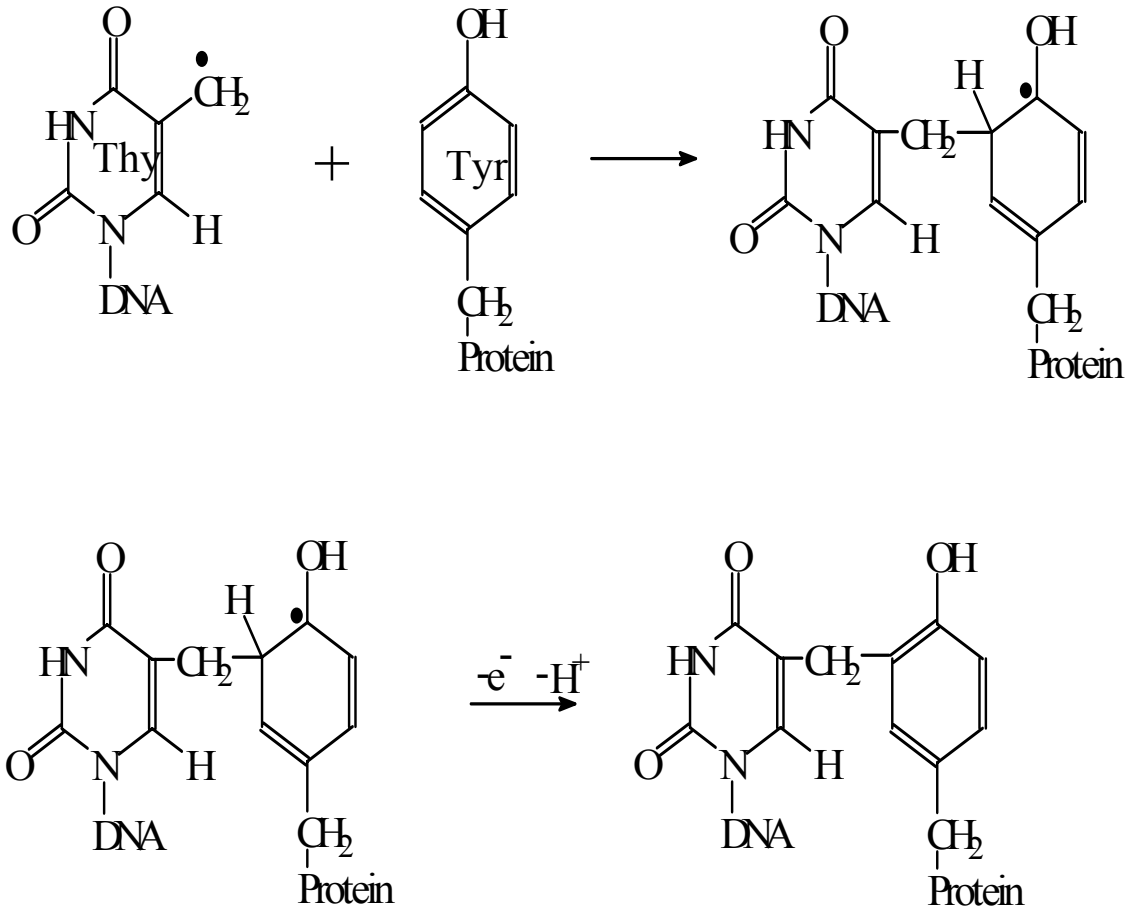

Figure 1.11. DNA-protein cross-link adducts.
(Peak GJ, Peak MJ, *et al*., (1985). *Photochem. Photobiol*. **41**. 295-302)

1.2.2. Lipid Peroxidation. Lipid peroxidation is a biological free radical chain reaction that is responsible for the formation of a wide range of products, in including aldehydes, ketones, and cyclic peroxide radicals in the cells [44]. The mechanism of lipid peroxidation is shown in Figure 1.12.

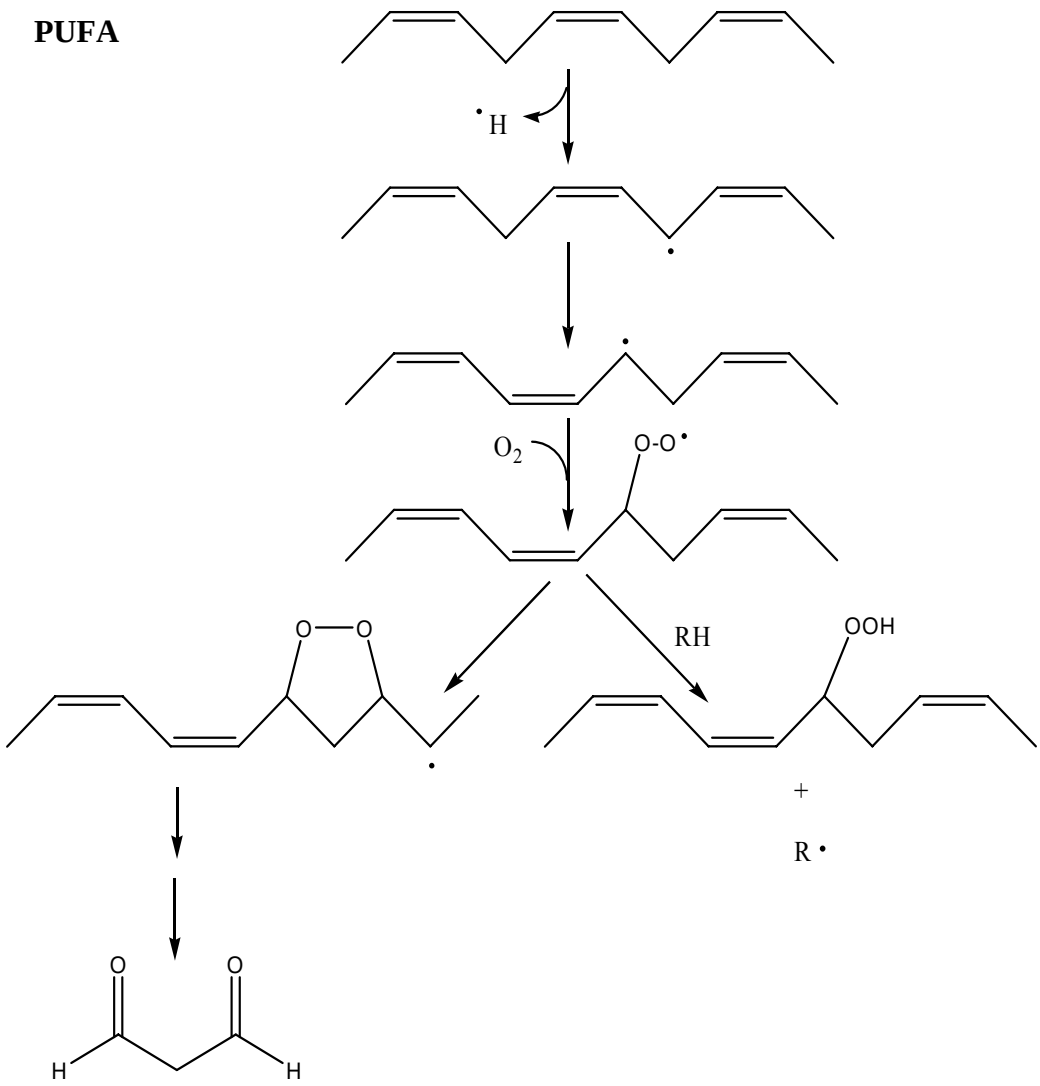

Malondialdehyde

Figure 1.12. Lipid peroxidation mechanism (polyunsaturated fatty acids).
(Bucher JR, Tien M. et al., (1983). *Biochem. Biophys. Res. Commun*. **111**: 777-784)

The lipid peroxidation chain reaction is initiated by an abstraction of a hydrogen atom from a methylene carbon in a polyunsaturated fatty acid (such as arachidonic acid) by a hydroxyl radical, forming lipid radicals. The presence of many carbon-carbon

double bonds makes the abstraction of hydrogen easier. The carbon-centered lipid radicals formed rearrange and react with molecular oxygen in an aerobic environment to form peroxyl radicals. The peroxyl radicals formed abstract hydrogen from the side chains of neighboring polyunsaturated fatty acids (PUFA) and combine with the abstracted hydrogen to form hydroperoxides, and propagate the chain reaction; combine with each other, and attack membrane proteins [45]. The lipid hydroperoxides decompose in the presence of metals, such as iron or copper to form products, which include ethane and pentane gas, unsaturated aldehydes such as 4-hydroxy-2-nonenal (4-HNE), and malondialdehyde (MDA) [46-48]. Lipid peroxidation has been implicated in the pathological conditions associated with atherosclerosis, ischemic or traumatic brain damage [44].

1.2.3. Protein Oxidation. Protein oxidation is the covalent modification of a protein induced either directly by reactive oxygen species or indirectly by reaction with secondary by-products of oxidative stress [49]. The damage caused on proteins due to oxidation can result in functional changes, which includes inhibition of enzymatic and binding activities; increased susceptibility to aggregation and proteolysis; decreased uptake by cells; altered immunogenisity; induction of apoptosis, and necrosis, altered gene regulation and expression, and modulation of cell signaling [50]. The oxidative changes can lead to backbone fragmentation, aliphatic-side chain oxidation, and aromatic side-chain oxidation. The ROS can abstract hydrogen from an α-carbon in an aliphatic residue as shown in Figure 1.13.

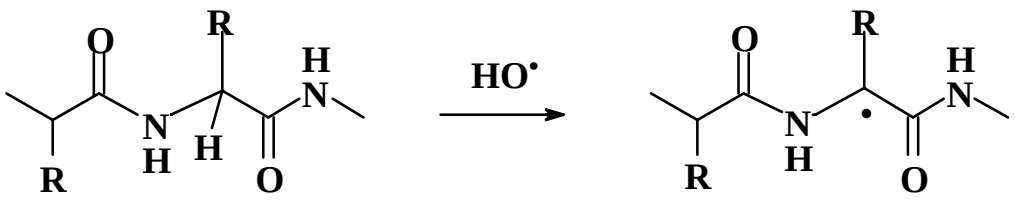

Figure 1.13. Sites of oxidant damage on proteins [51].
(Davis MJ. Protein oxidation: concepts, mechanisms and new insights. Sunrise Free Radical School)

The abstraction of hydrogen at an alpha-carbon can result in backbone fragmentation. Side chain oxidation on aliphatic residue can occur at a tertiary carbon or primary carbon, resulting in altered protein structure, shown in Figure 1.14.

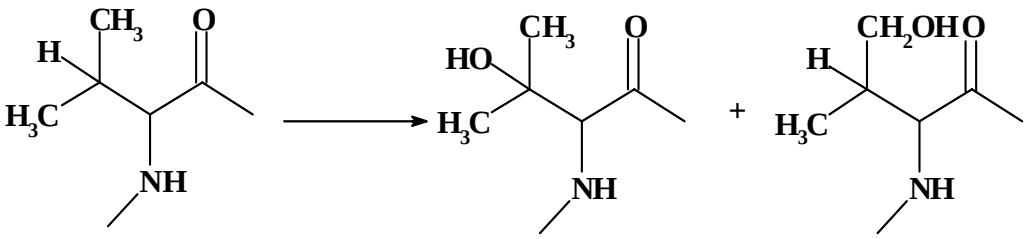

Valine side-chain

3° C radical 1° C radical

Figure 1.14. Side chain oxidation by radicals.
(Davis MJ. Protein oxidation: concepts, mechanisms and new insights. Sunrise Free Radical School)

Backbone fragmentation on a protein can occur when a hydrogen is abstracted from an alpha carbon, followed by addition of oxygen to form peroxyl radicals. The peroxyl radicals can undergo hydrolys, which results in fragmentation. Alternatively, the peroxyl radicals can abstract hydrogen from the neighboring molecules to form hydroperoxides, which eventually fragment to form products shown in Figure 1.15.

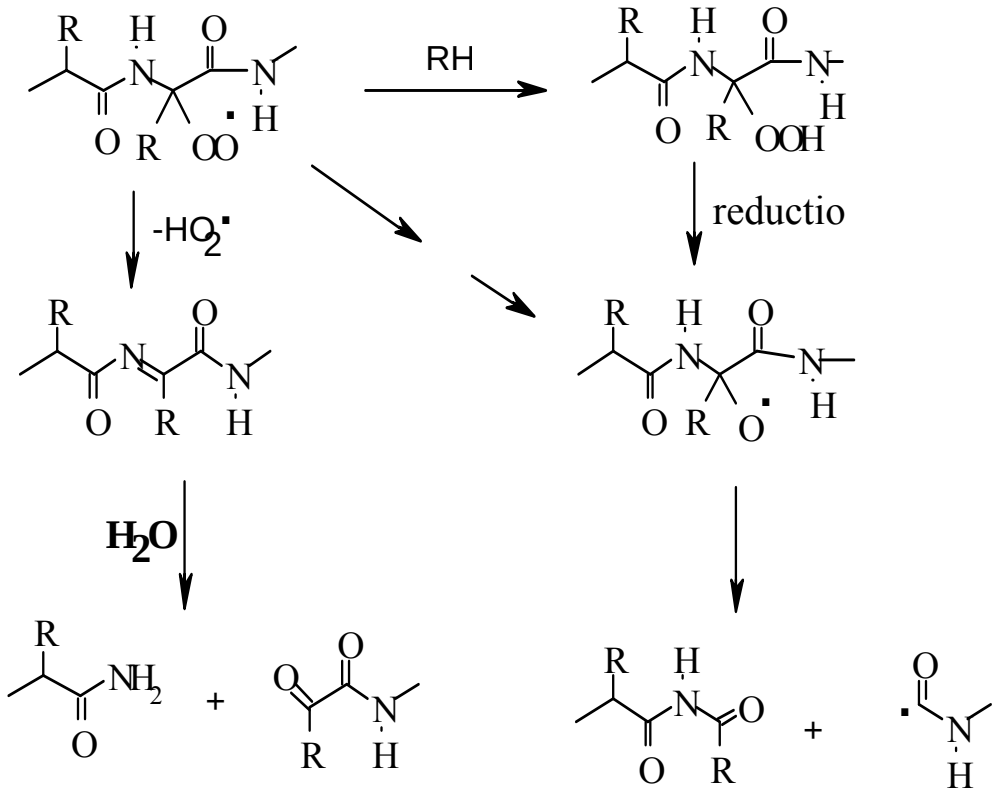

Figure 1.15. Backbone fragmentation induced by radicals [52].
(Davis MJ. Protein oxidation: concepts, mechanisms and new insights. Sunrise Free Radical School)

The aromatic side chain oxidation occur by addition of hydroxyl radical on to the aromatic ring, leading to transformations from phenyalanine to ortho and meta-tyrosine product, and from tyrosine to 2,3-dihydroxyphenyalanine (DOPA) [53]. The transformations are shown in Figure 1.16. Protein oxidation products have been used as biomarkers of oxidative stress.

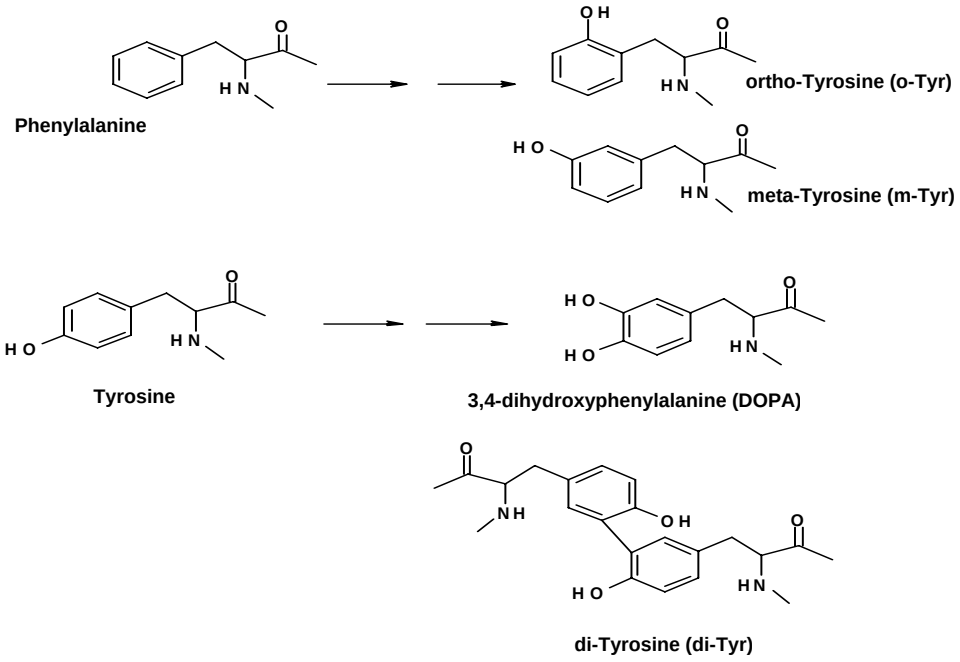

Figure 1.16. Specific aromatic side chain oxidation products [51].
(Davis MJ. Protein oxidation: concepts, mechanisms and new insights. Sunrise Free Radical School)

1.3. THE ANTIOXIDANT DEFENSE SYSTEM

Aerobic organisms have developed an elaborate system of antioxidant molecules and enzymes to counter the damaging effects of free radicals and reactive oxygen species

[54]. GSH is the most abundant antioxidant in the body, and is found in all mammalian cells. It is a tripeptide made of the amino acids: glutamate, cysteine, and glycine, as shown in Figure 1.17. The SH functional group in cysteine makes glutathione a potent antioxidant and the first line of defense against free radicals and xenobiotics. The antioxidant enzyme system is made of the enzymes: glutathione peroxidase, which decomposes organic and inorganic peroxides; glutathione reductase, which reduces oxidized glutathione to regenerate reduced glutathione; catalase, which decomposes hydrogen peroxide to water and oxygen; superoxide dismutase, which dismutates the superoxide radical [55-57]; and many others.

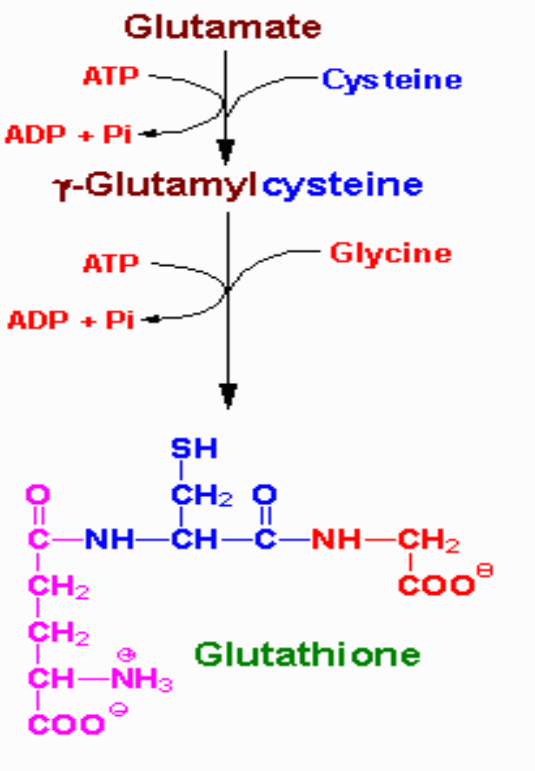

Figure 1.17. Glutathione, the principal antioxidant in mammalian cells. (web.indstate.edu/.../aminoacidderivatives.html)

Glutathione counters the oxidative stress by the following mechanisms:

Free radical scavenging,

$GSH + OH^{\bullet} \rightarrow GS^{\bullet} + H_2O$

Hydrogen donation.

$R^{\bullet} + GSH \rightarrow RH + GS^{\bullet}$

Restore oxidized DNA

$GSH + DNA^{\bullet} \rightarrow DNA + GS^{\bullet}$

Regenerate other antioxidants

$Vit\ C^{\bullet} + GSH \rightarrow Vit\ C + GS^{\bullet}$

Reduce lipid peroxides

$$2GSH + ROOH \xrightarrow{GPx} 2H_2O + ROH + GSSG$$

1.4. SIGNIFICANCE OF COMBINED EXPOSURE STUDIES

Studies have shown that, at high levels of exposure, chemical and physical agents may have additive/synergistic effects in the biological systems. Additionally, investigators have performed single agent exposure studies, while assuming that the agent under study would act independently of other preexisting conditions or agents [58]. Furthermore, the end points that have been measured by investigators in previous combined-exposure studies have been clinical outcomes, such as tumor induction, radiosensitization, or radioprotection, and not antioxidant status [59-61]. This investigation is the first complete combined-exposure investigation, using model *in vitro* and *in vivo* systems to determine the effects of a combination of ethanol and ionizing radiation on the antioxidant status of the systems. This study has the potential for

generating vital data that could be used to advise prospective radiation therapy patients. Additionally, this research offers a legitimate premise for advising the general public about the dangers of indulging in habits such as binge drinking and excessive use of alcohol. The on going research is bound to shed more light on effects of ethanol and radiation, and their interactions with biological systems. The onset of cancer generally occurs, in a majority of cases, from middle to old age, when habits such as cigarette smoking, alcoholism, and other habits are well established, and breaking such habits due to medical reasons always does not succeed. The data from this research can be used to offer advice against such harmful habits when there are still chances of recovery.

2. EFFECTS OF COMBINED EXPOSURE TO ETHANOL AND IONIZING RADIATION ON THE ANTIOXIDANT STATUS OF AN *IN VITRO* MODEL

2.1. INTRODUCTION

The combination of ionizing radiation and ethanol exposure can potentially be extremely toxic to tissues due to heightened oxidative stress. Ethanol and/or radiation exposure induce the production of reactive oxygen species (ROS) [62-66].

The enzymatic pathway of ethanol metabolism through cytochrome P4502E1 (CYP 2E1) generates directly, besides acetaldehyde and acetate, ROS [67-68]. The latter can trigger protein oxidation, enzyme inactivation, DNA damage, damage to the cell membrane through lipid peroxidation, and production of reactive lipid aldehydes such as MDA and 4-hydroxynonenal (4HNE). This pathway also consumes NADPH, which is used to reduce GSSG to GSH, leading to a drop in the GSH levels of cells. Moreover, ROS are formed during the non-enzymatic oxidation of ethanol. Numerous studies have shown that ionizing radiation also generates ROS in biological systems, resulting in oxidative damage to macromolecules such as DNA, lipids and proteins [69-71].

Ionizing radiation can interact directly with critical targets in the cells, such as DNA by energy transfer, causing ionization of the atoms, and subsequent biological changes. Additionally, the radiation may also interact with water molecules to produce free radicals indirectly in a series of reactions: $H_2O \rightarrow H_2O^+ + e^-$; $H_2O^+ + H_2O \rightarrow H_3O^+ + {}^{\bullet}OH$; ${}^{\bullet}OH + {}^{\bullet}OH \rightarrow H_2O_2$

These free radicals can then interact with macromolecules, such as DNA, to cause biological changes (indirect action).

Chemotherapeutic and radiotherapeutic treatment modalities have relied on the oxidative damage by free radicals to eradicate tumors [72] and in the process, unintended damage to normal tissues often occurs. Since ethanol and ionizing radiation can both increase free radical levels significantly, the need to better understand the interplay of exposure to ethanol prior to ionizing radiation (XRT) becomes necessary. Assessment of risks in having some other agent or condition present prior to or coincident with radiation exposure, has usually relied on the implicit assumption that radiation would act independently of other pre-disposing conditions or substances already present in the system at the time of exposure. Recent studies of interactions, however, have shown that at high exposures, the action of one agent or condition can be influenced by simultaneous exposure to other agents or conditions [73]. There are numerous reports of investigations conducted to determine the effect of combined exposure of radiation with other physical and chemical agents, namely, tobacco, bleomycin, 5-fluorouracil, glutamine, N-acetyl cysteine, paraquat (superoxide generating agent), cyclophosphamide, and many others. The end points measured have been various including combined action against cancers, radiation protection of normal tissues, and tumor induction [74-75]. Other medical conditions, such as diabetes, hypertension, or collagen vascular diseases, may also affect the risks of complications attributed to XRT. Therefore, in these sets of experiments, the effects of *in vitro* exposure of HepG2 cells to varying concentrations of ethanol for 24 h, followed by radiation, and then analysis 24 h later was investigated. In order to assess the antioxidant status, the parameters such as GSH, CYS, MDA, and activities of some antioxidant enzymes (catalase and glutathione reductase) were measured. Cell viability

was measured using the MTS assay and apoptosis by caspase-3 apoptotic assay and by fluorescence microscopy.

2.2. EXPERIMENTAL DESIGN

2.2.1. Ethanol Dose-Dependent Studies on HepG2 Cells. The ethanol dose dependent studies were conducted in order to determine the right concentration of ethanol to be used in the rest of the *in vitro* experiments. The cells were allowed a 24 h incubation period for attachment, followed by incubation with varying concentrations of ethanol (10-100 mM) for 48 h. At the end of the treatment period, the cells were collected by trypsinization, homogenized and derivatized, and levels of GSH determined.

2.2.2. Radiation Dose-Dependent Studies on HepG2 Cells. These experiments were done in order to determine the right radiation dose to be used for the rest of the experiments. The cells were incubated for 24 h to allow attachment, followed by a change of media and further 24 h incubation, after which the cells were exposed to varying radiation doses (2-10 Gy). The cells were collected, homogenized, and derivatized to determine the GSH levels 24 h after irradiation.

2.2.3. Oxidative Stress Studies. The cellular levels of oxidative stress markers such as GSH, CYS, and MDA were measured after the cells had been exposed to ethanol, followed by ionizing radiation. The activities of some antioxidant enzymes (GR and CAT) were also measured. The objective of performing these experiments was to determine the antioxidant status of the cells, in order to assess the effects of ethanol and radiation on HepG2 cells.

2.2.4. Cell Viability Studies. The cell viability was determined by the MTS assay. The tetrazolium compound (MTS) was reduced to a formazan product by NADPH produced by the dehydrogenase enzyme in the living cells. The formazan product has an absorbance at 490 nm, which is directly proportional to the number of the living cells. The cells were exposed to ethanol followed by radiation, then the MTS reagent was added to the cell in a 96-well plate, and the absorbance was read after 2 h. The cell viabilities in the various groups were determined as the percentage of the untreated control.

2.2.5. Apoptosis Studies. The caspase-3 assay and fluorescent microscopy procedures were used to determine the apoptotic process in the cells. The details of these procedures are given under the materials and methods section.

2.3. MATERIALS AND METHODS

2.3.1. Materials. HPLC-grade acetonitrile, glacial acetic acid, water, and phosphoric acid, used for the preparation of mobile phase, were purchased from Fisher Scientific (Fair Lawn, NJ USA). N-(1-pyrenyl)-maleimide (NPM), used as a derivatizing agent for measurement of CYS and GSH, 1,1,3,3-tetramethoxypropane, and ethanol were purchased from Aldrich (Milwaukee, WI USA). Protein concentration was evaluated with the Bradford reagent obtained from BioRad (Melville, NY USA). Dulbecco's Modified Eagle Medium (DMEM), heat inactivated fetal bovine serum, L-glutaMax, penicillin and/streptomycin, sodium pyruvate, and non-essential amino acids were purchased from Invitrogen Corporation (Carlsbad, CA USA). Acridine orange (AO), ethidium bromide

(EB), and all other chemicals were purchased from Sigma (St. Louis, MO USA). 25 cm^2 culture flasks and 0.2-µm filters were purchased from Advantech MFS, Inc. (Dulin, CA USA). Human hepatocellular liver carcinoma (HepG2) cells were provided by Dr. Helen Anni from Thomas Jefferson University in Philadelphia, PA USA. Caspase-3 activity assay kit was purchased from R&D Systems, USA, while CAT and GR activity assay kits were purchased from OxisResearch ™.

2.3.2. Culture of HepG2 Cells. HepG2 cells were grown in high glucose DMEM, supplemented with 1 % of L-glutaMax, penicillin and streptomycin, sodium pyruvate, non-essential amino acids, and 10 % heat inactivated fetal bovine serum (FBS). The cells were seeded at a density of 1.5 million cells per ml in T-25 culture flasks with 5 ml of complete medium and cultured at 37 ^{o}C with 5 % carbon dioxide.

2.3.3. Ethanol and Radiation Treatment. After 24 h, attached cells were treated with varying concentrations of ethanol (10-100 mM), for 24 h. Irradiation of the cells (8 Gy) was performed with a 9 MeV beam generated by a Varian Linear accelerator, model 21 EX (Varian Associates, Walnut Creek, CA, USA) using a 20 x 20 or 25 x 25 cm field at the Radiation Oncology Department of the Phelps County Regional Medical Center in Rolla, Missouri. The cells were further incubated for 24 h after radiation, and then trypsinized, homogenized, and immediately analyzed, or stored at -80 ^{o} C for later analysis of CYS, GSH, MDA, and antioxidant enzymatic activities.

2.3.4. Thiols Determination. The derivatizing agent, N-(1-pyrenyl) maleimide, reacts with thiols (GSH, CYS, NAC, HCYS) to form a fluorescent adduct that can be quantified by the HPLC method, with fluorescent detection. This procedure was used to

determine the levels of glutathione and cysteine in HepG2 cells after homogenization and derivatization.

2.3.5. Protein and Enzyme Activity Determination. A Hitachi U-2000 double beam UV-Vis spectrophotometer (Tokyo, Japan) was used to measure protein concentration using the Bradford assay [76] and antioxidant enzyme activities. A Fluostar OPTIMA microplate reader (BMG Labtechnologies. Inc, Durham, NC) was used for MTS and caspase-3 assays.

2.3.6. Determination of GSH and CYS Levels. Cellular levels of GSH and CYS were determined by RP-HPLC, according to the method developed in our laboratory [77]. The HPLC system (Thermo Electron Corporation) consisted of a Finnigan Spectra System vacuum membrane degasser (model SCM1000), gradient pump (model P2000), autosampler (model AS3000), and fluorescence detector (model FL3000) with λex = 330nm and λem = 376 nm. The HPLC column was a Reliasil ODS-1 C_{18} column (5 µm packing material) with 250 x 4.6 mm (Column Engineering, Ontario, CA, USA). The mobile phase was 70% acetonitrile and 30% water and was adjusted to a pH of 2 with acetic acid and o-phosphoric acid. The NPM derivatives of CYS and GSH were eluted from the column isocratically at a flow rate of 1mL/min.

2.3.7. MDA Determination. The MDA determination was done by RP-HPLC method using λexc = 515 nm; the λem 550 nm [78]. Cell homogenate (350 µl) was mixed with butylated hydroxytoluene (100 µl of 500 ppm), and 10% trichloroacetic acid (550 µl) and boiled for 30 min. After the solution was cooled on ice and centrifuged for 10 min at 1500 x g, the supernatant (500 µl) was mixed with thiobarbituric acid (TBA) (500 µl). The tubes were boiled again for 30 min, and then cooled on ice. A solution (500 µl) was

added to n-butanol (1.0 ml), vortexed, and centrifuged for 5 min at 60 x g to facilitate a phase separation. The top layer was then filtered through 0.45 μm filters and injected onto a 5 μm C_{18} column (250 x 4.6 mm) on a RP- HPLC system. The mobile phase consisted of 69.4% 5mM sodium phosphate buffer pH = 7.0, 30% acetonitrile, and 0.6% tetrahydrofuran.

2.3.8. Cell Viability Determination. This assay uses the novel tetrazolium compound, MTS (3-(4,5-dimethylthiazol-2-yl)-5-(3-carboxymethoxyphenyl)-2-(4-sulfophenyl)-2H-tetrazolium), that is reduced by NADPH or NADH (produced by dehydrogenase enzyme in the living cells) into formazan, which is soluble in tissue culture medium. The Cell Titer 96® AQ_{ueous} Cell Proliferation Assay (Promega Corporation, Madison, WI, USA) was used to determine of cell viability in the various groups. The absorbance of the formazan product was measured using 96-well microplates at 490 nm [79-80]. The production of formazan is proportional to the number of living cells; therefore, the intensity of the color produced is a good measure of cell viability. 100 μL cell suspension of HepG2 cells (approximately 5 x 10^3 cells) were seeded into each well of the 96-well microplate and incubated for 24 h for the cells to attach. The old media was removed and fresh medium, with different concentrations of ethanol, was added to the ethanol groups. The control and XRT only groups received complete media without ethanol. The cells were incubated for an additional 24 h, then the XRT and ethanol and XRT groups were exposed to radiation, while the control group did not receive any radiation. The cells were returned to an incubator maintained at 37 ^{o} C, 95% air, and 5% CO_2 for an additional 24 h after radiation. Then 20 μL of MTS tetrazolium

reagent were added to each well. The absorbance at 490 nm was read after 2 h incubation with the MTS reagent.

2.3.9. Apoptosis Measurements. The caspase-3 apoptotic assay was performed using a colorimetric substrate, as per the manufacturer's instructions (R&D Systems, Inc. MN). Briefly, 25µl of lysis buffer per $1x10^6$ cells were added to each pellet that was collected after treatment. The cell suspension was incubated on ice for 10 min and then centrifuged at 10,000 x g for 3 min. 50 µl of the supernatant, along with 50 µl of the 2X reaction buffer containing 0.1 M dithiothreital (DTT) and 5 µl of the caspase-3 colorimetric substrate (DEVD-pNA) were added to each well in a 96-well plate. The plate was then incubated for 2 h before the absorbance was read by a microplate reader at 405 nm.

Apoptosis was also evaluated by fluorescence microscopy. HepG2 cells (3.5 x 10^6 cells/ml), were centrifuged at 150 x g for 5 min to pellet the cells, and then washed once with cold PBS (5 ml). The cells were resuspended in cold PBS (1 ml), and then 25 µl of the cell suspension was mixed with 2 µl of EB/AO dye mix. Stained cells (10 µl) were placed on a clean microscope slide and covered with a cover slip and viewed using an Olympus IX51 inverted microscope at 400X total magnification using a UPLFLN 60X NA 1.25 objective. FITC (EX 482/35 506DM EM536/40) and TexasRed (EX 562/40 593DM EM 692/40) filters were used (Brightline). Images were captured with a Hamamatsu ORCA285 CCD camera. Shutters, filters, and camera were controlled using SlideBook software (Intelligent Imaging Innovations, Denver, CO).

2.3.10. Catalase Activity. The activity of catalase (CAT; EC 1.11.1.6) in the cell homogenates was measured spectrophotometrically at 240 nm following the exponential

disappearance of hydrogen peroxide (H_2O_2; 10 mM) according to the method described by Aebi [81]. The catalase activity is calculated from $A_{60} = A_{initial}\, e^{-kt}$ where k, is the rate constant, $A_{initial}$, is the initial absorbance, and A_{60} is the absorbance at 60 s.

2.3.11. Glutathione Reductase Activity Assay. Glutathione reductase (GR; EC 1.6.4.2) activity was measured spectro-photometrically at 340 nm following the decrease of NADPH using a commercial kit from OxisResearch™ (Portland, Oregon, U.S.A). This reaction maintains the normal levels of cellular glutathione, essential for keeping the levels of free radicals and organic peroxides down.

2.3.12. Statistical Analysis. The data were analyzed with Student's *t* test and one way ANOVA. Calibration curves were plotted and linear equations from the calibration standards were used to determine the parameters to be measured. All experiments were performed in triplicate, and the values reported are mean ± SD.

2.4. *IN VITRO* RESULTS

2.4.1. Ethanol Concentration Dependent Experiments. Figure 2.1 shows the results of increasing concentrations of ethanol (10 – 100 mM) on the levels of GSH in HepG2 cells The cells were exposed to different concentrations of ethanol for 48 h, and then GSH was measured. This experiment was performed to determine the optimal concentration of ethanol to be used in the combined exposure group. As can be seen from this figure, there is a nearly linear decrease in the level of GSH with an increasing concentration of ethanol. The GSH levels of the ethanol treated groups were significantly lower as compared to those of the control group.

.

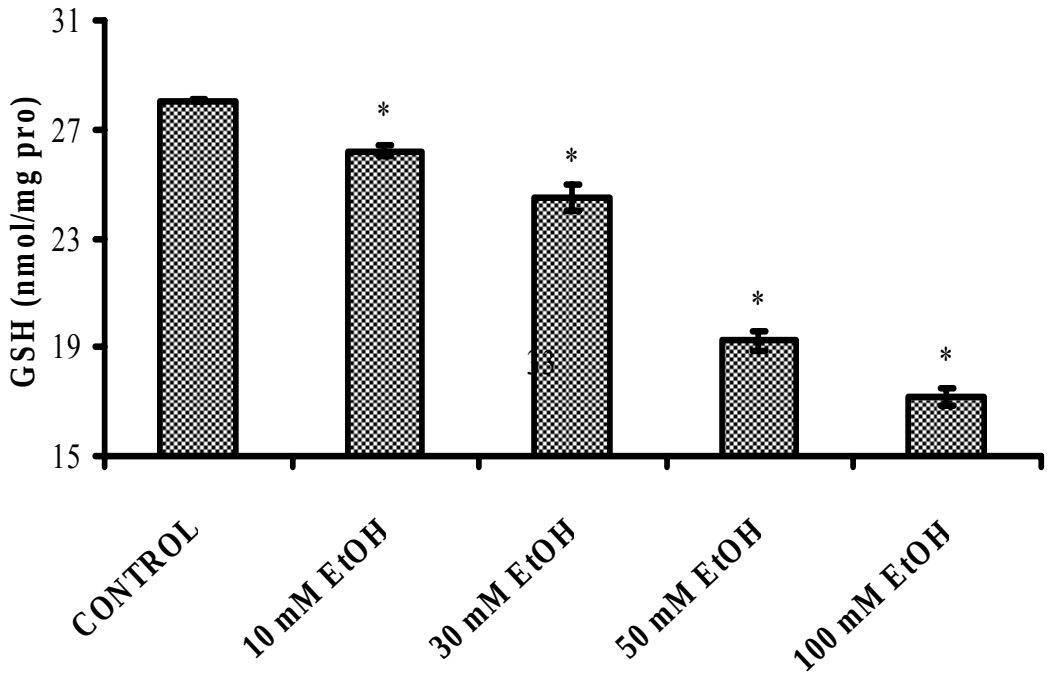

Figure 2.1. Effects of ethanol (10 – 100 mM) on the levels of GSH in HepG2 cells. The cells were incubated with ethanol for 48 h, and then GSH levels were measured by the HPLC method after derivatization with NPM. The GSH levels decreased linearly with increases in ethanol concentration (pro: protein).

2.4.2. Radiation Dose Dependent Experiments. Figure 2.2 shows how the levels of GSH in HepG2 cells vary when exposed to varying radiation doses (2 – 10 Gy). There is a nearly linear decrease in the levels of GSH that coincides with increases in radiation doses. The GSH levels in the radiation exposed groups are significantly lower than those of the control. This experiment was performed to determine the appropriate radiation dose to be used in combined exposure studies.

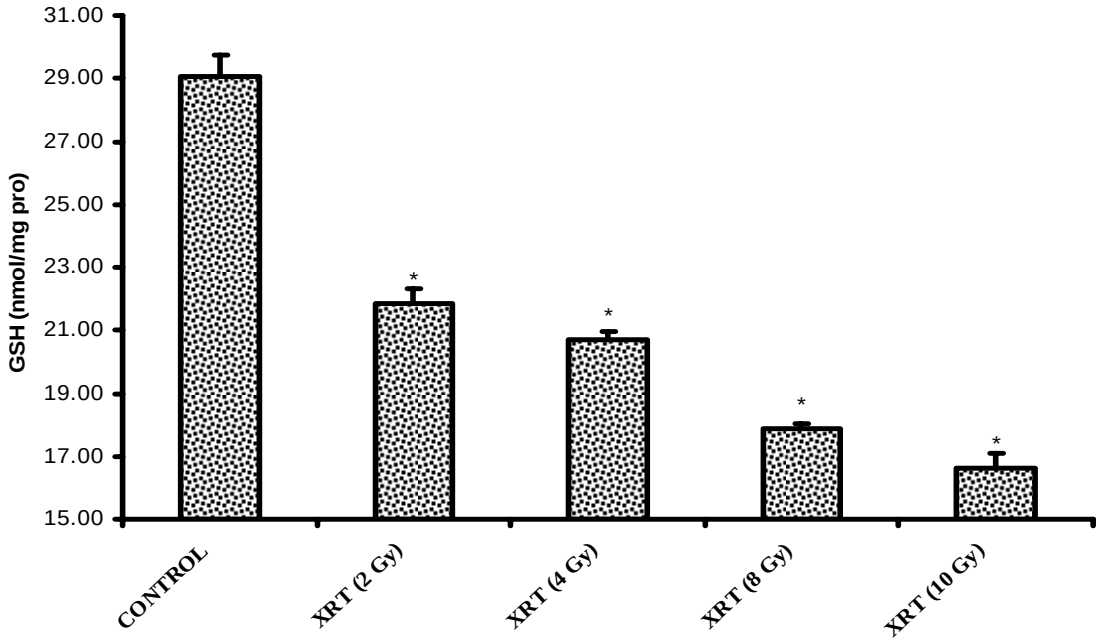

Figure 2.2. Effects of radiation (2 – 10 Gy) on the levels of GSH in HepG2 cells. Confluent cells were exposed to doses of radiation ranging from 2 to 10 Gy, and then analyzed 24 h later. The GSH levels decreased linearly with increasing doses of radiation.

2.4.3. GSH levels in Combined Exposure Experiments. Figure 2.3 shows the GSH levels in different treatment groups. Four groups, in triplicate, were designated as: (I) Control: no exposure to ethanol or radiation; (II) 50 mM ethanol, no radiation; (III) radiation (8 Gy), no ethanol; (IV) ethanol (50 mM) for 24 h, followed by radiation (8 Gy). The GSH level in the control group was significantly higher than those in the single agent and combined exposure groups. The GSH levels in the single agent (ethanol or radiation) exposure groups were significantly higher than those in the combined exposure group. The chromatograms in Figures 2.4 to 2.7 show changes in the areas under the curves, indicating variations in the levels of GSH and cysteine in the four experimental groups.

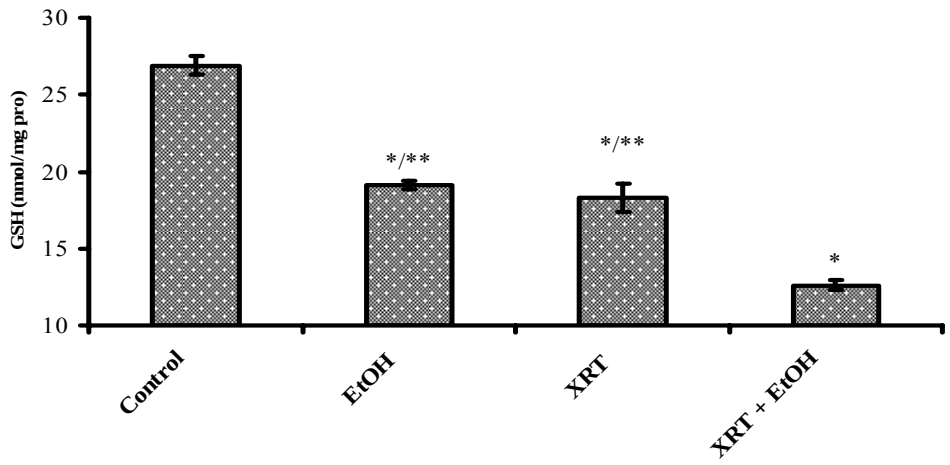

Figure 2.3. Combined effects of ethanol and radiation on the levels of GSH.
The levels of GSH were determined in groups designated as: control, ethanol only (50 mM), radiation only (8 Gy), and ethanol (50 mM) + radiation (8Gy). The ethanol and radiation group was exposed to ethanol (50 mM) for 24 h, followed by radiation (8 Gy), then analysis 24 h later. * Significantly different compared to control ($p < 0.05$). ** Significantly different compared to combined exposure group ($p < 0.05$).

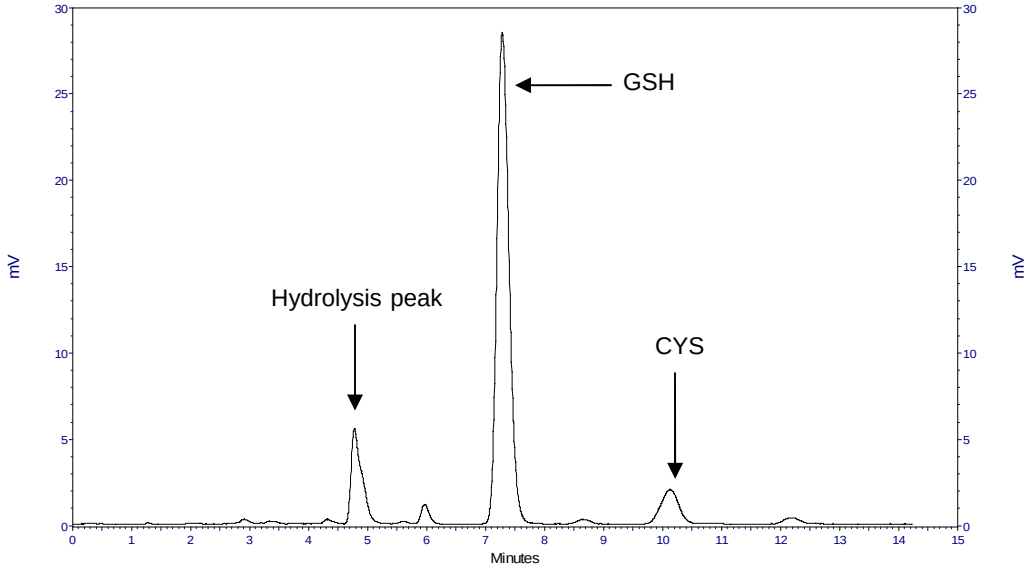

Figure 2.4. Chromatogram of control HepG2 cells.

The cells were incubated with a complete media only. Separation conditions: An ODS-1 C_{18} Column (5 µm packing material) with 250 x 4.6 mm (i.d) was used for the separation. The NPM derivatives were measured by a fluorescence detector (λ_{ex} = 330 nm and λ_{em} = 376 nm). Flow rate was 1ml/min. The GSH peak at a retention time of 7.90 min was the highest, and the CYS peak was at retention time of 10.73 min. The hydrolysis peak (due to excess NPM) came earlier than the analyte peaks.

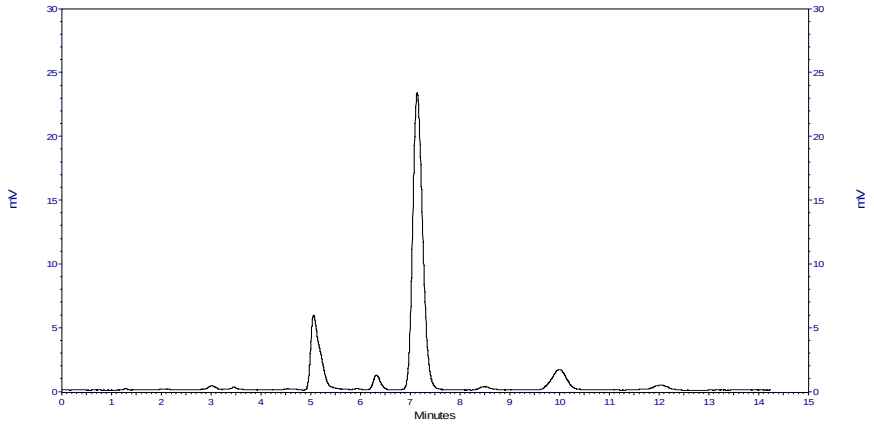

Figure 2.5. Chromatogram of HepG2 cells incubated with 50 mM ethanol. The separation conditions were the same as mentioned in Figure 2.4.

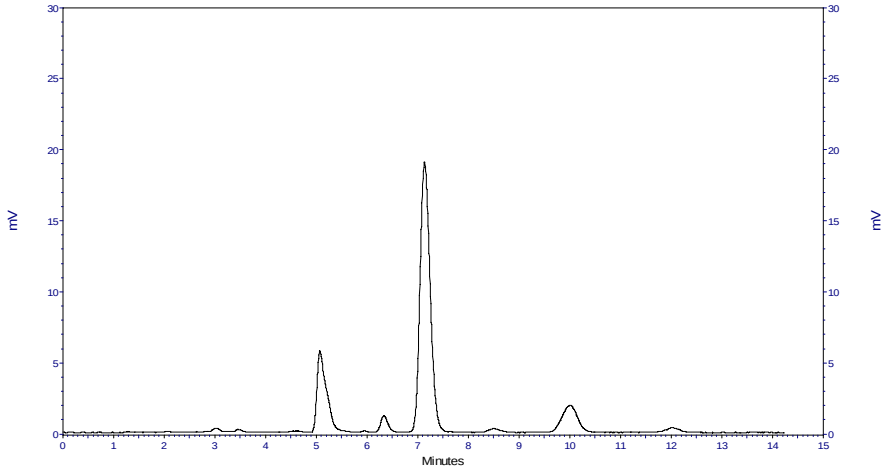

Figure 2.6. Chromatogram of HepG2 cells exposed to radiation (8 Gy). The separation conditions were the same as mentioned in Figure 2.4.

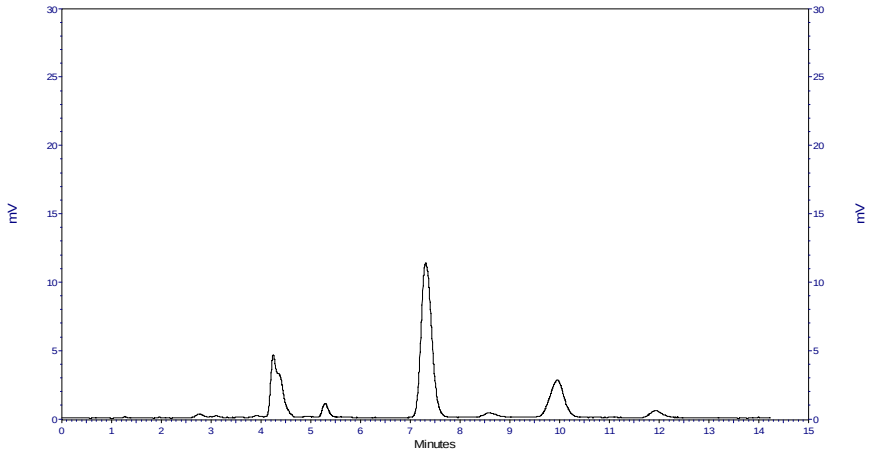

Figure 2.7. Chromatogram of HepG2 cells exposed to ethanol and radiation. The separation conditions were the same as mentioned in Figure 2.4.

2.4.4. Cysteine Levels. Figure 2.8 shows changes in the cysteine levels in the different treatment groups. The cysteine level in the control group was higher than that in the ethanol (50 mM) only group, but significantly lower than the ethanol (50 mM) and radiation (8 Gy) groups. The control and radiation (8 Gy) only groups had almost the same levels of cysteine.

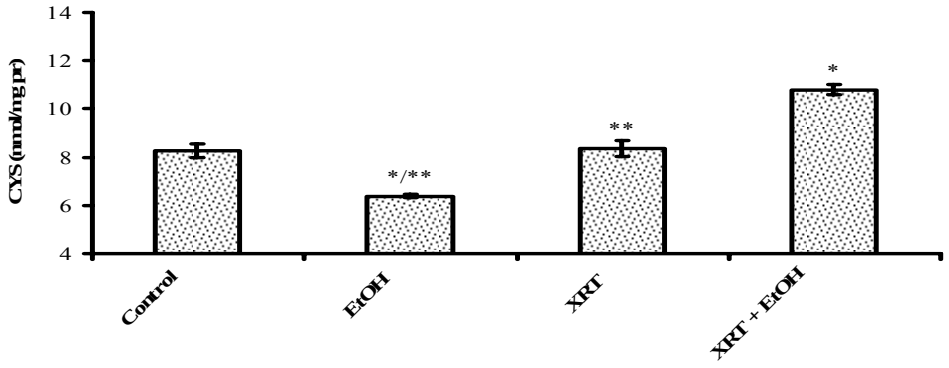

Figure 2.8. Cysteine levels in the control and treatment groups. 50 mM ethanol decreased the level of cysteine significantly compared to control, while 8 Gy radiation had the same

level of cysteine as the control. The ethanol (50 mM) + radiation (8Gy) group had significantly higher levels of cysteine as compared to all the other groups.

2.4.5. Catalase, Glutathione Reductase and Caspase-3 Results. Table 2.1 displays the results of catalase, glutathione reductase, and caspase-3 activities as determined using enzyme assays. The catalase activity was significantly higher in the control as compared to the treatment groups. The single agent treatment groups had significantly higher catalase activity compared to that in the combined exposure groups. Glutathione reductase and caspase-3 activities were significantly higher in the combined exposure groups than those in both the single agent exposure groups and the control.

Table 2.1. CAT, GR, and CAS-3 activities.

Groups	CAT (mU/mg pro)	GR (U/mg pro	CAS-3
Control	2.47± 0.21	40.13 ± 2.44	0.262 ± 0.012
EtOH	1.4 ± 0.12*/**	45.43 ± 2.59*/**	0.325 ± 0.037*/**
XRT	1.65 ± 0.15*/**	47.4 ± 2.89*/**	0.366 ± 0.045*/**
XRT + EtOH	1.16 ± 0.09*	51.15 ± 1.12*	0.661 ± 0.027*

All the experiments were performed in triplicate, and the values reported are mean ± SD. * $p < 0.05$ compared to corresponding value of control group, ** $p < 0.05$ compared to combined exposure group.

2.4.6. MDA and MTS Results. Table 2.2 shows the results of ethanol and radiation exposure on MDA and MTS. The level of MDA, a marker of lipid peroxidation, was measured by using the HPLC method. The combined exposure groups had significantly higher MDA levels than both the single agent exposure and the control groups. Treating HepG2 cells with ethanol, and then exposing them to radiation, elevated MDA levels far beyond the levels obtained in the control, ethanol only, or radiation only groups. Metabolically active cells bioreduce the MTS to a colored formazan product in the culture media. The number of viable cell is determined by measuring the absorbance at 490 nm. A decrease in absorbance indicates less viability. The number of viable cells, as determined by the MTS assay was significantly higher in the control than in both the single agent exposure and the combined exposure groups. The single agent exposure groups had significantly higher cell viability than the combined exposure groups. The free radicals produced by irradiation attack on polyunsaturated fatty acids (PUFA) leads to the formation of MDA, along with other products. Ethanol increases the levels of CYP2E1 by a post-transcriptional mechanism, leading to the formation of stable adducts. During its catalytic cycle, CYP2E1, which has high NADPH oxidase activity [96], generates ROS and hydrogen peroxide, and in the presence of iron, Fenton reaction takes place, producing more harmful free radicals such as hydroxyl radicals, ferryl species, and 1-hydroxyethyl radicals. These ROS damage the cell membranes through lipid peroxidation and the production of lipid aldehydes such as MDA and 4-hydroxynonenal. Increased levels of MDA is an indicator of elevated toxicity.

2.4.7. Detection of Apoptosis in HepG2 Cells. Figure 2.9 (panels A through D) shows the images of HepG2 cells that were treated with 50 mM ethanol, 8 Gy radiation, 50 mM ethanol and 8 Gy radiation for induction of apoptosis, and blank control.

Table 2.2. MTS and MDA results.

Groups	MTS (% untreated control)	MDA (nmol/100 mg pro)
Control	100 ± 9.8	22.8± 1.83
EtOH	84.5 ± 6.39*/**	27.9 ± 1.55*/**
XRT	72.8 ± 9.46*/**	24.7 ± 2.06*/**
XRT + EtOH	60.4 ± 4.8*	29.5 ± 2.23*

The experiments were performed in triplicate, and values presented as mean ± SD. * $p < 0.05$ compared to corresponding value of control group, ** $p < 0.05$ compared to combined exposure group.

The cells were observed using a fluorescent light microscope, with a differential uptake of fluorescent DNA binding dye (AO/EB dye mix). Acridine orange (AO) permeates all cells and makes the nuclei appear green, while ethidium bromide (EB) is taken up only by cells that have lost cytoplasmic membrane integrity, and stains the nuclei red. Panel A shows images of control group cells, with most of the cells stained green, indicating that there is little apoptosis taking place in the control group. Panel B cells were treated with 50 mM ethanol, while panel C cells were treated with radiation (8Gy). In both panels, there is evidence of increased apoptosis because of the number of cells with highly condensed red/orange nuclei. Panel D cells were exposed to 50 mM ethanol, followed by radiation (8 Gy). There is a significantly elevated level of apoptosis in this group as compared to both the control and the single agent exposure groups, as

evidenced by the number of red/orange-stained cells with highly condensed chromatin matter.

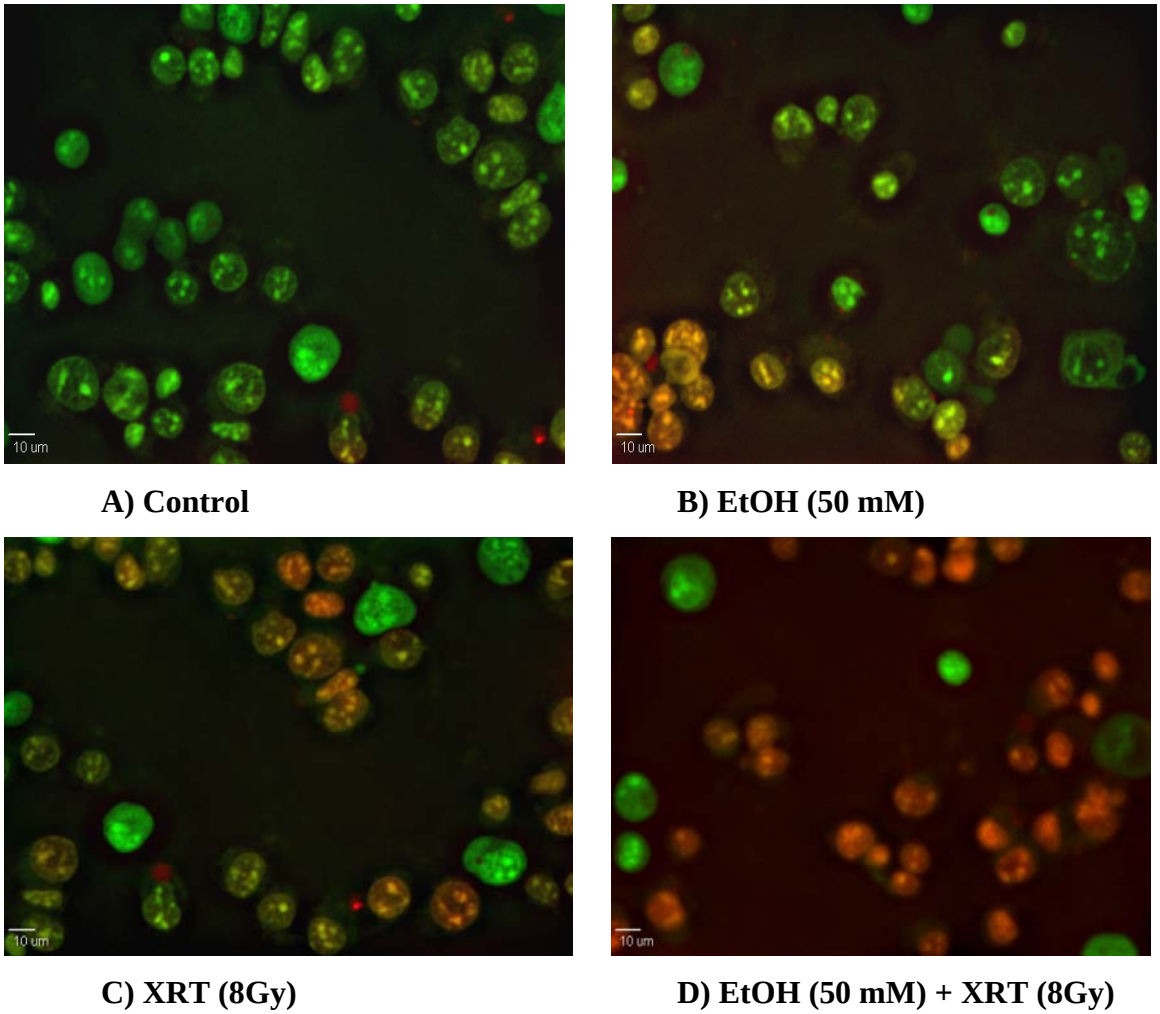

Figure 2.9. Morphological changes in different treatment groups of HepG2 cells.
The cells were treated as described in the method section, washed with cold PBS, and stained with AO/EB dye mixture, and then observed using a fluorescent microscope (original magnification 400x). (A) Microphotograph of blank control HepG2 cells, incubated with the media only. The normal non-apoptotic cells were dyed green, while apoptotic cells, with highly condensed chromatin material, were dyed red with the AO/EB dye mixture. (B) HepG2 cells treated with 50 mM ethanol. There are more apoptotic cells compared to the control group. (C) HepG2 cells exposed to radiation (8 Gy). The number of apoptotic cells is comparable to that in the ethanol treated group, but significantly higher than the number in the control group. (D) The group treated with 50 mM ethanol for 24 h, then exposed to radiation (8 Gy). The number of apoptotic cells is

higher than that in both the control and the single agent treatment groups. Apoptosis was induced more by combined exposure than by single agent exposure.

2.5. DISCUSSION

This investigation reports on the *in vitro* assessment of the toxic effects of ethanol and ionizing radiation on HepG2 cells by measuring antioxidant levels and antioxidant enzyme activities. Consumption of ethanol is widespread and many cancer patients who undergo radiotherapy have consumed ethanol at one time or another. In a majority of cases, it has been assumed that consumption of ethanol will not affect the outcome of radiotherapy, in spite of the well known fact that both ethanol and radiation produce free radicals that can be very damaging to tissues. Radiation oncologists who administer radiotherapy are, for the most part, not aware that significant alcohol consumption is a possible predisposing conditions that could potentially endanger the lives of patients. Most investigations on the effects of ethanol and radiation on biological systems have focused on single agent treatments. A few combined exposure studies have been reported, including tobacco and radiation [82], but most investigations have concentrated on radiation and other chemical agents [83-85]. Moreover, the end points measured in these studies were biological or clinical outcomes such as radiosensitization, radiation protection or tumor induction, not antioxidant status.

No study has been conducted to determine the toxic effects of exposure to ethanol, followed by ionizing radiation in a model system, such as HepG2 cells. The aim of this investigation was to determine the mechanism of toxicity of combined exposure to ethanol, followed by radiation, and show that the toxicity of ethanol enhances the toxicity

of ionizing radiation *in vitro*. Linear decreases in GSH levels with increases in ethanol concentrations and radiation doses were established, leading to the choice of an ethanol concentration of 50 mM and a radiation dose of 8 Gy to be used for the rest of the experiments.

2.5.1. Effects of Combined Exposure on GSH Levels. The results showed that the levels of GSH in HepG2 cells exposed to ethanol followed by ionizing radiation were significantly lower than GSH levels in cells exposed to ethanol or radiation only. GSH is present in all mammalian cells and is a powerful antioxidant that scavenges free radicals and hydrogen peroxide, and neutralizes toxic metabolites by condensing with them both enzymatically and nonenzymatically [86]. GSH is found in both the cytosol and mitochondria of cells. Most ROS are formed in the mitochondria during tissue respiration as a result of leakage of electrons through the mitochondrial electron transport chain. Neuman et al. have reported a dramatic decrease in mitochondrial GSH in isolated hepatocytes exposed to alcohol [87]. Cytotoxicity of ethanol has been attributed to GSH depletion according to studies conducted by Hirano et al. [88]. Devi et al. reported that exposure of rat hepatocytes to ethanol increased ROS production, decreased GSH, and increased lipid peroxidation [89]. Incubation of HepG2 cells with ethanol induces oxidative stress and leaves the cells vulnerable to further injury by ROS. When cells are exposed to ionizing radiation after ethanol exposure, they are not able to cope with elevated levels of ROS. In conditions of severe oxidative stress, the ability of the cells to reduce GSSG to GSH is overcome, leading to GSSG accumulation within the cytosol. To prevent a shift in a cell's redox equilibrium, GSSG is actively exported out of the cell or reacted with the protein sulfhydryl group, producing mixed disulfide. Under such

circumstances, GSH is not regenerated; thus depletion of cellular GSH can be potentiated by severe oxidative stress [90]. This explains the significant decreases in the GSH levels in the combined exposure groups as compared to single agent exposure, suggesting that exposure to ethanol enhances the toxicity of ionizing radiation through hightened oxidative stress.

2.5.2. MDA Levels. Significantly higher levels of MDA were identified in the HepG2 cells in the combined exposure groups as compared to both the control and the single agent exposure groups. MDA is a marker of lipid peroxidation [91] and there are numerous reports on induction of lipid peroxidation by both ethanol and radiation [92-95]. The free radicals produced by irradiation attack on polyunsaturated fatty acids (PUFA) leads to the formation of MDA, along with other products. Ethanol increases the levels of CYP2E1 by a post-transcriptional mechanism, leading to the formation of stable adducts. During its catalytic cycle, CYP2E1, which has high NADPH oxidase activity [96], generates ROS and hydrogen peroxide, and in the presence of iron, Fenton reaction takes place, producing more harmful free radicals such as hydroxyl radicals, ferryl species, and 1-hydroxyethyl radicals. These ROS damage the cell membranes through lipid peroxidation and the production of lipid aldehydes such as MDA and 4-hydroxynonenal. Increased levels of MDA is an indicator of elevated toxicity.

2.5.3. GR and Caspase-3 Activities. Levels of glutathione reductase and caspase-3 activities were more elevated in the combined exposure groups than those in the single agent treatment groups. Previous investigations have reported that both ethanol and radiation increase the activities of these enzymes [97-101]. The hydrogen peroxide produced by ethanol metabolism and ionizing radiation is metabolized by GSH

peroxidase (GPx) in the cytosol and by catalase in the peroxisomes. Metabolism of hydrogen peroxide by GPx consumes GSH and produces GSSG. GPx then converts GSSG back to GSH, at the expense of NADPH, to restore the cells' redox status. Under conditions of elevated levels of ROS, more GSH is consumed and considerable GSSG is produced. The activity of GR increases to cope with the enormous amount of GSSG being produced. Changes in the levels of caspase-3 are discussed further under detection of apoptosis by EB/AO staining.

2.5.4. Catalase Activity. The results showed significant decreases in catalase activity in all treatment groups, as compared to the control groups. Additionally, the combined exposure groups had significantly lower catalase activity than that in the single agent exposure groups. This is in agreement with findings of previous investigations which have reported decreases in catalase activity, due to exposure to ethanol and ionizing radiation [102-105], and inactivation of catalase by superoxide radical [106]. Lipid peroxidation has been shown to damage membrane proteins, inactivating receptors and enzymes. These observations are supported by the *in vitro* catalase activity results. The elevated levels of ROS in the combined exposure groups produce the greatest toxic effects on the catalase enzyme.

2.5.5. MTS Assay. The cell viability of HepG2 cells was reduced to the lowest level in the combined exposure groups as compared to the control, and significantly lower as compared to the single agent exposure groups. Previous studies have shown that ethanol and radiation reduce cell viability [107-109]. The deleterious changes produced by ROS in essential biomolecules (such as DNA, lipids, and proteins) in the cells eventually lead to cell death, reducing cell viability. ROS induce oxidative damage to

DNA, which suffers double and single strand breaks, deoxyribose damage, and base modifications. The proteins and lipids undergo oxidation, forming lipid aldehydes (such as MDA) and oxidized proteins. These alterations affect vital cellular functions and lead to cell death. Our investigation showed that combined exposure has a greater toxic effect on cell viability than single agent exposure does.

2.5.6. Cysteine Levels. The results of this investigation showed that CYS levels significantly increased in the combined exposure group, but remained unchanged in the radiation only group as compared to the control, and decreased significantly in the ethanol only group. Increases in CYS levels could have resulted from the degradation of GSH by the ectoenzyme, γ-glutamyltranspeptidase (GGT), located on the external surface of certain cells. Degradation of GSH by GGT yields cysteinylglycine, which is broken down by dipeptidase to produce CYS and glycine. The amino acid linkage in GSH is such that glutamate and CYS are linked by a peptide bond through the γ-carboxyl group of glutamate, instead of the usual α-carboxyl group. This amino acid linkage prevents degradation of GSH by intracellular peptidases. The only enzyme capable of degrading GSH is the extracellular enzyme, GGT [110]. Under normal conditions, GSH is transported out of a cell by carrier-mediated transporters [111], across the cell membrane, to participate in the γ-glutamyl cycle for the regeneration of CYS. When oxidative stress sets in, however, the cell membrane is destroyed through lipid peroxidation and protein oxidation, releasing the cellular contents, including GSH.

2.5.7. Detection of Apoptosis by EB/AO Staining. Significantly more HepG2 cells were stained red/orange with EB/AO staining in the combined exposure groups than there were in the single agent exposure groups or the control. Apoptotic cells have

condensed or fragmented chromatin, which stain red/orange with EB/AO, while live cells have normal nuclei with organized chromatin and stain green [112-113]. Damage to mitochondrial membrane by ROS produced by both ethanol and ionizing radiation leads to the releases of cytochrome *c* molecules from the mitochondria into the cytosol. Proapoptotic enzymes, caspases, are activated by cytochrome *c* in the cytosol to trigger the apoptotic process [114]. Studies have shown that decreases in the GSH levels in cells triggers apoptosis. Another mechanism of apoptosis induction is the involvement of Fas and Fas ligand. Fas is a receptor found on hepatocytes, and can interact with Fas ligand found on the surface of certain T-cells to trigger chemical processes that lead to apoptosis. The binding of Fas to Fas ligand to trigger the process of apoptosis is mediated by ROS, like those produced by ionizing radiation and ethanol metabolism [115]. In this investigation, combined exposure lead to greater elevated levels of apoptosis than did single agent exposure, due to increased levels of ROS in the combined exposure groups.

2.6. CONCLUSION

The results of this investigation have shown that combined exposure of HepG2 cells to ethanol and ionizing radiation has a significantly greater toxic effect on cells than single agent exposure does. Since both ethanol and ionizing radiation have been proven to produce free radicals in biochemical environments, it seems reasonable to suggest that pre-radiation exposure of cells to ethanol induces oxidative stress in the cells, and leaves them vulnerable to further attacks by ROS. When these cells are later exposed to ionizing radiation, the antioxidant defense system is not able to withstand the renewed onslaught of ROS, and more oxidative damage results. Therefore, it is concluded that a possible

mechanism to account for enhanced toxicity of ethanol and ionizing radiation on HepG2 cells is through increased oxidative stress. This investigation could be an eye-opener for doctors and oncologists to consider recent drinking histories of cancer patients before radiotherapy is administered. Combined exposure studies are relevant since the environment contains many diverse agents that can enter the biological systems, and interact with each other leading to greater toxic effects.

3. EFFECTS OF COMBINED EXPOSURE TO ETHANOL AND IONIZING RADIATION ON THE ANTIOXIDANT STATUS OF AN *IN VIVO* MODEL

3.1. INTRODUCTION

The data from the *in vitro* investigation showed that combined exposure to ethanol and ionizing radiation results in significantly higher oxidative stress compared to single agent exposure [116]. Numerous investigations have shown that ethanol and ionizing radiation can individually induce a state of oxidative stress in biological systems through increased production of reactive oxygen species (ROS), such as hydrogen peroxide (H_2O_2), hydroxyl radical ($^{\bullet}OH$), superoxide radical ($O_2^{\bullet-}$), and many other types of ROS, proteins and lipid aldehydes [117-123].

Ethanol metabolism by the enzyme cytochrome P4502E1 (CYP 2E1) is well documented to induce the production of reactive oxygen species [124-127]. This pathway has been identified as the central pathway by which ethanol produces free radicals and pathological transformations that are associated with chronic ethanol intake [128-129]. Moreover, investigators have found a positive correlation between increased levels of CYP 2E1 and heightened deleterious changes in organs such as the liver [130]. Additionally, enzymatic metabolism of ethanol by alcohol dehydrogenase and acetaldehyde dehydrogenase enzymes result in increased levels of NADH, which induce the conversion of xanthine dehydrogenase (XDH) to xanthine oxidase (XO), and subsequent generation of free radicals [131]. Non-enzymatic metabolism of ethanol generates α-hydroxyethyl radical ($CH_3C^{\bullet}HOH$), which can react with oxygen to form a peroxy radical intermediate, which then undergoes rearrangement to produce acetaldehyde and superoxide radical. The ROS produced during enzymatic and non-

enzymatic ethanol metabolism proceed to attack cellular components such as cell membranes, mitochondrial membranes, and DNA, resulting in protein oxidation, lipid peroxidation, breaks in single and double stranded DNA, and tissue damage.

Ionizing radiation is known to produce tissue damage through direct ionization by energy transfer of the atoms comprising the targeted proteins, lipids, and DNA [132]. Radiation-induced DNA damage has been reported in rats and mice by many investigators [133]. Interaction of ionizing radiation with water molecules, which constitutes up to 80% of the cells in the living organisms, results in the fission of O-H bonds in water to produce hydrogen ($H^{\bullet}$) and hydroxyl ($^{\bullet}OH$) radicals. Hydroxyl radical is the most lethal of all the ROS formed from radiolysis of water molecules, and reacts at a diffusion-controlled rate with the majority of the molecules in the living cells [134]. It is commonly believed that most, if not all, of the deleterious effects of exposure to ionizing radiation in the living systems are initiated by the attack of $^{\bullet}OH$ on carbohydrates, lipids, proteins, and DNA molecules [135], resulting in loss of cell membrane integrity, lipid peroxidation, mitochondrial permeability transition, and formation of other harmful adducts such as MDA and 4- hydroxynonenal (4-HNE).

Ethanol and ionizing radiation produce ROS in biological systems. Exposure of an organism to certain levels of these agents simultaneously should be viewed as having a potential to cause increased pathological damage. Due to increased application of radiotherapeutic procedures to cancer patients, who may have other predisposing conditions likely to negatively impact on the outcome of radiotherapy, it has become necessary to engage in combined exposure studies to investigate how various agents and conditions would interact with each other in model systems. In spite of widespread use of

ethanol as an alcoholic beverage, and increased exposure to ionizing radiation in radiotherapy situations, combined exposure investigations have not been performed. The use of ethanol in the context of chronic heavy and light drinking, followed by exposure to ionizing radiation, would model a cancer patient with a chronic heavy drinking recent history undergoing radiotherapy. Furthermore, it is well documented that the risk of serious complications following therapeutic irradiation is heightened by a variety of predisposing conditions, including diabetes, ataxia telangiectasia, prior abdominal/pelvic surgeries, and collagen vascular diseases such as scleroderma or lupus [136-139].

In this investigation the CD-1 mice were used to model chronic light and heavy drinking followed by exposure to a sub-lethal dose of ionizing radiation, as would be the case in a chronic alcohol user who undergoes therapeutic irradiation. The mice were chronically exposed to low-dose (5%) ethanol or high-dose (10%) ethanol in their drinking water for 6 weeks, followed by exposure to 8 Gy of ionizing radiation, before being sacrificed 4 d later. To assess the effects of combined exposure on the mice, various parameters were measured, including total blood count, GSH, CYS, GSSG, and MDA levels, and the antioxidant activities of the enzymes catalase and glutathione reductase.

3.2. EXPERIMENTAL DESIGN

3.2.1. Chronic Light Ethanol Treatment. The animals in this group received ethanol in increasing concentrations, to a final concentration of 5% (v/v) ethanol solution as their sole drinking fluid for 6 weeks.

3.2.2. Chronic Heavy Ethanol Treatment. The chronic high dose ethanol group received ethanol in increasing concentrations to a final concentration of 10% (v/v) ethanol solution as their sole drinking fluid. The ethanol treatment period lasted 6 weeks.

3.2.3. Exposure to Ionizing Radiation. The animals in the combined exposure and radiation only groups were exposed to ionizing radiation in the middle of the 6 weeks of treatment, as detailed under the material and methods section.

3.2.4. Oxidative Stress Studies. The antioxidant status of the animals was determined by measuring the GSH, CYS, and GSSG levels, along with the activities of some antioxidant enzymes (GR and CAT). MDA, which is a lipid peroxidation biomarker, was also measured. The aim of these procedures was to determine how the combined exposure to ethanol and radiation affected the antioxidant status of the mice (*in vivo* model).

3.3. MATERIALS AND METHODS

3.3.1. Materials. HPLC-grade acetonitrile, glacial acetic acid, water, and phosphoric acid, used for the preparation of the mobile phase, were purchased from Fisher Scientific (Fair Lawn, NJ USA). N-(1-pyrenyl)-maleimide (NPM), used as a derivatizing agent for measurement of CYS and GSH, 1,1,3,3-tetramethoxypropane, and ethanol were purchased from Aldrich (Milwaukee, WI USA). Protein concentration was evaluated with the Bradford reagent obtained from BioRad (Melville, NY USA). The CD-1 mice were from our breeding colony (VA Medical Center, St Louis, MO USA). Heparin was provided by Dr. Mark Ranney (University of MO-Rolla). Safety syringes were purchased from Fisher Scientific (Fair Lawn, NJ USA).

3.3.2. Animals. The mice were housed in a temperature-controlled (25^{o}C) room, that was equipped to maintain a 12 h light-dark cycle. Tap water and standard rat chow (Purina rat chow) were given *ad libitum* for 3 weeks while the mice were being acclimated before the experiments began. 40 mice were randomly divided into six groups (6 or 7 animals per group), and housed 3 or 4 per cage in polycarbonate cages with wooden chips as bedding. The groups were designated as follows: Group I (n=6): Control (no exposure to ethanol or XRT); Group II (L-EtOH) (n=6): Chronic low-dose ethanol (5% v/v ethanol in the drinking water); Group III (H-EtOH) (n=7): Chronic high-dose ethanol drinking (10% v/v ethanol solution as the sole drinking fluid); Group IV (XRT) (n=7): Radiation only (8 Gy XRT); Group V (L-EtOH + XRT) (n=7): Chronic low-dose ethanol drinking (5% v/v ethanol solution) and 8 Gy XRT; Group VI (H-EtOH + XRT) (n=7): Chronic high-dose drinking (10% v/v ethanol solution) and 8 Gy XRT. The same treatments were continued after the mice were irradiated until the day of sacrifice. All of the procedures performed with the animals were approved by the University of Missouri – Rolla Animal Care and Use Committee

3.3.3. Exposure of Animals to Ethanol. The control group mice were kept for the same period as the treatment groups, but were fed only the mouse food and tap water. The chronic low-dose ethanol drinking groups received 2% (v/v) ethanol solution diluted from 99.8% ethanol as their only drinking fluid for 3 days, followed by a 4% ethanol solution (v/v) for 4 days. Finally, a 5% (v/v) ethanol solution was provided for the next 5 weeks to complete the chronic drinking treatment period. The chronic high-dose ethanol drinking treatment groups received a 2% (v/v) ethanol solution as their only drinking fluid for 3 days, followed by 4% for the next 3 days, 6 % for 3 days, and 8 % for another

5 days. Finally, a 10 % (v/v) ethanol solution was provided for the next 4 weeks to complete the chronic drinking treatment period. 3 % (w/v) food grade white sugar was added to the drinking fluids of both the control and the treatment groups to improve the palatability of the ethanol solutions. The average peak ethanol intake was 5.4g/kg body weight for the chronic low-dose ethanol drinking groups, and 11.2g/kg body weight for the chronic heavy ethanol drinking groups.

3.3.4. Exposure of Animals to Ionizing Radiation. At the end of the ethanol treatment period, the mice in the combined exposure groups and the radiation only groups were exposed to radiation. The animals were exposed to 8 Gy of radiation at a dose rate of 3 Gy/min using a 9 MeV beam generated by a Varian Linear accelerator, model 21 EX (Varian Associates, Walnut Creek, CA, USA), at the Radiation Oncology Department of the Phelps County Regional Medical Center in Rolla, Missouri, USA. A 25 x 25 cm field was used, and output factors were checked once a week. Flatness of the field was also checked once a week and was maintained within 2 %. A 25 x 25 cm field showed the 90% isodose at 2.75 cm depth. The 95% fall-off point was at 2.5 to 2.6 cm depth. Less than 10% dose variation through the thickness of a mouse was achieved under these conditions. All of the animals were anesthetized and heparinized blood was collected via cardiac puncture 4 days after radiation treatment. After perfusion with an antioxidant buffer, the livers were removed. The blood samples were kept on ice or at 4-8^{o}C, and taken to the University of Missouri-Columbia, Research Animal Diagnostic Laboratory (RADIL) the very next day for complete blood count analysis. The liver tissue samples were analyzed immediately for GSH, CYS, and GSSG levels and the remaining samples were kept in a -80 ^{o}C freezer for later analysis.

3.3.5. Preparation of Tissue Homogenates. The tissue samples from the livers, kidneys, and brains of the mice were homogenized (0.15 g/ml) in antioxidant buffer to avoid oxidation. The antioxidant buffer was prepared by dissolving 1.2 g disodium phosphate, 0.32 g sodium dihydrogen phosphate, 100 µL butylated hydroxytoluene (BHT) solution (0.1102 g BHT in 1 mL 100 % ethanol), 0.841 g aminotriazole, 0.039 g DETAPAC, and 0.065 g sodium azide in 1 L HPLC-grade water.

3.3.6. Determination GSH and CYS. Tissue levels of GSH and CYS were determined by RP-HPLC, according to the method developed by Winters (Winters et al., 1995). The HPLC system (Thermo Electron Corporation) consisted of a Finnigan Spectra System vacuum membrane degasser (model SCM1000), gradient pump (model P2000), autosampler (model AS3000), and fluorescence detector (model FL3000) with λex = 330nm and λem = 376nm. The HPLC column was a Reliasil ODS-1 C_{18} column (5 µm packing material) with 250 x 4.6 mm (Column Engineering, Ontario, CA, USA). The mobile phase was 70% acetonitrile and 30% water and was adjusted to a pH of 2 with acetic acid and o-phosphoric acid. The NPM derivatives of CYS and GSH were eluted from the column isocratically at a flow rate of 1mL/min.

3.3.7. Determination of Oxidized Glutathione (GSSG). Straight tissue homogenate (84 µL) was mixed with 16 µL of 2-vinyl pyridine and incubated for 1 h at room temperature to block the preexisting GSH. At the end of the incubation period, 95 µL of 2 mg/ml solution of NADPH and 5 µL of a 2 units/ml glutathione reductase enzyme were added to the tissue homogenate and mixed. An aliquot (100 µL) of this mixture was removed and mixed with 150 µL of HPLC grade water and 750 µL of NPM (1 mM in acetonitrile). This mixture was incubated for 5 min at room temperature, after

which 5 µL of 2N HCl was added to stop the reaction. The samples were filtered into vials through 0.2 µm filters and injected into the HPLC system.

3.3.8. Determination of Malondialdehyde (MDA). The MDA determination was done by the RP-HPLC method using λex = 515 nm; the λem 550 nm (Gutteridge, 1975). Tissue homogenate (350 µL) was mixed with butylated hydroxytoluene (BHT) (100 µL of 500 ppm solution) and 10% trichloroacetic acid (550 µL), and boiled for 30 min. After the solution was cooled on ice and centrifuged for 10 min at 1500 xg, the supernatant (500 µL) was mixed with thiobarbituric acid (500 µL). The tubes were boiled again for 30 min, and then cooled on ice. A solution (500 µL) was added to n-butanol (1.0 ml), vortexed, and centrifuged for 5 min at 60 xg to facilitate a phase separation. The top layer was then filtered through 0.2 µm filters and injected onto a 5 µm C_{18} column (250 x 4.6 mm) on a RP- HPLC system. The mobile phase consisted of 69.4% 5mM sodium phosphate buffer pH = 7.0, 30% acetonitrile, and 0.6% tetrahydrofuran.

3.3.9. Glutathione Reductase (GR) Activity Determination. Glutathione reductase (GR; EC 1.6.4.2) activity was measured spectrophotometrically at 340 nm following the decrease of NADPH using a commercial kit from OxisResearch™ (Portland, Oregon, USA). This reaction maintains the normal levels of cellular glutathione, essential for keeping the levels of free radicals and organic peroxides down.

3.3.10. Catalase (CAT) Activity Determination. The activity of catalase (CAT; EC 1.11.1.6) in the cell homogenates was measured spectrophotometrically at 240 nm following the exponential disappearance of hydrogen peroxide (H_2O_2; 10 mM) according to the method described by Aebi (Aebi, 1984). The catalase activity was calculated from

$A_{60} = A_{initial}\, e^{-kt}$ where k, is the rate constant, $A_{initial}$, is the initial absorbance, and A_{60} is the absorbance at 60 s.

3.3.11. Total Blood Count. Immediately following blood collection, with a 23 g needle into a heparinized syringe, peripheral blood smears were made on microscope slides, according to the standard operating procedure set by the Research Animal Diagnostic laboratory (RADIL) of the University of Missouri-Columbia, USA. 500 µL of whole blood in Ependorf tubes on ice, together with the blood smears, were taken to MU RADIL for complete blood count analysis. All of the red blood cell and platelet parameters were measured by an automated hematology instrument (Abbott Cell-Dyn 3500 Hematology analyzer, Abbott Labs., Abbott Park, IL, USA). White blood cell counts, including a differential count, were also measured. White blood cell differentials were obtained from blood smears prepared at the time of blood collection.

3.3.12. Protein Determination. A Hitachi U-2000 double beam UV-Vis spectrophotometer (Tokyo, Japan) was used to measure protein concentration using the Bradford assay (Bradford, 1976) and antioxidant enzyme activities.

3.3.13. Statistical Analysis. Means are reported with their standard deviations. The results were analyzed with the student's *t*-test when only two means were compared and by one-way analysis of variance (one-way ANOVA) to assess the significance of the difference between the control and the treatment groups, and between the single agent exposure and combined exposure groups. Calibration curves were plotted and linear equations from the calibration standards were used to determine the parameters to be measured. $P < 0.05$ was considered significant.

3.4. *IN VIVO* RESULTS

3.4.1. Weight Changes During the Treatment Period. The mice were weighed on a weekly basis to monitor changes in weight in each group. The results of the weight changes are shown in Figures 3.1 to 3.6. There were increases in weight in all the groups during the 41 d treatment period, but the control group had the most steady weight increase, and higher weight gain as compared to the rest of the groups. All the ethanol treatment groups had similar patterns in weight fluctuations, and comparable weight changes. There was a drop in the weight of the mice in all the groups that were irradiated, starting from the day of irradiation. The radiation only group had the sharpest drop in weight.

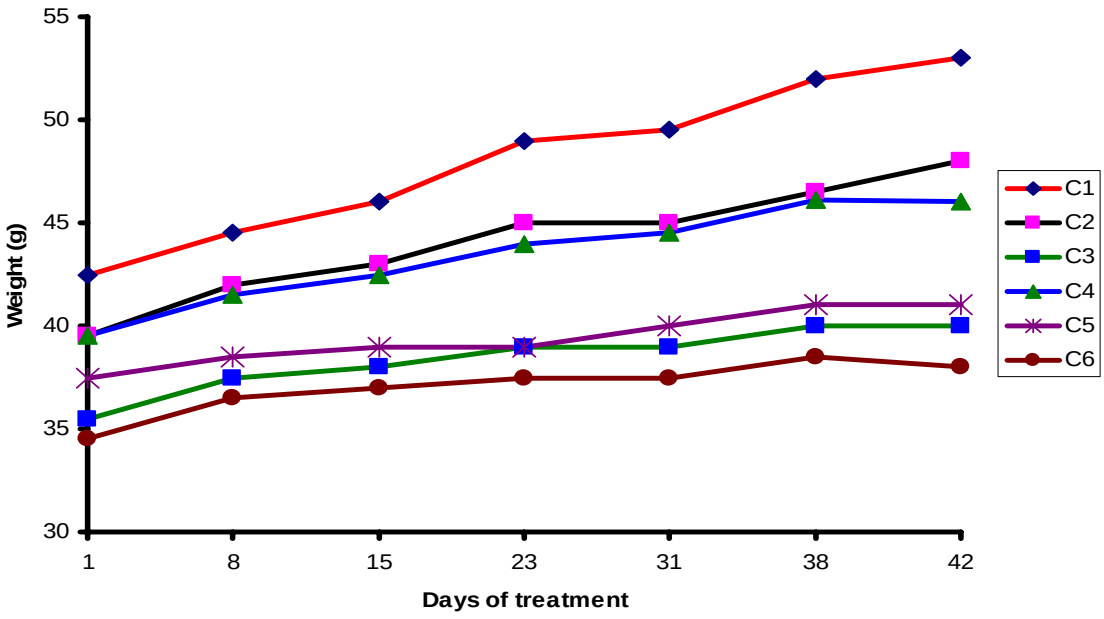

Figure 3.1. Weight changes in mice of the control group.

The mice were kept for 6 weeks, and were provided food and water *ad libitum*. There was a steady increase in weight in all the mice in the control group. (C: control, C_1, C_2, C_3, C_4, C_5, C_6 represent each control animal).

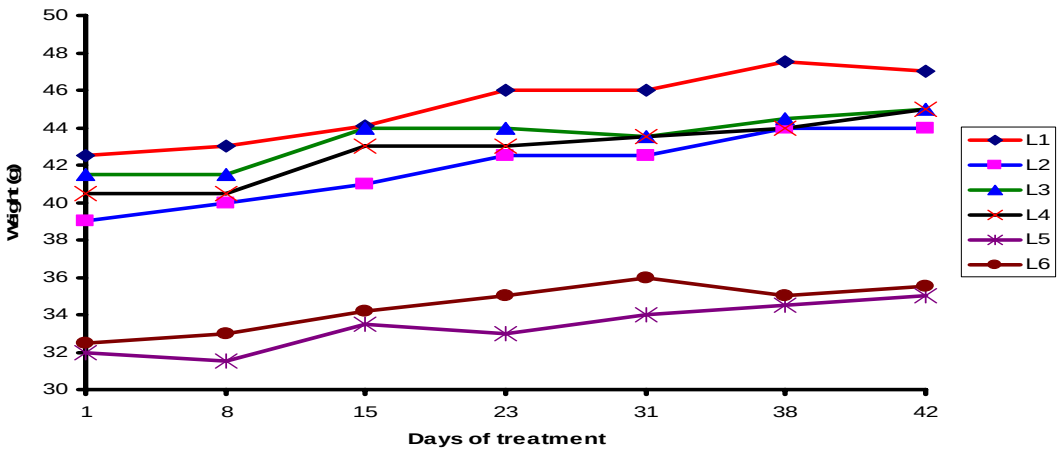

Figure 3.2. Weight changes in mice treated with light/low-dose ethanol.
The mice were provided the ethanol (5% v/v) solution as their only drinking fluid, and rodent food *ad libitum*. There were fluctuations in weight during the treatment period, but the general trend was a gradual increase. (L: light/low-dose ethanol treatment, L_1, L_2, L_3, L_4, L_5, L_6 represent each animal in the light/low-dose ethanol treatment group)

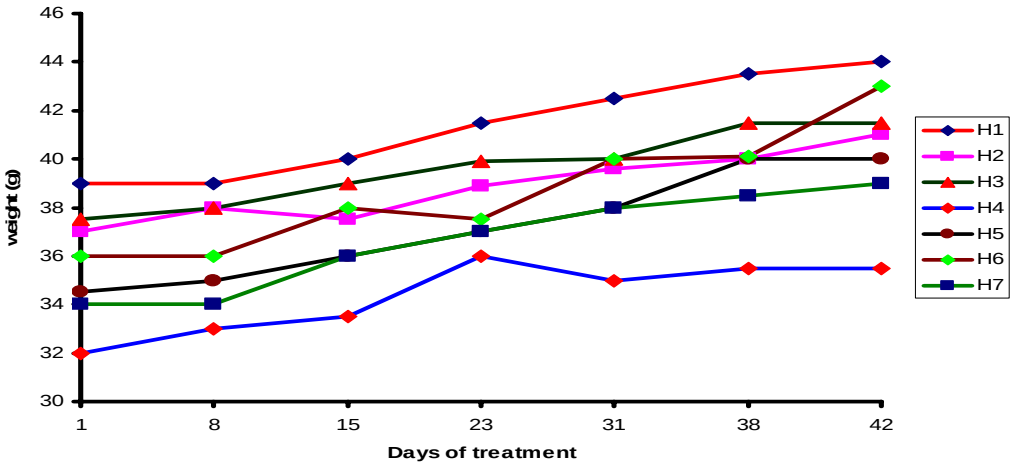

Figure 3.3. Weight change in the heavy/high-dose ethanol group.

The mice in this group were given ethanol solution at a final concentration of 10 % (v/v), and the treatment lasted 6 weeks. There were fluctuations in weght during the treatment period, but the trend was a gradual increase. (H: heavy/high-dose ethanol treatment, H_1,H_2, H_3, H_4, H_5, H_6, H_7 represent each animal in the heavy/high-dose ethanol treatment group).

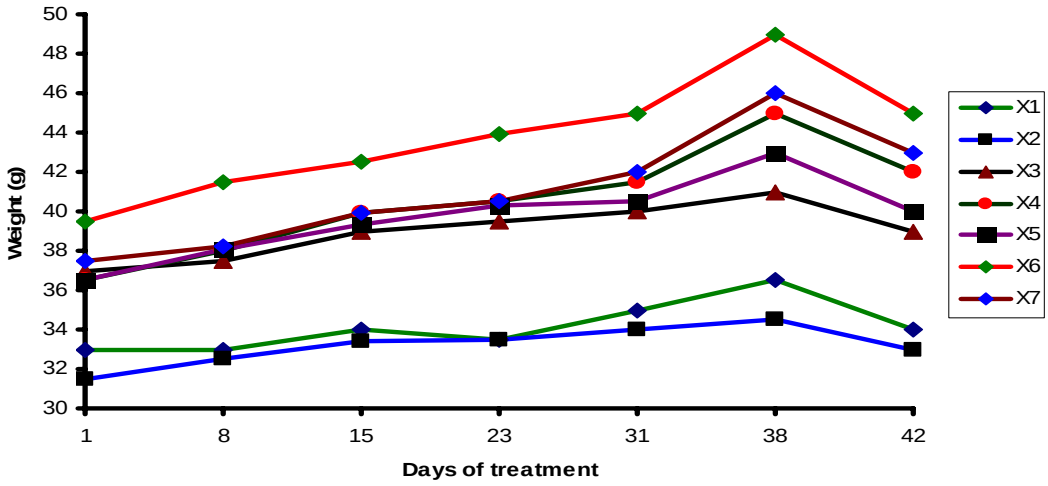

Figure 3.4. Weight changes in the mice of the radiation only group.
The mice were provided food and water *ad libitum* for six weeks, and were exposed to 8 Gy of ionizing radiation on the 38th day. There was a steady increase in weight up to the 38th day, but the weight dropped sharply after the exposure to radiation. (X: radiation only, X_1-X_7 represent animals in the XRT only group)

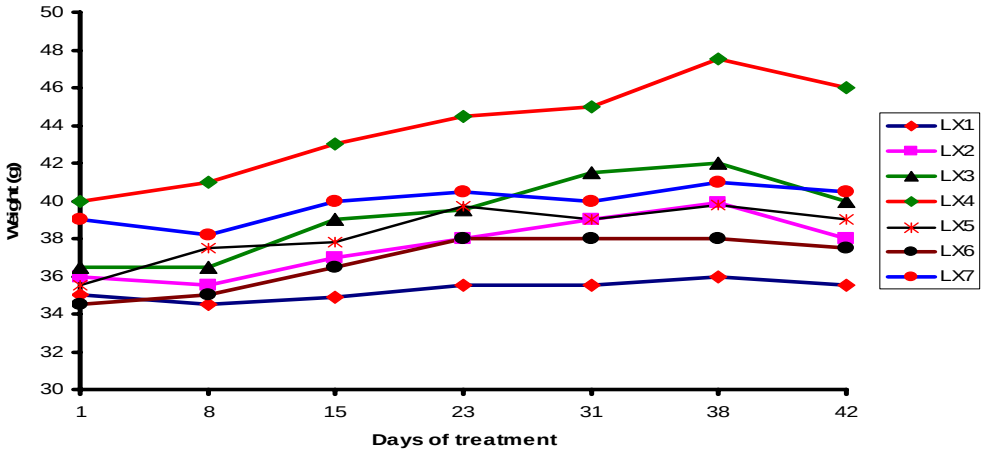

Figure 3.5. Weight changes in light/ low-dose ethanol and radiation group.

The entire treatment period was 6 weeks (42 d). Food and ethanol solution (5% v/v), as the only drinking fluid, were given *ad libitum.* There were fluctuations in weight, but the trend was that of a gradual increase up to the 38th day, then the weight dropped. (LX: light/low-dose ethanol + XRT, LX_1-LX_7 represent all the animals in the light/low-dose ethanol combined exposure group).

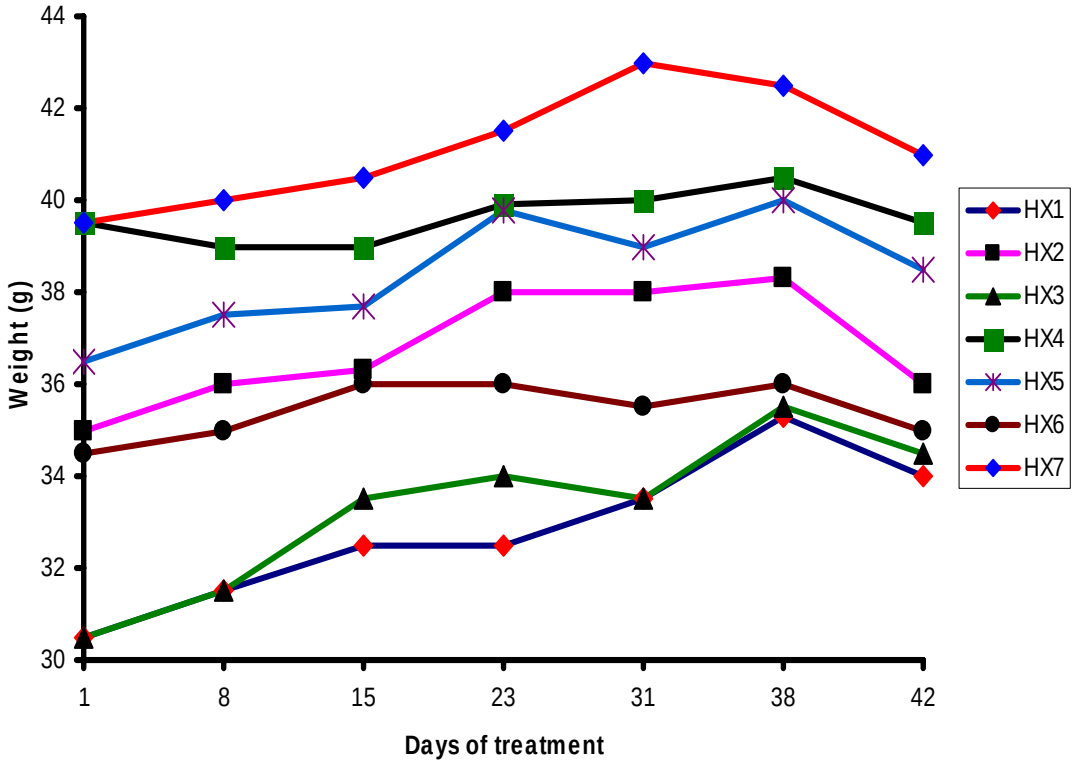

Figure 3.6. Weight changes in heavy/high-dose ethanol combined exposure group.
The mice were given ethanol solution at a final concentration of 10 % (v/v) as their only drinking fluid, and rodent chow *ad libitum* for 38 days, then exposed to 8 Gy of ionizing radiation. There were fluctuations in weight, but the general trend was that of an increase up to the 38th day, followed by a decrease. (HX: heavy/high-dose ethanol + XRT treatment, HX_1-HX_7 represent all the animals in the heavy/high-dose ethanol combined exposure group).

3.4.2. Percentage Weight Gain up to the 38th Day. The percentage weight gain in each of the experimental groups are shown in Figure 3.7. The weight gain percentage

was determined by subtracting the initial weight of each animal from the weight on the 38th day, and expressing the difference as a percentage. The control group had a slightly higher weight gain than the rest of the groups, but the difference was not significant. The ethanol treatment groups had comparable percentage weight gain.

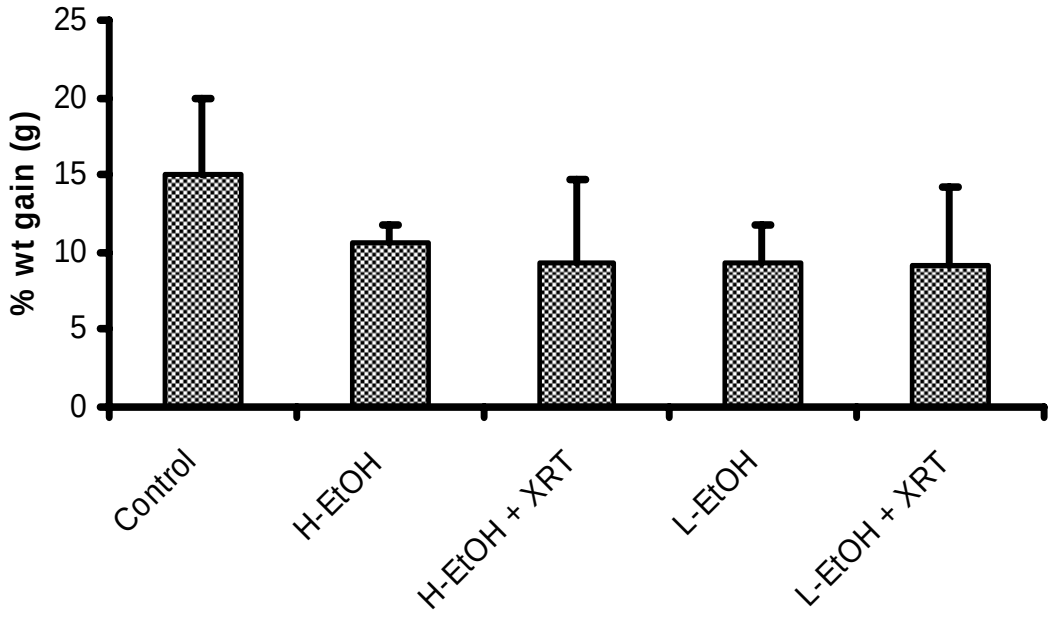

Figure 3.7. Percentage weight gain in grams in each group up to the 38th day.
There were weight gains in each group, which averaged 10 to 15 grams. The control group gained a little more weight than the ethanol treatment groups. The percentage weight gains in all the ethanol treatment groups were not significantly different. (H-EtOH: heavy/high-dose ethanol treatment group, L-EtOH: light/low-dose ethanol treatment group, H-EtOH + XRT: high-dose ethanol combined exposure, L-EtOH + XRT: light-dose ethanol combined exposure)

3.4.3. Daily Fluid Intake. The average daily fluid in take of the mice during the treatment period are shown in Figures 3.8 to 3.11. There were fluctuations within a narrow range in the daily fluid intake of the mice in all the groups. The control group had

a slightly higher fluid intake than the ethanol treatment groups. The light/low-dose ethanol groups had slightly higher, but insignificant fluid intake as compared to the heavy/high-dose ethanol treatment group.

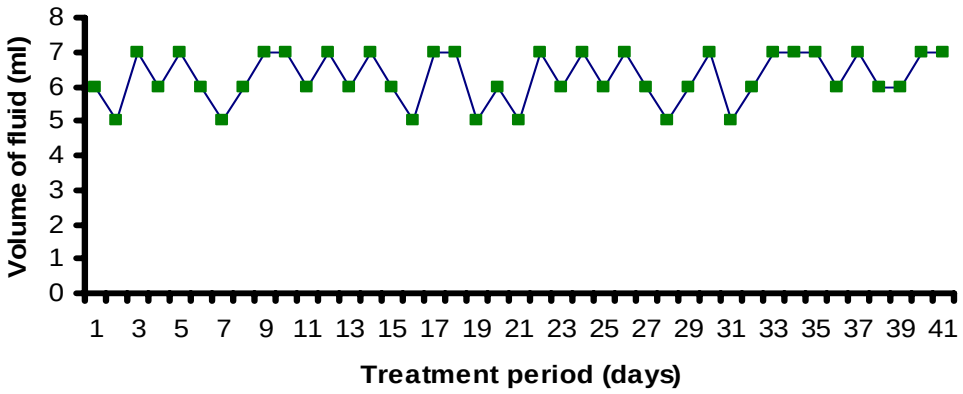

Figure 3.8. Daily fluid intake for the control group.
The fluid intake was measured after every 24 h for 41 d. The volume taken by each mouse in the control group fluctuated within a narrow range. The control group had insignificantly higher fluid intake as compared to the ethanol treatment groups.

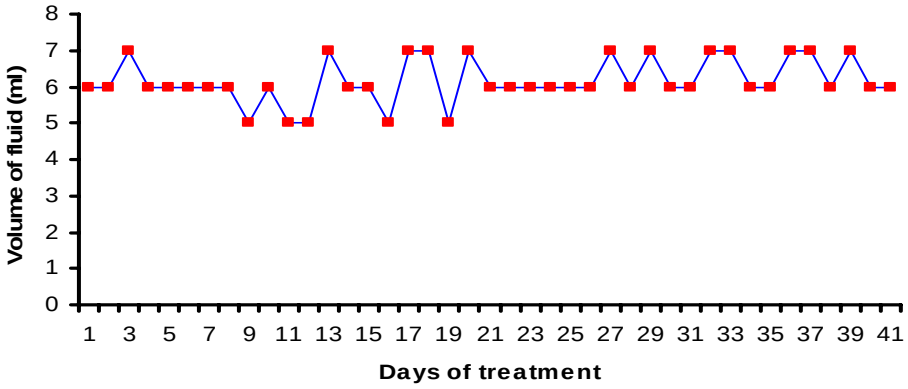

Figure 3.9. Daily fluid intake for the light/ low-dose ethanol treatment group.

The volume of drink was measured after every 24 h. The mice were provided ethanol solution (5% v/v) as their only drinking fluid. The drinking pattern fluctuated within a narrow range.

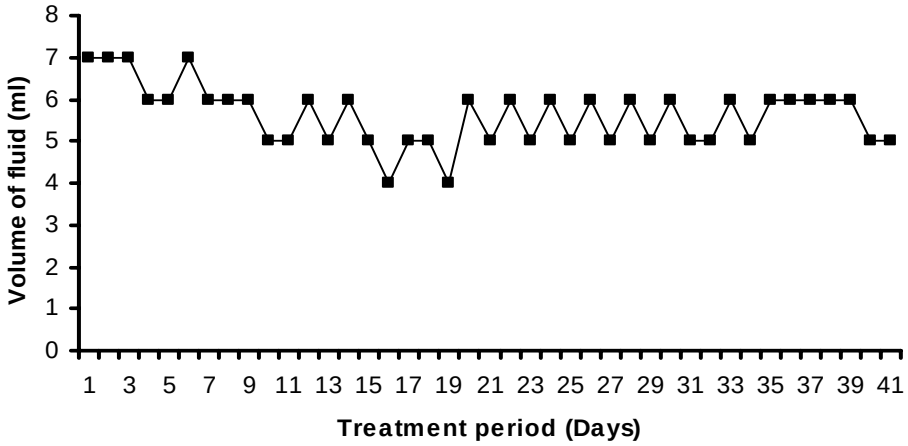

Figure 3.10. Daily fluid in take for the mice in heavy/high-dose ethanol group.
The mice were provided ethanol solution (10 % v/v) as their only drinking fluid. The mice in this group had the lowest fluid in take, but the difference was insignificant compared to the other groups.

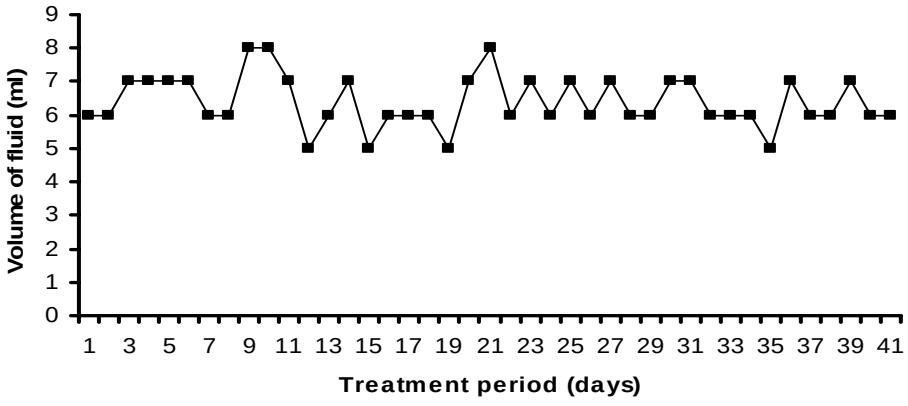

Figure 3.11. Daily fluid intake for the mice in the radiation only group.
Water was provided ad libitum, and the volume of drink was measured after every 24 h. The volume taken by each mouse fluctuated within a narrow range.

3.4.4. Complete Blood Count Results. Table 3.1 displays the protein content and the white blood cell parameters (WBC numbers, neutrophils, lymphocytes, monocytes, eosinophils, and basophils) obtained from manual differential data using the blood smears that were prepared from the blood of the mice immediately after sacrifice. The protein content of the blood was significantly higher in the control group than that in both the single agent and combined exposure groups. The combined exposure groups had lower protein content as compared to the single agent exposure groups, except for the XRT group, which had the lowest protein content. The number of white blood cells (WBC) was significantly higher in the control compared to the single agent and combined exposure groups, with the exception of the high-dose ethanol group. The high-dose ethanol combined exposure group had the lowest number of WBC. The control and high-dose ethanol groups had the same numbers of neutrophils, while the low-dose ethanol and XRT groups had the lowest number. The numbers of neutrophils in the high-dose ethanol combined exposure and XRT only groups were too few to be determined. The numbers of lymphocytes, monocytes, and eosinophils in the high-dose ethanol combined exposure and XRT only groups were too few to be determined, while the control had the highest numbers and the low-dose ethanol combined exposure had the lowest. The high-dose ethanol group seemed to deviate from this trend, with numbers closer to those of the control. The number of basophils was significantly higher in the control, as compared to that of the single agent and the combined exposure groups. The combined exposure groups had the lowest numbers of basophils.

The red blood cell and platelet parameters (RBC numbers, hemoglobin content, hematocrit %, mean corpuscular volume (MCV), mean corpuscular hemoglobin (MCH),

Table 3.1. Effects of ethanol and XRT on white blood cell parameters.

	Total pro (g/dL)	Leucocytes (x1.0+03/ µL)	Neutrophils (x1.0+03/ µL)	Lymphocytes (x1.0+03/ µL)	Monocytes (x1.0+03/ µL)	Eosinophils (x1.0+03/ µL)	Basophils (x1.0+03/ µL)
Normal range	5.9 - 10.3	5.0 - 13.7	N/A	N/A	N/A	N/A	0.0 - 0.2
Control	6.3 ± 0.3	3.4 ± 1.0	0.4 ± 0.2	3.0 ± 0.8	0.08	0.05 ± 0.007	0.19 ± 0.03
L-EtOH	6.2 ± 0.8	1.0 ± 0.6*/**	0.2 ± 0.1*	0.9 ± 0.4*	0.06	0.02	0.04 ± 0.006*/**
H-EtOH	5.8 ± 0.6	3.9 ± 1.0**	0.4 ± 0.08	3.4 ± 0.9	0.12± 0.09	0.03	0.15 ± 0.08**
XRT	5.0 ± 0.9	0.3 ± 0.2*	0.0000	0.000	0.000	0.00	0.013 ± 0.005
L-EtOH + XRT	5.2 ± 0.4	0.7 ± 0.1*	0.16	1.7	0.12	0.00	0.01 ± 0.0
H-EtOH + XRT	5.5 ± 0.5	0.2 ± 0.06*	0.0000	0.000	0.000	0.00	0.01 ± 0.0

mean corpuscular hemoglobin concentration (MCHC), platelet numbers, and mean platelet volume (MPV)) were obtained from automated differential data, which was acquired on a Cell Dyne 3500 (Abbot) analyzer, are displayed in Table 3.2. The RBC numbers, hemoglobin content, and hematocrit percentage were highest in the ethanol only treatment groups, but lowest in the XRT only group. Nevertheless, all of these parameters fell within the normal range in all the groups. The MCV and MCH were slow-dosely higher in the control, but not significant when compared to the treatment groups; the measurements for these parameters fell within the normal range in all of the groups. There was no significant difference in MCHC in all of the groups. The number of platelets was highest in the control and lowest in the XRT only group, but they were too few to be counted in the high-dose ethanol combined exposure group. The MPV values fell within the normal range in all of the groups, and were not significantly different from

each other; values could not be determined for the high-dose ethanol combined exposure group.

Table 3.2. Effects of ethanol and XRT on red blood cell parameters.

	RBC (M/µL)	Hb (g/dL)	Hem (%)	MCV (fL)	MCH (pg)	MCHC (g/dL)	Plts (x1.0+03/ µL)	MPV (fL)
Normal range	6.36 - 9.42	11.0 - 15.1	35.1 - 45.4	45.4 - 60.3	14.1 - 19.3	30.2 - 34.2	592-2972	5.0 - 20.0
Control	8.9 ± 0.6	14.8 ± 0.7	44.5 ± 1.9	51.2 ± 0.9	16.6 ± 0.4	32.4 ± 0.7	960 ± 25	9.5 ± 1.2
L-EtOH	9.9 ± 0.7	15.8 ± 1.1	48.3 ± 4.0	49.2 ± 0.7	15.9 ± 0.2	32.3 ± 0.5	768	7.7 ± 0.4
H-EtOH	10.4 ± 0.7	15.6 ± 0.6	48.7 ± 2.9	47.5 ±1.0	15.05 ± 0.5	31.8 ± 0.7	952 ± 92	8.9 ± 2.3
XRT	7.7 ± 0.7	12.4 ± 0.9*	37.2 ± 3.8*/**	48.8 ± 0.9	16.07 ± 0.4	32.9 ± 1.4	692 ± 36*	8.1 ± 1.6
L-EtOH + XRT	8.9 ± 0.8	14.2 ± 1.3	43.0 ± 4.9	48.6 ± 1.3	16.0 ± 1.7	32.9 ± 0.7	787	9.7 ± 1.0
H-EtOH + XRT	9.2 ± 0.6	14.2 ± 1.1	44.0 ± 3.6	48.2 ± 1.4	15.4 ± 0.2	31.8 ± 0.6	0.00	0.00

All of the red blood cell and platelet parameters were measured by an automated hematology instrument (Abbott Cell-Dyn 3500 Hematology analyzer) at the UMC Research Animal Diagnostic Laboratory (RADIL), Columbia, MO, USA. The number of platelets and MPV could not be determined in the high-dose ethanol combined exposure group. (Hb: hemoglobin, Plts: platelets, Hem: hematocrit)

3.4.5. Liver GSH Levels. The GSH levels in all the groups were determined following homogenization of the liver tissue samples, and derivatization using NPM. Figure 3.12 shows how the levels of GSH varied in the livers of mice that were treated with low-dose ethanol and/or radiation. The GSH levels were highest in the control group, and lowest in the combined exposure group (group treated with ethanol plus

radiation exposure). The combined exposure group had significantly lower GSH levels compared to the single agent exposure groups. The results for the GSH levels of high-dose ethanol combined exposure groups are shown in Figure 3.13. The GSH levels in this figure followed a pattern similar to that in Figure 3.5 (a), but the differences were larger. Chronic high-dose ethanol combined with radiation exposure resulted in significantly lower GSH levels than chronic low-dose ethanol combined with radiation exposure. In both of these groups, combined exposure resulted in significantly lower GSH levels than the control and single agent exposure groups. The high-dose ethanol combined exposure group resulted in significantly lower GSH levels compared to low-dose ethanol combined exposure group. The sample chromatograms shown in Figures 3.14 to 3.19 are from the liver samples, with the area under the curve being largest in the control group and smallest in the high-dose ethanol combined exposure group.

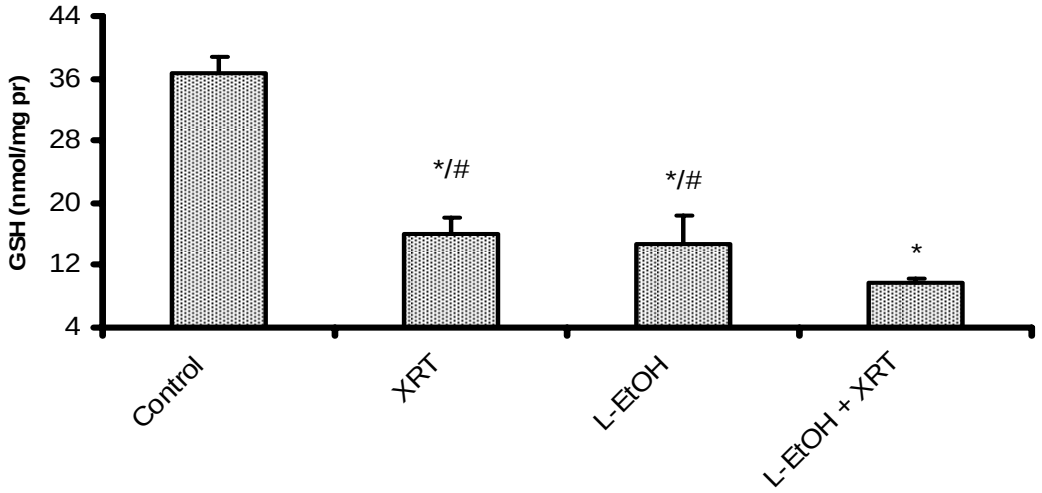

Figure 3.12. GSH levels in the chronic low-dose ethanol groups (liver).
The mice were treated with ethanol (5%v/v) for 5 weeks, and then exposed to 8 Gy radiation. The GSH levels were measured by the HPLC method after homogenization of

the liver tissue samples and derivatization with NPM. The GSH levels were significantly lower in the treatment groups as compared to the control. The combined exposure group had a significantly lower GSH level as compared to the single agent treatment groups. * Significantly different compared to control ($p < 0.05$). # Significantly different compared to combined exposure group ($p < 0.05$). (H-EtOH: heavy/high-dose ethanol treatment group, L-EtOH: light/low-dose ethanol treatment group, H-EtOH + XRT: high-dose ethanol combined exposure, L-EtOH + XRT: light-dose ethanol combined exposure, XRT: radiation only group, pr: protein)

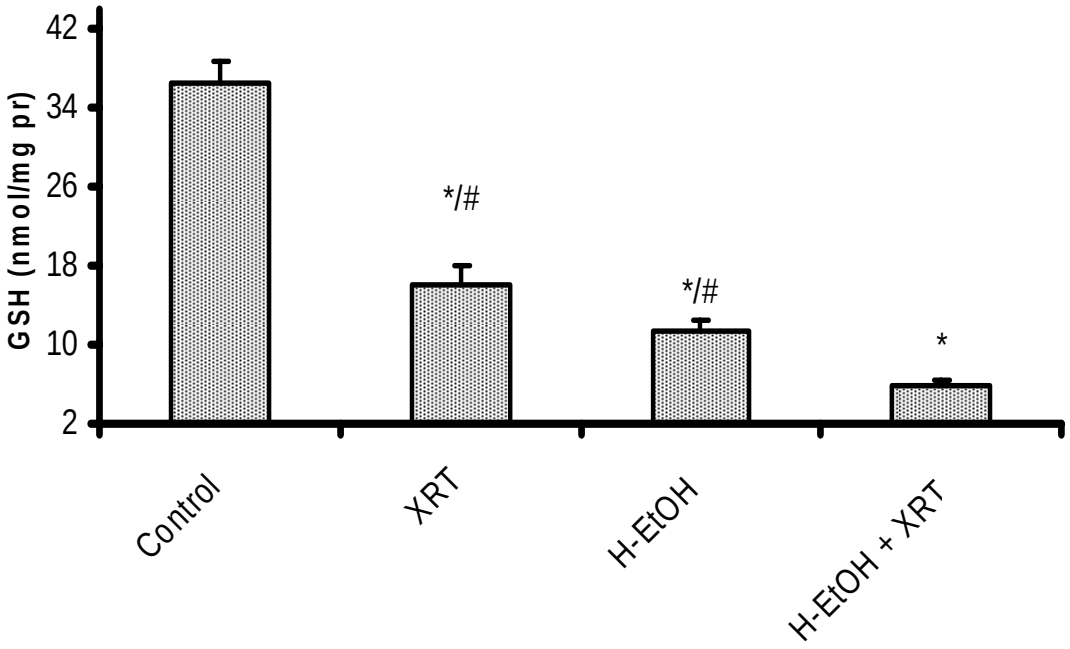

Figure 3.13. GSH levels in the high-dose ethanol groups (liver).
The mice were treated with ethanol (10 %v/v) for 5 weeks, and then exposed to 8 Gy radiation. The GSH levels were measured as described above. The combined exposure group had significantly lower GSH levels as compared to the control and single agent exposure groups. (H-EtOH: heavy/high-dose ethanol treatment group, L-EtOH: light/low-dose ethanol treatment group, H-EtOH + XRT: high-dose ethanol combined exposure, L-EtOH + XRT: light-dose ethanol combined exposure, XRT: radiation only group, pr: protein)

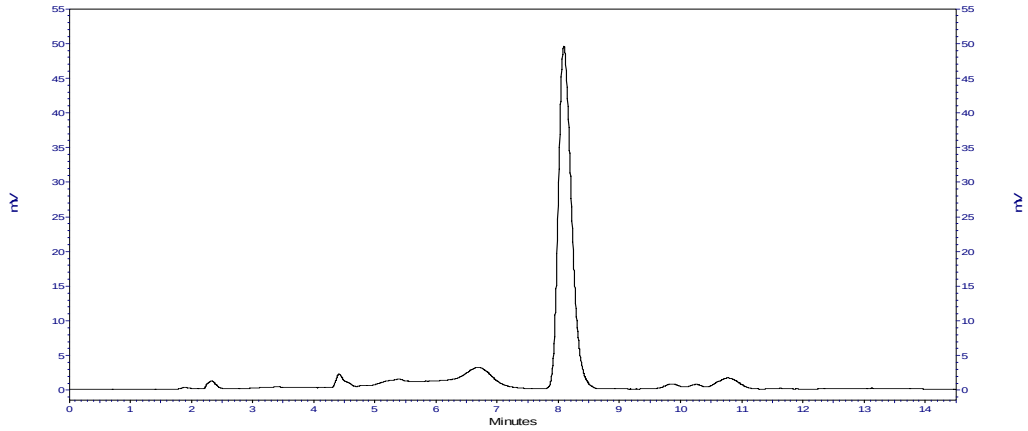

Figure 3.14. The control liver sample Chromatogram.
The animals in the control group were not exposed to ethanol or radiation. Food and tap water was provided *ad libitum.* Separation conditions: An ODS-1 C_{18} Column (5 µm packing material) with 250 x 4.6 mm (i.d) was used for the separation. The NPM derivatives were measured by a fluorescence detector (λ_{ex} = 330 nm and λ_{em} = 376 nm). Flow rate was 1ml/min.The GSH peak at a retention time of 8.20 min was the highest, and the CYS peak was at the retention time of 10.73 min. The hydrolysis peak (due to excess NPM) came earlier than the analyte peaks.

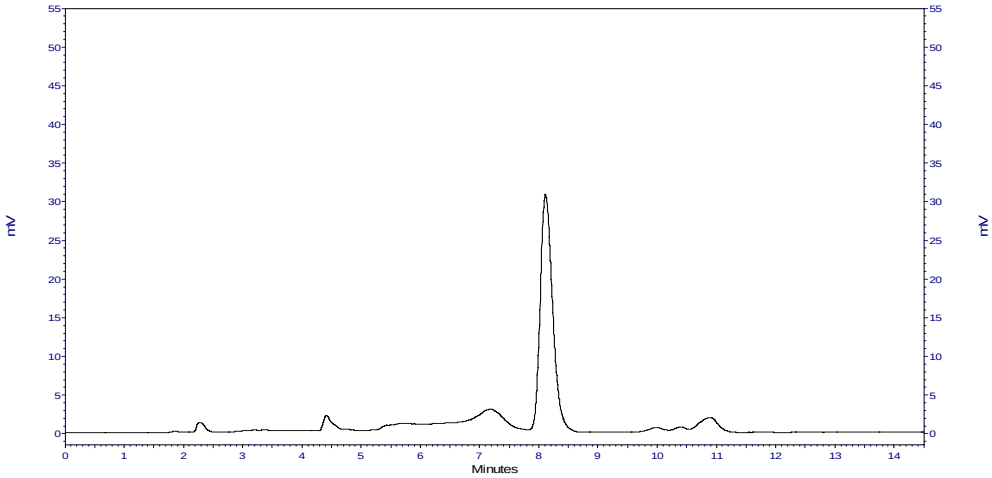

Figure 3.15. The light/low-dose ethanol group liver sample Chromatogram.
The separation conditions were the same as mentioned in Figure 3.14.

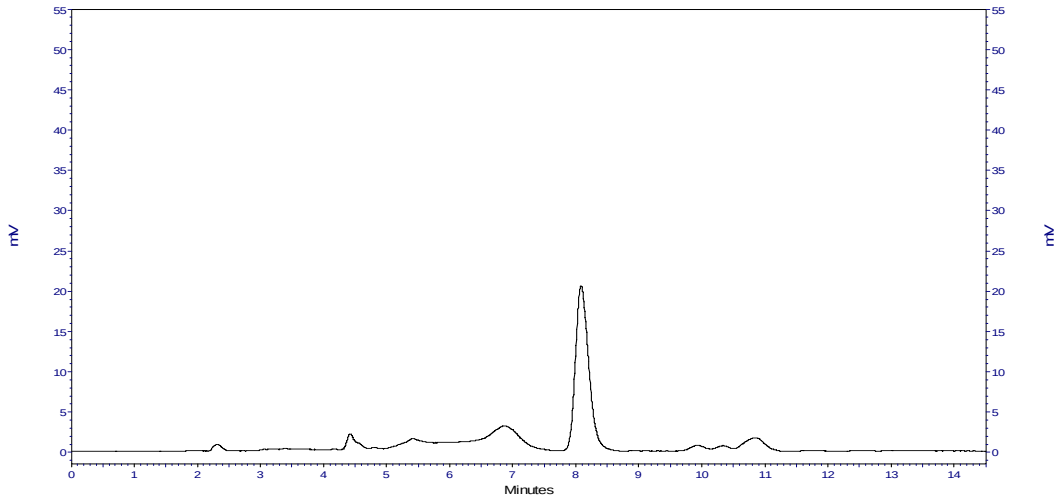

Figure 3.16. The high-dose ethanol group liver sample Chromatogram.
The mice received ethanol (10% v/v) solution as their only drinking fluid.

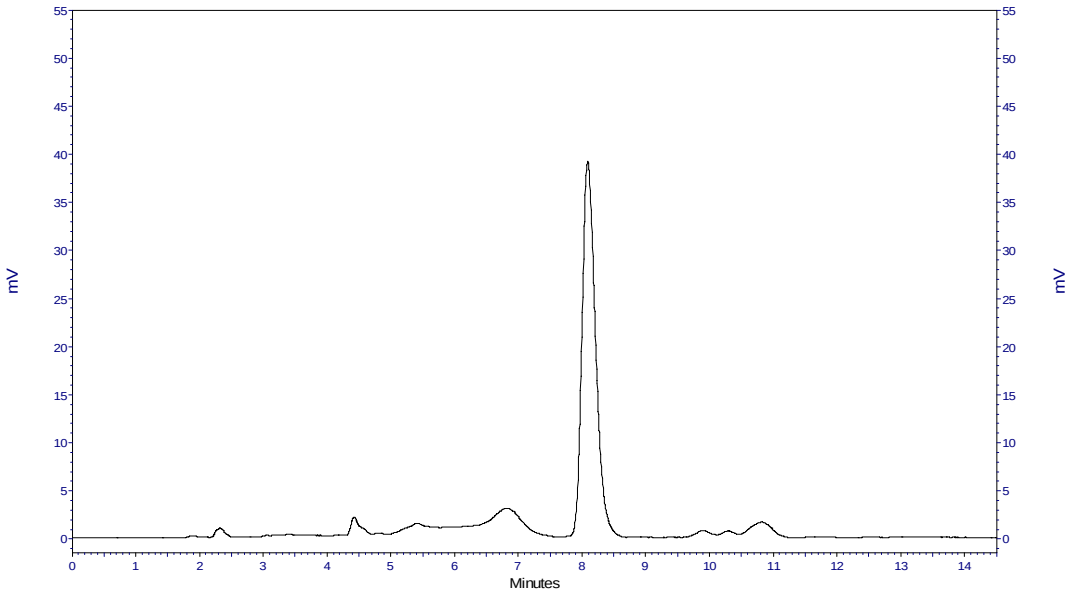

Figure 3.17. The radiation only group liver sample chromatogram.
The mice received the same treatment as the control, but were exposed to the radiation at the end of the treatment period.

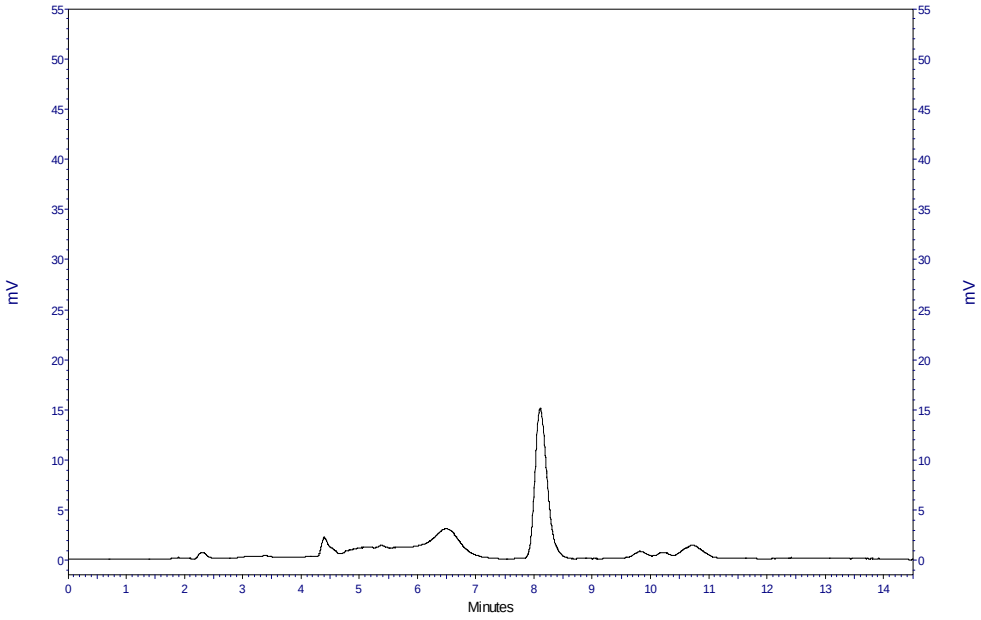

Figure 3.18. The light-dose ethanol combined exposure group chromatogram (liver). The separation conditions were the same as described in Figure 3.14.

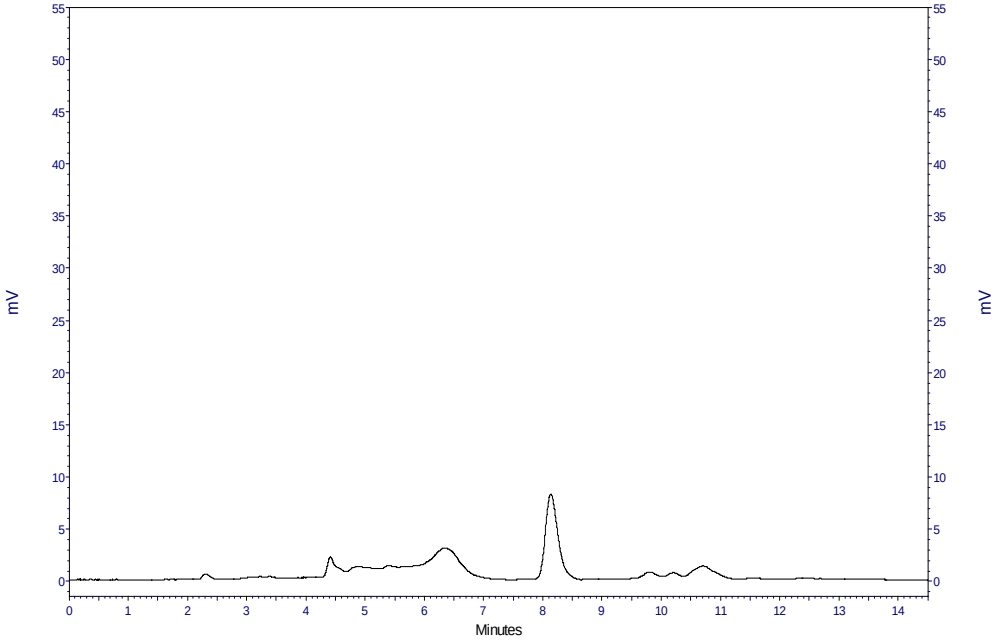

Figure 3.19. The high-dose ethanol combined exposure group chromatogram (liver). The separation conditions were the same as described in Figure 3.14.

3.4.6. Brain GSH Levels. The results of the brain GSH levels displayed in Figures 3.20 and 3.21, show that the control group had the highest GSH level; while high-dose ethanol combined exposure group had the lowest GSH levels. The single agent treatment groups had significantly higher GSH levels than the combined exposure groups. The GSH levels in the liver were significantly higher than the GSH levels in the brain in all the experimental groups.

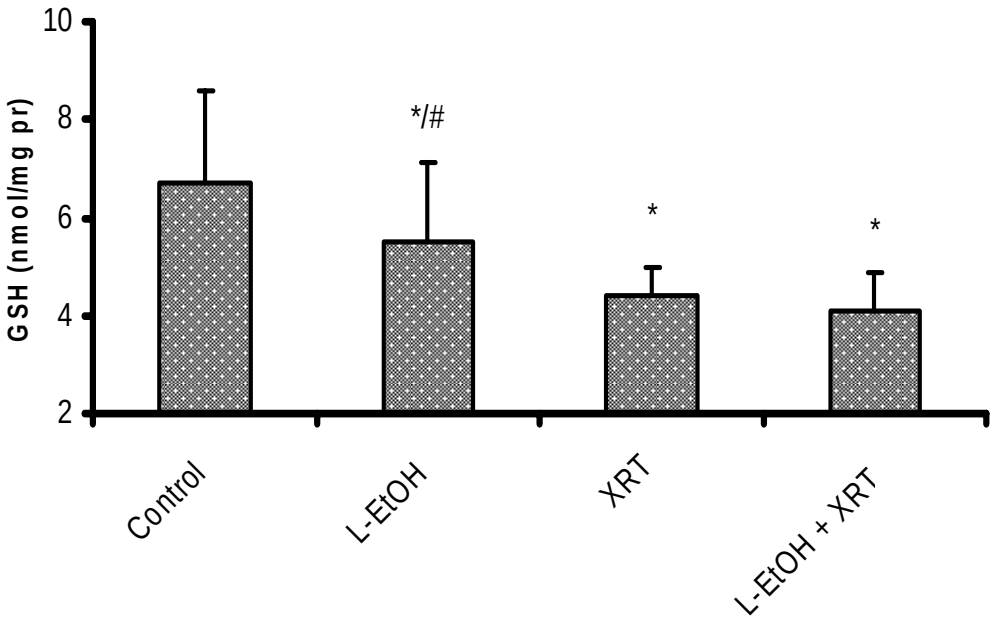

Figure 3.20. The GSH levels in the chronic low-dose ethanol groups (brain).
The treatment of the mice and GSH determinations were done as described in Figure 3.5. (a). (H-EtOH: heavy/high-dose ethanol treatment group, L-EtOH: light/low-dose ethanol treatment group, H-EtOH + XRT: high-dose ethanol combined exposure, L-EtOH + XRT: light-dose ethanol combined exposure, XRT: radiation only group, pr: protein)

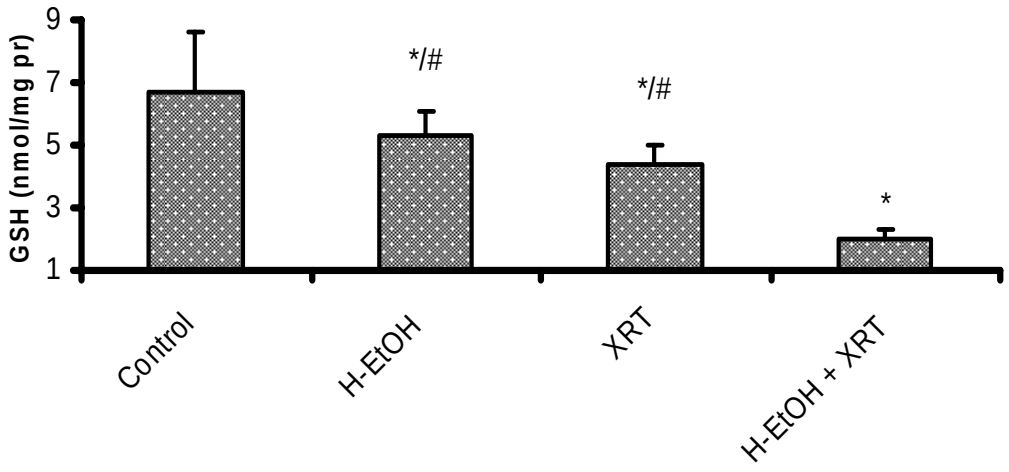

Figure 3.21. The GSH levels in the chronic high-dose ethanol groups (brain).
The treatment of the mice and GSH determinations were done as described in Figure 3.5. (b). (H-EtOH: heavy/high-dose ethanol treatment group, L-EtOH: light/low-dose ethanol treatment group, H-EtOH + XRT: high-dose ethanol combined exposure, L-EtOH + XRT: light-dose ethanol combined exposure, XRT: radiation only group, pr: protein)

3.4.7. Liver cysteine levels. The results of the liver cysteine levels are shown Figures 3.22 and 23. The cysteine levels in the chronic low-dose ethanol only group (Group II) were the highest, whereas the high-dose ethanol combined exposure group (Group VI) had the lowest CYS levels. Combined exposure groups (Groups V and VI) had significantly lower cysteine levels compared to the single agent (Groups II, III, and IV) exposure and control groups. The high-dose ethanol only group had similar CYS levels as the control group.

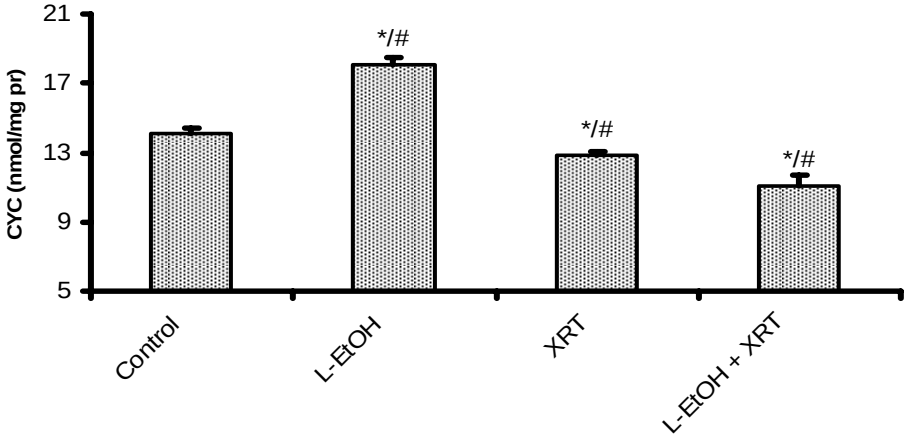

Figure 3.22. The liver CYS levels in low-dose ethanol groups.
The treatment of the mice and CYS determinations were done as described in Figure 3.12. (H-EtOH: heavy/high-dose ethanol treatment group, L-EtOH: light/low-dose ethanol treatment group, H-EtOH + XRT: high-dose ethanol combined exposure, L-EtOH + XRT: light-dose ethanol combined exposure, XRT: radiation only group, pr: protein)

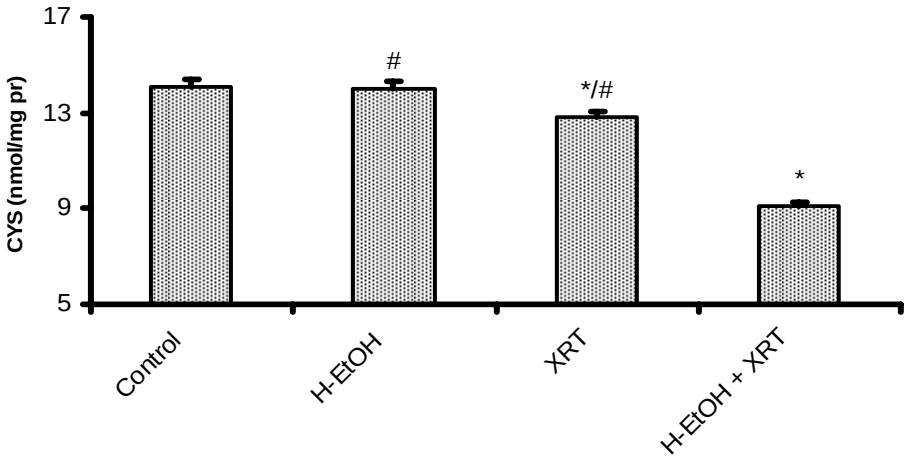

Figure 3.23. The liver CYS levels in high-dose ethanol groups.
The treatment of the mice and CYS determinations were done as described in Figure 3.12. (H-EtOH: heavy/high-dose ethanol treatment group, L-EtOH: light/low-dose ethanol treatment group, H-EtOH + XRT: high-dose ethanol combined exposure, L-EtOH + XRT: light-dose ethanol combined exposure, XRT: radiation only group, pr: protein)

3.4.8. Brain and Kidney Cysteine Levels. The kidney and brain CYS levels are displayed in Table 3.3. There was no consistent pattern in CYS levels in the kidney, while the CYS levels in the brain decreased gradual from the control, which had the highest level, to the high-dose ethanol combined exposure group, which had the lowest CYS levels.

Table 3.3. The kidney and brain CYS levels.

GROUPS	Kidney CYS (nmol/mg pro)	Brain CYS (nmol/mg pro)
Control	8.4 ± 0.4	8.1 ± 1.2
L-EtOH	9.4 ± 1.7*	7.4 ± 1.9*/#
H-EtOH	6.7 ± 1.1*/#	6.8 ± 1.4*/#
XRT	9.1 ± 1.2*/#	6.7 ± 1.3*/#
L-EtOH + XRT	9.3 ± 1.5*	6.0 ± 1.7*
H-EtOH + XRT	8.1 ± 1.3	5.3 ± 1.1*

The treatment procedures and CYS determinations were done as described figure 3.5. a and b. (pro: protein)

3.4.9. GSSG Levels in the Liver Samples. The same liver tissue samples used to determine the GSH levels were derivatized and used for the determination of the GSSG levels. This was done in order to facilitate the determination of GSH:GSSG ratio. Figures 3.24 and 3.25 shows the results of the GSSG levels in the two categories of the treatment groups. In both of the treatment categories, the control group had the lowest GSSG level, while the combined exposure groups had the highest GSSG levels. The single agent exposure groups had significantly lower GSSG levels as compared to combined exposure

groups. The high-dose ethanol combined exposure group had significantly higher GSSG level than the low-dose ethanol combined exposure group.

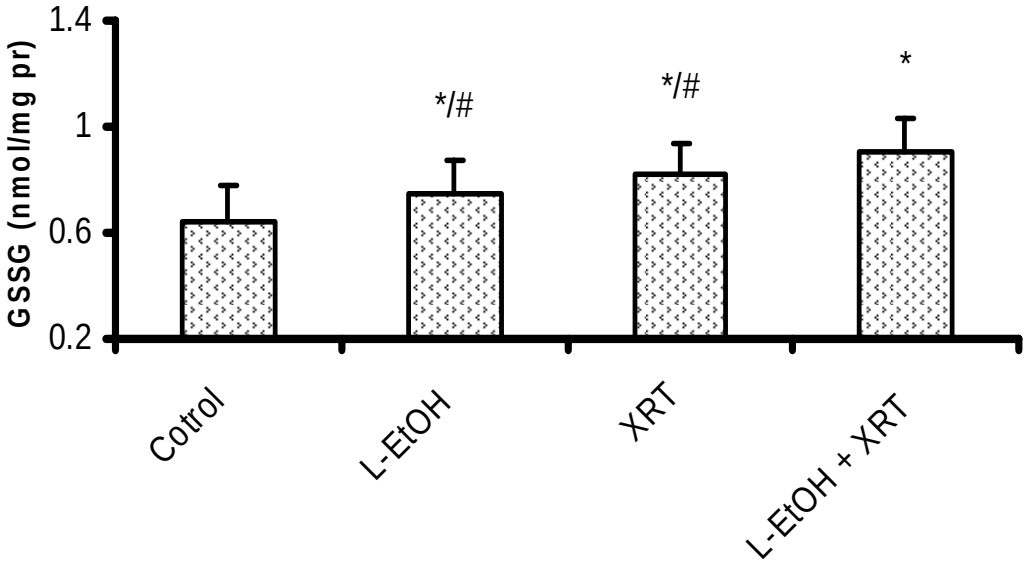

Figure 3.24. The GSSG levels in the chronic low-dose ethanol groups (liver).
The mice in this group received an ethanol solution (5% v/v) as their sole drinking fluid for 5 weeks, and then were irradiated and sacrificed 4 d later. The GSSG levels were determined by the HPLC method as described under the methods section. The control group had the lowest GSSG level, while the combined exposure group had the highest level. (H-EtOH: heavy/high-dose ethanol treatment group, L-EtOH: light/low-dose ethanol treatment group, H-EtOH + XRT: high-dose ethanol combined exposure, L-EtOH + XRT: light-dose ethanol combined exposure, XRT: radiation only group, pr: protein)

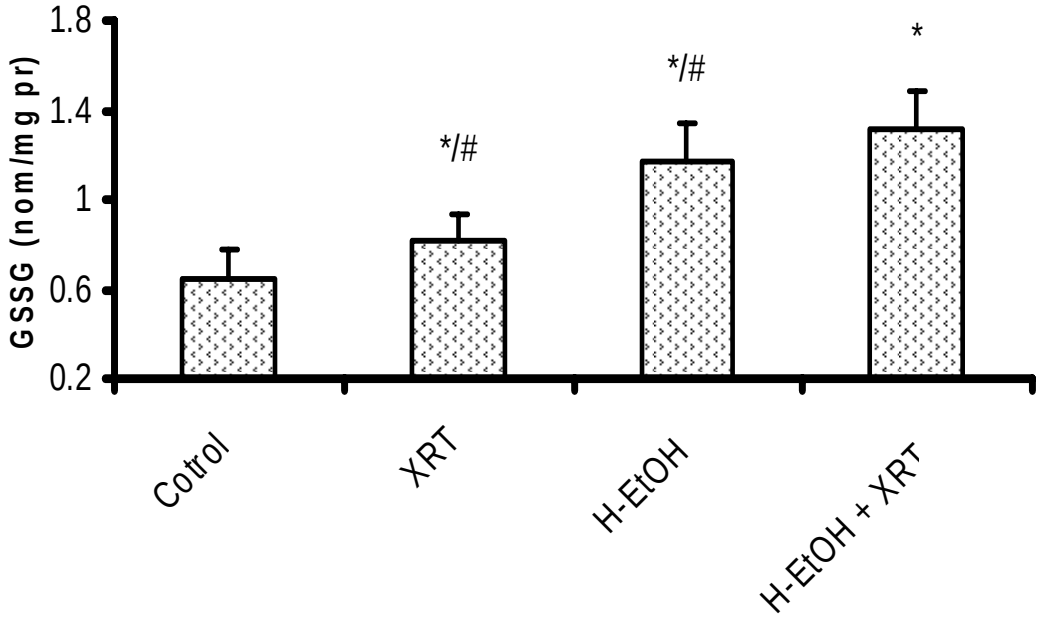

Figure 3.25. The GSSG levels in the chronic high-dose ethanol groups (liver).
The mice received an ethanol solution (10% v/v) as their sole drinking fluid. The GSSG level was determined as described above. The combined exposure group had the highest GSSG level. (H-EtOH: heavy/high-dose ethanol treatment group, L-EtOH: light/low-dose ethanol treatment group, H-EtOH + XRT: high-dose ethanol combined exposure, L-EtOH + XRT: light-dose ethanol combined exposure, XRT: radiation only group, pr: protein)

3.4.10. GSH:GSSG Ratio in the Liver Samples. The GSH levels from the liver samples were divided by the corresponding GSSG levels in order to determine the GSH:GSSG ratio in the liver. The control group, with the highest GSH level, and the lowest GSSG level, had the highest GSH:GSSG ratio as compared to the single agent and combined exposure groups, as can be seen in Figures 3.26 and 3.27. In the single agent exposure groups, low-dose ethanol treatment and XRT groups had nearly equal

GSH:GSSG ratios, while the high-dose ethanol treatment group had the lowest ratio. The high-dose ethanol treatment combined exposure group had a significantly lower ratio compared to the low-dose ethanol combined exposure group.

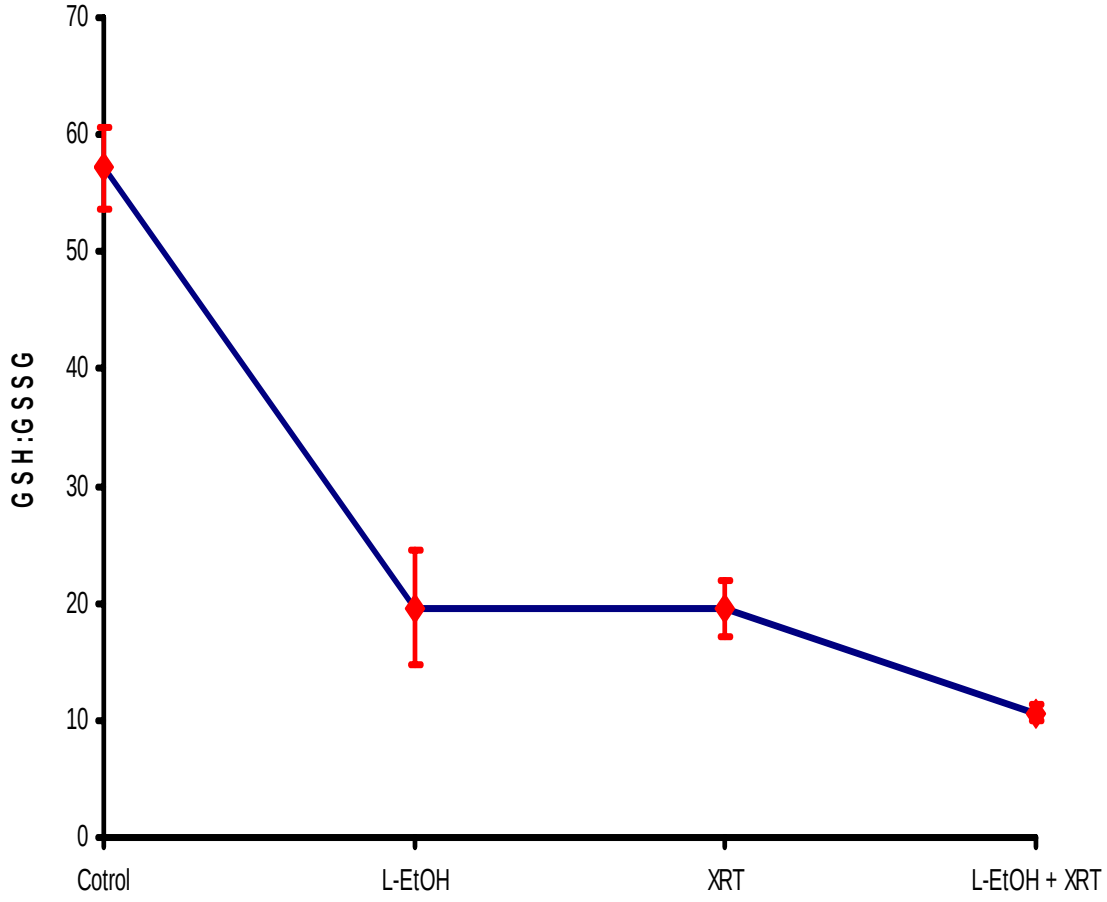

Figure 3.26. The GSH:GSSG ratio in the chronic low-dose ethanol groups (liver). The ratio was determined after separately determining GSH and GSSG levels, and then dividing the corresponding values of the two parameters. The highest GSH:GSSG ratio was in the control group, while the combined exposure group had the lowest ratio.

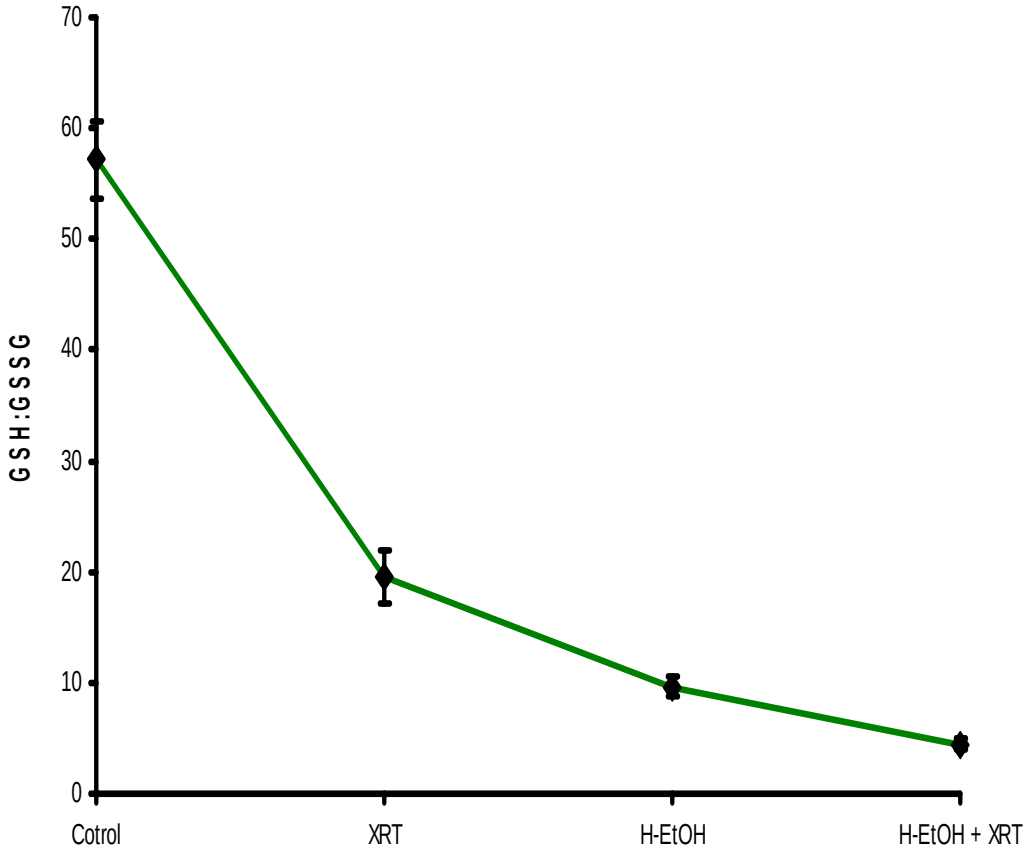

Figure 3.27. The GSH:GSSG ratio in the chronic high-dose ethanol groups (liver). The ratio was determined as described above. The combined exposure group had the lowest ratio.

3.4.11. Liver MDA Levels. The high-dose ethanol combined exposure group had the highest MDA level, while the control group had the lowest MDA level, as can be seen in Figures 3.28 and 3.29. The differences in the MDA levels of the control, low-dose ethanol, and XRT only groups, were not significant. High-dose ethanol resulted in higher MDA levels than low-dose ethanol treatment in the liver. The MDA levels in the high-

dose ethanol combined exposure group were significantly higher than those in the high-dose ethanol and radiation only groups.

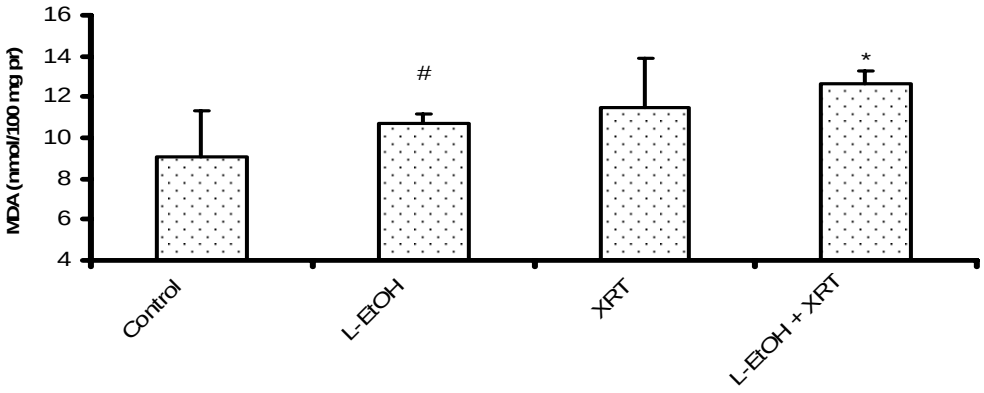

Figure 3.28. The MDA levels in the chronic low-dose ethanol groups (liver).
The MDA levels were measured by the reversed-phase HPLC method with fluorescence detection. The mobile phase consisted of 69.4% 5mM sodium phosphate buffer pH = 7.0, 30% acetonitrile, and 0.6% tetrahydrofuran. The flow rate was 1ml/min. The MDA levels were significantly higher in the treatment groups as compared to the control group. The combined exposure group had significantly higher MDA levels as compared to the single agent exposure groups.

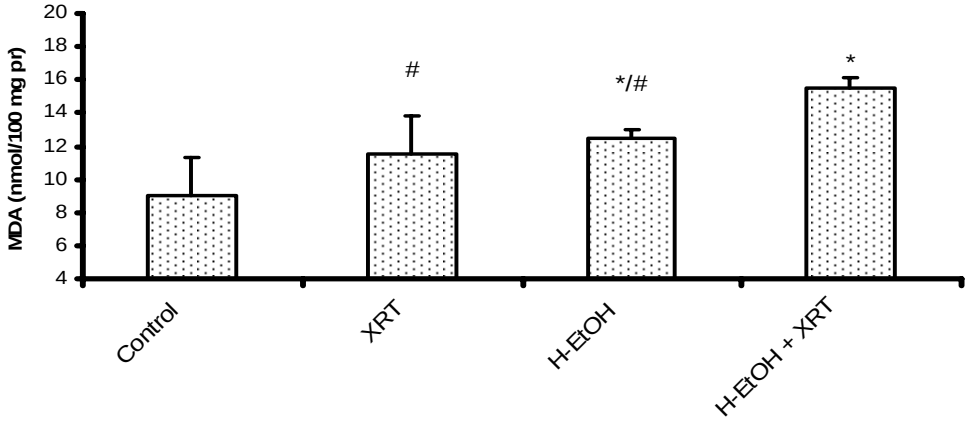

Figure 3.29. The MDA levels in the chronic high-dose ethanol groups (liver).
The combined exposure group had the highest MDA levels, while the control group had the lowest.

3.4.12. Catalase and GR Activities in the Liver. The results for the catalase and glutathione reductase activities are displayed in Table 3.4. The activities of these enzymes were determined by a spectrophotometric enzyme assay method. The activity of catalase enzyme was the highest in the control group, and lowest in the high-dose ethanol combined exposure group. The single agent exposure groups had significantly higher catalase activity than the combined exposure groups. Between the combined exposure groups, the high-dose ethanol combined exposure group had lower catalase activity as compared to the low-dose ethanol combined exposure group. The glutathione reductase activity was the lowest in the control group, and highest in the high-dose ethanol combined exposure group. The single agent exposure groups had significantly lower GR activities, as compared to the combined exposure groups. The high-dose ethanol combined exposure group had significantly higher GR activity as compared to the low-dose ethanol combined exposure group.

Table 3.4. CAT and GR activities in the liver of CD-1 mice.

Groups	CAT (units/mg pro)	GR (units/mg pro)
Control	0.25 ± 0.07	23.0 ± 5.0
L-EtOH	0.16 ± 0.02 */#	28.0 ± 3.1*/#
H-EtOH	0.13 ± 0.03*/#	32.4 ± 4.2*/#
XRT	0.15 ± 0.04*/#	39.7 ± 4.9*/#
L-EtOH + XRT	0.13 ± 0.02*	52.0 ± 6.5*
H-EtOH + XRT	0.10 ± 0.02*	63.8 ± 5.4*

Effects of chronic ethanol treatment followed by radiation exposure on catalase (CAT) and glutathione reductase (GR) activities in the liver of CD-1 mice. [CAT activity was measured spectrophotometrically at 240 nm following the exponential disappearance

of hydrogen peroxide (H_2O_2; 10 mM) according to the method described by Aebi (Aebi, 1984), while GR activity was measured at 340 nm following the decrease of NADPH. The values reported are mean ± SD. * $p < 0.05$ compared to the corresponding value of the control, while $^{\#}$ $P < 0.05$ compared to the corresponding value of the combined exposure group.

3.5. DISCUSSION

It has been shown by many investigators that oxidative stress plays a major role in many human pathological conditions such as cancer, diabetes, cardiovascular disease, neurological disorders, ischemia/reperfusion, and many other diseases as well as in aging [140-143]. Any agent that affects the antioxidant status of living systems, such as ethanol and ionizing radiation, has the potential of producing a negative impact on the health condition of an individual [144-146]. After the *in vitro* investigation showed that a combination of ethanol and ionizing radiation induces elevated oxidative stress [116], the *in vivo* investigation of combined exposure using a CD-1 mice model was performed. This study reinforces the need to have a thorough background check on patients in terms of their previous and current drinking behaviors by doctors and oncologists before procedures such as radiotherapy are administered. Unfortunately, the risk assessment in most cases is performed with an assumption that the agent being studied acts independently of other agents, even though interaction studies have shown that, at high exposures, the action of one agent can be influenced by simultaneous exposure to the other agents [147]. Previous combined exposure studies involving radiation and other agents have focused on the measurements of various end points, including lung cancer, mutations, tumor incidence, liver carcinomas and foci, and many others, but not antioxidant status [148-151]. In this study, therefore, the levels of reduced glutathione,

which is the most important antioxidant in the living systems, having a thiol functional group that enables it to scavenge free radicals and maintains the redox status of the cells was measured. The GSSG levels were also measured, and the GSH:GSSG ratios, MDA levels, and antioxidant enzyme activities (CAT and GR) as a way of determining how combined exposure to ethanol, followed by ionizing radiation, affects the antioxidant status of mice were determined . Since ethanol metabolism, which takes place primarily in the liver is associated with most pathological conditions of the liver [152-154], all of the parameters mentioned were determined for the liver. Additionally, the GSH and CYS levels in the brains of the mice were determined, since ethanol has been documented to cross the blood brain barrier [155-156], and CYS levels in the kidneys.

The GSH levels in the livers and brains of CD-1 mice were lowest in our chronic high-dose ethanol combined exposure group, and highest in the control. The ROS and free radicals produced during ethanol metabolism have been shown to cause oxidative stress and lipid peroxidation in the liver and brain [157-159]. Lieber reported depletion of hepatic GSH after chronic alcohol consumption in experimental animals and humans [160], and Borek reported that radiation at doses used in radiotherapy depletes tissue antioxidants such as alpha tocopherol, and Vitamins A, C and E [161]. An investigation conducted by Zentella et al. [162] concluded that ethanol intoxication decreased GSH levels. GSH performs many essential functions in cells, such as scavenging free radicals, maintaining the essential thiol status of proteins by preventing oxidation of –SH groups or by reducing difulfide bonds induced by oxidative stress, detoxifying electrophiles, modulating critical cellular processes such as DNA synthesis and immune function, and providing a reservoir for cysteine [163-166]. Here, chronic ethanol administration

induced a state of oxidative stress in the mice, lowering the levels of antioxidants and interfering with the normal functioning of the antioxidant enzymes. When the mice were exposed to ionizing radiation, further oxidative stress resulted, since the antioxidant levels were already too low to cope with the increased production of ROS. Antioxidants and antioxidant enzymes form the defense system against oxidative damage by ROS in biological systems [167]. When this defense system is broken, tissue damage and pathological conditions result.

The result of this investigation showed that GSSG levels were significantly higher in the high-dose ethanol combined exposure group as compared to both the control and the single agent exposure groups. The hydrogen peroxide formed in the cells is reduced by GSH in the presence of glutathione peroxidase enzyme to form water, and in the process, GSH is oxidized to GSSG. The GSSG is then reduced back to GSH by glutathione reductase enzyme at the expense of NADPH. This forms a redox cycle which keeps the levels of GSSG low and maintains the equilibrium between oxidants and antioxidants in the cell [168]. When the cells experience conditions of severe oxidative stress because of chronic exposure to ethanol or ionizing radiation, their ability to reduce GSSG back to GSH can be overcome, resulting in accumulation of GSSG within the cytosol. The cells, therefore, have high GSSG levels and low GSH levels, resulting in a low GSH:GSSG ratio. The results of this investigation showed that the GSH:GSSG ratio was significantly lower in the combined exposure groups in comparison to the control and the single agent exposure groups, suggesting that the GSH-GSSG redox cycle could not cope with the substantial amounts of GSSG that were being formed to maintain the oxidant-antioxidant equilibrium of the cells.

The catalase activity in the livers of the mice in this study was significantly lower in the combined exposure groups as compared to the control and single agent exposure groups. The study conducted by Escobar et al. on superoxide dismutase and catalase inactivation by singlet oxygen and peroxyl radicals showed that these ROS lowered the activity of catalase [169]. Ribiere et al. have shown that ethanol administration lowers the activity of the catalase enzyme [170], while Potier et al. reported a decrease in catalase activity in ox liver by radiation [171]. The catalase enzyme, which is most abundant in the liver, decomposes hydrogen peroxide to oxygen and water by a dismutation process. The active sites of catalase enzyme is altered by reactive oxygen species, rendering them unable to carry out their catalytic functions. The results showed that the increased levels of ROS induced by exposure to ethanol and ionizing radiation significantly decreased the activity of catalase in the liver.

Glutathione reductase activity was significantly higher in the liver of the mice in the combined exposure groups as compared to both the control and the single agent exposure groups. Studies have shown that exposure to both ethanol and ionizing radiation increase the activity of GR [171-173]. GR catalyzes the reduction of oxidized glutathione (GSSG) to reduced glutathione (GSH), maintaining adequate levels of reduced cellular GSH in the glutathione redox cycle. This reaction requires one mole of NADPH as a cofactor, which is oxidized to $NADP^+$ for every mole of GSSG reduced, and two moles of GSH are produced. When the cells are experiencing oxidative stress, more GSH is consumed and large amounts of GSSG are produced. The activity of GR rises to cope with the increased amounts of GSSG being produced. The highest activity of GR observed in the liver of the combined exposure groups suggests that combined exposure

induced greater oxidative stress in the liver than single agents did and most affected the antioxidant status.

The liver cysteine levels in this study were lowest in the combined exposure groups as compared to single agent and control groups, while the brain cysteine levels showed gradual decrease from the control, which had the highest level, to the high-dose ethanol combined exposure, which had the lowest level. CYS levels in the kidney showed fluctuations, without any particular pattern. Wlodek et al. have reported a decrease in the levels of cysteine in the livers of mice after chronic exposure to ethanol [174], and Dewey et al. [175] have shown that interconversion of cysteine to cystine, which is an oxidation process, is induced by X-rays, and can induce alterations in cysteine levels. The low levels of cysteine in the livers of combined exposure groups as compared to the control and the single agent exposure groups could have been orchestrated by exposure to ethanol and ionizing radiation, both of which have been proved to induce ROS capable of initiating the oxidation of cysteine. Fluctuations of cysteine levels in the brains and kidneys could have been brought about by degradation of GSH, a process that is induced by ROS, and by oxidation of cysteine to cystine.

The MDA data from this investigation showed that the high-dose ethanol combined exposure group had the highest levels of MDA while the control group had the lowest. Both ethanol and ionizing radiation have been individually shown to induce lipid peroxidation, which is indexed by the increased levels of MDA [176-180]. Ethanol metabolism is characterized by events such as acetaldehyde formation, CYP2E1-mediated 1-hydroxyethyl radical formation, ROS production, increase in the $NADH/NAD^+$ ratio, causing the reduction of ferric iron to ferrous iron, with

accompanying production of hydroxyl radicals. These events lead to lipid peroxidation and production of MDA and 4-hydroxynonenal (4-HNE). The ROS produced by ionizing radiation attack polyunsaturated fatty acids (PUFA) in the liver, producing MDA and lipid peroxides. Exposure to ethanol, followed by radiation, enhanced the generation of enormous amounts of ROS. These, in turn, attacked the cell membrane lipids, mitochondrial membrane and other cellular organelles, forming lipid aldehydes and peroxides. The data from the investigation supported this observation.

The findings from this investigation showed that all of the white blood cell parameters were significantly lower in the high-dose ethanol combined exposure and XRT only groups than in all of the other groups, while the control had the highest values, with exception of the high-dose ethanol only group, which seemed to deviate from this observation. The red blood cell parameters also followed this general trend, more notably, the platelet and mean platelet volume values, which were lowest in the high-dose ethanol combined-exposure group. The destructive effects of the ROS are more pronounced on the DNA molecules, causing single and double strand breaks. Rapid proliferation of the blood cells does not allow for the repair of the damaged DNA molecules, resulting in heightened apoptosis. This explains the dramatic changes in the white and red blood cell and platelet parameters after exposure to ethanol and ionizing radiation.

3.6. CONCLUSION

This investigation has elucidated the effects of chronic ethanol exposure, followed by ionizing radiation on CD-1 mice as a model *in vivo* system, completing the

investigation on the effects of combined exposure to ethanol and ionizing radiation on model *in vitro* and *in vivo* systems. The *in vivo* results are in agreement with the *in vitro* data from all of the major parameters that were measured, confirming that there seems to be an interaction between ethanol and ionizing radiation in the biological systems, which is more significant with higher doses of radiation and ethanol. Based on these findings, it would appear to be good practice by doctors and oncologists to seriously consider the recent drinking histories of cancer patients before radiation therapy is administered. In view of the fact that both ethanol and ionizing radiation have individually been shown to induce oxidative stress in biological systems, a deliberate effort should be made to educate patients on the potential dangers of these agents, particularly when present in biological systems simultaneously. Further investigation of combined exposure that would involve chronic ethanol intake, tobacco smoking, and ionizing radiation in a clinical setup is recommended. This would model a chronic high-dose alcohol and tobacco user who undergoes radiation therapy, and provide interesting data on combined exposure.

APPENDIX

High performance liquid chromatography analysis of 2-Mercaptoethylamine (Cysteamine) in biological samples by derivatization with *N*-(1-pyrenyl) maleimide (NPM) using fluorescence detection

Joshua Ogony[1], Suneetha Mare[1], Wei Wu[1], and Nuran Ercal*

(J. Chromatogr. B. 843: 57-62 (2006))

([1] Department of Chemistry, University of Missouri-Rolla, Rolla, MO 65409, USA)

*Corresponding Author
Address: Department of Chemistry
University of Missouri – Rolla
1870 Miner Circle
Rolla, MO 65409
Voice: 573-341-6950
Fax: 573-341-6033
Email: nercal@umr.edu

ABSTRACT

2-Mercaptoethylamine (cysteamine) is an aminothiol compound used as a drug for the treatment of cystinosis, an autosomal recessive lysosomal storage disorder. Because of cysteamine's important role in clinical settings, its analysis by sensitive techniques has become pivotal. Unfortunately, the available methods are either complex or labor intensive. Therefore, we have developed a new rapid, sensitive, and simple method for determining cysteamine in biological samples (brain, kidney, liver, and plasma), using N-(1-pyrenyl) maleimide (NPM) as the derivatizing agent and reversed-phase high performance liquid chromatography (HPLC) with a fluorescence detection method (λex = 330 nm, λem = 376 nm). The mobile phase was acetonitrile and water (70:30) with acetic acid and o-phosphoric acid (1 ml/L). The calibration curve for cysteamine in serine borate buffer (SBB) was found to be linear over a range of 0-1200 nM (r^2 = 0.9993), and in plasma and liver matrix, the r^2 values were 0.9968 and 0.9965, respectively. The coefficients of the variation for the within-run and between-run precisions ranged from 0.68% to 9.90% and 0.63% to 4.17 %, respectively. The percentage of relative recovery ranged from 94.1% to 98.6%.

Keywords: *CSH; cysteamine; NPM, thiols; cystinosis; oxidative stress; HPLC; 2-mercaptoethylamine*

INTRODUCTION

2-Mercaptoethylamine (cysteamine) is an aminothiol compound used as a drug for the treatment of cystinosis [1]. The deficiency of a cystine carrier in the lysosomal membrane leads to cystine accumulation within the lysosomes, ultimately crystallizing in vital organs such as the liver, kidney, spleen, intestines, and cornea [2, 3]. The kidney is most sensitive to cystine accumulation that causes renal tubular Fanconi syndrome to develop in children 6 to 12 months of age [4, 5]. Cysteamine crosses the plasma and lysosomal membranes and reacts with the crystallized cystine within the lysosomes to form cysteine and cysteine-cysteamine mixed disulfides, which leave through the lysine porter [6]. The thiol functional group in cysteamine makes it a potential antioxidant in oxidative stress conditions such as after radiotherapy.

Because of cysteamine's important role in clinical settings and its potential future applications as an antioxidant, it has become necessary to develop an analytical method for detecting cysteamine in biological samples. Various derivatizing reagents and procedures have been described in the literature for cysteamine analysis [7-9]. These procedures, however, are either complex or time-consuming, involving incubation of samples in the dark, deproteinisation, coupled enzyme reactions, and pre-treatment of the biological samples. We have, thus, developed a method that is simple, sensitive, and rapid for analyzing cysteamine in tissues from the brain, kidney, liver, and plasma. In this study, we have used N-(1-pyrenyl) maleimide (NPM), which has high affinity for free thiols as the derivatizing agent [10]. The derivatization procedure does not require previous extraction and takes place at room temperature with an incubation period of only 5 min. The adduct formed is stable for at least 4 weeks at 4^{o}C and reversed-phase

HPLC is used for the quantitation. Various analytical methods have been cited in the literature for the determination of cysteamine in biological fluids, such as ion exchange column chromatography [11], high voltage electrophoresis [12], electrochemical detection [13, 14], and gas chromatography with flame photometric detection [15]. However, these methods lack sensitivity and have generally not been used with tissue samples to determine cysteamine. Because of this, we used reversed-phase HPLC with fluorescence detection since this method is very sensitive and specific for NPM-thiol adducts, in detecting and quantitating cysteamine in tissues of rats.

EXPERIMENTAL

Reagents and chemicals

Acetonitrile, acetic acid, and phosphoric acid (all HPLC grade) were purchased from Fisher (Fair Lawn, NJ, USA). NPM and diethylenetriaminepentaacetic acid (DETAPAC) were obtained from Aldrich (Milwaukee, WI, USA). Cysteamine and Tris-HCl (Trizma hydrochloride), and all the other chemicals were obtained from Sigma (St Louis, MO, USA).

Animals

Adult Sprague Dawley rats, weighing 250-280 g each, were obtained from Charles River Laboratories (Wilmington, MA, USA). The rats were housed in a temperature-controlled (25^{o}C) room equipped to maintain a 12 h light-dark cycle. Standard rat chow (Purina rat chow) and water were given *ad libitum.* After over-night fasting, cysteamine was administered intraperitoneally at 300 mg/kg of body weight in 1 ml of saline solution. The animals were then anesthetized according to the University of

Missouri Animal Care Regulations. Blood samples were collected after 30 min via intracardiac puncture into the sterile polystyrene tubes containing heparin as an anticoagulant. The animals were then sacrificed and liver, kidney, and brain samples were obtained and kept on ice for immediate derivatization and analysis. The remaining tissue samples were kept at -70^{o}C for later analysis. The blood was centrifuged for 5 min at 1000 x g to obtain plasma, which was immediately derivatized with NPM.

Preparation of solutions for calibration

Stock solutions of cysteamine were prepared by dissolving 1.2 mg of cysteamine in 10 mL of serine borate buffer (SBB) to make a 1 mM solution of cysteamine, which was further diluted with SBB to obtain 100 μM and 10 μM stock solutions. The stock solutions were used to prepare standards for the calibration curve. Appropriate volumes of cysteamine stock solutions were added to plasma and tissue samples in order to obtain final concentrations of 50, 100, 200, 400, 600, 800, 1000, and 1200 nM for the calibration standard. SBB was prepared by adding 15.74 g Tris-HCl, 0.618 g borate, 0.525 g serine, and 0.393 g diethylenetriaminepentaacetic aced (DETAPAC) in 1 L of HPLC grade water (pH = 7.0). NPM (1 mM) solution was prepared by dissolving 0.003 g of NPM in 10 mL acetonitrile. Antioxidant buffer was prepared by dissolving 1.2 g disodium phosphate, 0.32 g sodiumdihydrogen phosphate, 100 μL butylated hydroxytoluene (BHT) solution (0.1102 g BHT in 1 mL 100 % ethanol), 0.841 g aminotriazole, 0.039 g DETAPAC, and 0.065 g sodium azide in 1 L HPLC-grade water.

HPLC system

The HPLC system (Thermo Electron Corporation) consisted of a Finnigan ™ Spectra SYSTEM SCM1000 Vacuum Membrane Degasser, Finnigan ™ Spectra SYSTEM P2000 Gradient Pump, Finnigan ™ Spectra SYSTEM AS3000 Autosampler, and Finnigan ™ Spectra SYSTEM FL3000 Fluorescence Detector (λex = 330 nm and λem = 376 nm). The HPLC column was a Reliasil ODS-1 C_{18} column (5 μm silica packing material) with 250 x 4.6 mm (Column Engineering, Ontario, CA, USA). The mobile phase was 70% acetonitrile and 30% HPLC water and was adjusted to a pH of about 2 through the addition of 1 mL of both acetic acid and o-phosphoric acid. The NPM derivatives were eluted from the column isocratically at a flow rate of 1 mL/min. The chromatographic column temperature was ambient. There were very minor fluctuations of retention times which could be neglected.

Assay procedures

Derivatization of cysteamine

The tissue samples from the livers, kidneys, and brains of adult Sprague Dawley rats were homogenized (0.15 g/ml) in antioxidant buffer (prepared as described above under solution preparation) to avoid oxidation. The plasma samples were diluted (1/5) before derivatization. 10 μL of tissue homogenates or diluted plasma samples were mixed with 240 μL of SBB and then derivatized at room temperature with 750 μL of NPM to form fluorescent derivatives. Standard solutions of cysteamine were prepared by taking appropriate volumes of stock solutions to obtain concentrations of 0, 50, 100, 200, 400, 600, 800, 1000, and 1200 nM in the tissue matrix. The resulting mixtures were derivatized with 750 μL of 1.0 mM NPM solution in acetonitrile and left to stand for 5

min at room temperature. At the end of the reaction time, 10 µL of 2 N HCl solution were added to stop the reaction and stabilize the adducts. The final pH of the solution was maintained at about 2 which is ideal for the stability of the NPM-cysteamine adducts. The derivatized samples were filtered through a 0.45 µm acrodisc filter, and then injected into the column in a reversed-phase HPLC system.

Protein assay

The protein contents of different tissue samples were determined by using the Bradford method [16] in order to compare the concentration levels of CSH obtained from the tissue samples. The homogenized samples were diluted to appropriate concentrations prior to determination of protein levels. Concentrated coomasie blue (Bio-Rad) was diluted 1:5(v/v) with distilled water; then 2.5 mL of the diluted dye were added to 50 µL of the homogenized sample. The mixture was incubated at room temperature for 5 min, then the absorbance was measured at 595 nm by a spectrophotometer. The concentrations of protein present in the homogenized samples were obtained by comparing the absorbance values of the samples against the standard curve. The standard curve was constructed using the bovine serum albumin (BSA), 0.25-1 mg/mL.

METHOD VALIDATION

Calibration curves

The calibration curves of CSH were plotted by using integrated peak areas as the y-axis vs. standard CSH concentrations (0, 50, 100, 200, 400, 600, 800, 1000, and 1200 nM) as the x-axis. Linearity for the standards (without the tissue matrix) was obtained

over a full range of 0-1200 nM with the calibration curve: y = 876.35x -5224.7 and a correlation coefficient: r^2 = 0.9993. Linearity for standards (with the tissue matrix) was also obtained over a full range of 0-1200 nM, with the calibration curves in the plasma and liver tissue matrix: y = 890.33x – 12871 and y = 856.62x – 14886 respectively. The correlation coefficients were r^2 = 0.9968 in the plasma matrix and r^2 = 0.9965 in the liver tissue matrix.

Accuracy, precision, and recovery

Six replicates of plasma and tissue samples were prepared, spiked with 50 nM, 100 nM, 600 nM, and 1000 nM of CSH, and then analyzed in order to determine accuracy. The concentration points (50, 100, 600, and 1000 nM) were used as the true values in the calculation of the deviations between the true values and the measured values. The calculated deviations were then expressed as percentage to yield a relative deviation (RD), which was used as a measure of accuracy. Within-run precision was determined by analyzing six replicates of CSH-spiked control plasma and tissue samples, at concentrations ranging from 50-1000 nM in one analytical run, and comparing the CSH concentrations calculated from the peak areas of the six replicates in the matrix. Between-run precision was determined by derivatizing six replicates of CSH-spiked control plasma and tissue samples, at concentrations ranging from 50-1000 nM in three different analytical runs, and comparing the CSH concentrations calculated from the peak areas of the six replicates in each matrix. The coefficients of variation were calculated in each matrix and used as a measure of precision. Relative recovery was determined by spiking the brain, kidney, liver, and plasma samples with 50 nM, 100 nM, 600 nM, and

1000 nM CSH in three replicates. The recoveries were calculated by comparing the analytical results for the spiked samples with the unspiked pure standards at the four mentioned concentrations that represented 100 % recovery. The coefficients of variation (CV) for between-run and within-run precision, accuracy, and relative recovery of the samples spiked with CSH (50, 100, 600, 1000 nM) in the tissue matrix and standards are reported in Table 1. The coefficients of variation for within-run precision and between-run precision ranged from 0.68% to 9.90% and 0.63% to 4.17 %, respectively. The within-run precision of 9.90% was obtained at 50 nM. The percentages of relative recovery ranged from 94.1% to 98.6%.

Sensitivity and stability

The lower limit of quantitation (LLOQ) was the concentration of CSH when its peak area was 10 times that of the peak area of the blank (signal-to-noise = 10). The LLOQ of CSH was 50 nM (0.05 nmol/ml), and the detection limit was 10 nM (0.01 nmol/ml) (signal-to-noise = 3) with 5 µL injected sample volume. The autosampler stability was measured by determining the six replicates of derivatized CSH spiked plasma and tissue samples at three concentrations (100, 600, and 1000 nM). These were kept in HPLC autosampler vials and stored at room temperature following 0, 6, 12, 24, and 48 h of sample derivatization, or stored at 4^{o}C for 1, 3, 7, and 14 days after sample derivatization. The relative standard deviation was found to be less than 8 % when the derivatized samples were stored at room temperature, and less than 15 % for samples stored at 4^{o}C.

Investigating interference from other thiols

A standard mixture of 600 nM of cysteamine (CSH), N-acetyl-L-cysteine (NAC), glutathione (GSH), cysteine (CYS), and homocysteine (HCYS), in a plasma matrix was derivatized with NPM and analyzed by reversed-phase HPLC, as shown in the chromatogram in Figure 2. All of the biological thiols mentioned above elute before CSH and do not interfere with its detection.

RESULTS

In this investigation, CSH was derivatized with NPM and analyzed using the reversed-phase HPLC with fluorescence detection method in isocratic mode. The tissue samples (brain, kidney, liver) from treated adult Sprague Dawley rats were homogenized, derivatized with NPM, and analyzed. The plasmas were also analyzed. Tissues of control animals were spiked with varying concentrations of CSH and analyzed. Figure 1 shows the derivatization reaction in which the thiols reacted with NPM to form fluorescent adducts. Figure 2 shows the chromatogram of derivatized standard mixed thiols (600 nM): NAC, GSH, CYS, HCYS, and CSH in a plasma matrix. The biological thiols (CYS, GSH, NAC, and HCYS) do not interfere with the detection of CSH since their peaks come out before the CSH peak. Figure 3 is the chromatogram of a kidney sample obtained from an animal administered 300 mg/kg body weight of CSH and sacrificed 30 min later. Figure 4 (a) shows the chromatogram of the control liver sample from a Sprague Dawley rat given phosphate buffered saline solution only. There is no CSH peak in this chromatogram. Figure 4 (b) shows the chromatogram of the liver sample obtained from a rat that was administered 300 mg/kg body weight of CSH and sacrificed 30 min

later. The CSH peak was observed at 17 min. The concentrations of CSH obtained in the plasma and tissues are reported in Table 2. The levels of other important biological thiols (such as GSH and CYS) in the tissue samples and plasma were calculated using the thiol concentrations (nM) of homogenized tissue solutions, divided by the protein content in the tissue and expressed as nmol/mg protein. This data is reported in Table 2. The hydrolysis peak is the peak of NPM-water adduct, which results from the reaction of excess NPM with water.

DISCUSSION

In spite of the attempts that have been made to analyze cysteamine in biological samples, to the best of our knowledge, no detailed study has been reported in the recent past on determination of cysteamine in biological samples. Ricci et al. (1983) published an analytical method for determining cysteamine in biological samples but the derivatization procedure used is complex, involving coupled enzyme reactions along with detailed pre-treatment of the samples. Furthermore, no clear detection method has been shown. Stachowicz et al. (1998) have reported determination of cysteamine in human serum. However, their work did not include the determination of cysteamine in other tissue samples such as the brain, kidney, and liver. Moreover, the derivatizing agent they used was mono bromobimane (mBBr) as a fluorescent probe, which can measure many biologically important thiols since it is both specific and sensitive to thiols. However, the sample preparation and derivatization are complex and time consuming, and involve the incubation of samples in the dark. In our study, we used N-(1-pyrenyl) maleimide (NPM) as the derivatizing agent [17]. NPM is very specific for thiols. The derivatization

procedure using NPM is very simple (not requiring any special conditions), and the reactions take place at room temperature under ordinary laboratory conditions. NPM has the added advantage of increased sensitivity and rapid analysis, compared to the mBBr method. Although NPM has hydrolysis peaks, these come up well before the cysteamine peak; no interference has been observed.

The methods of detection reported in the literature, such as high performance liquid chromatography with ultraviolet detection [18], ion exchange column chromatography, and capillary electrophoresis [19, 20, 21], are well documented as lacking sensitivity [22]. Therefore, we focused on the use of reversed-phase HPLC with fluorescence detection for determining cysteamine in biological samples. This is a very sensitive method with high reproducibility and precision. The LLOQ of CSH in biological samples by our method was 0.05 nmol/ml, and the detection limit was 0.01 nmol/ml (signal-to-noise = 3), which is better than the LLOQ of 0.1 nmol/ml of plasma reported by Kusmierek et al. using HPLC with ultraviolet detection after precolumn derivatization, and the LOD of 0.061 μmol/L reported by Lochman et al using high-throughput capillary electrophoretic method for determination of total aminothiols in plasma and urine [18, 9]. A plasma cysteamine concentration of 5μM in humans 8 hours after an oral dose of 1200 mg is reported by Stachowicz et al [8]. It is important to note that cysteamine easily undergoes oxidation at room temperature to form mixed disulfides, therefore, cysteamine should be dissolved in serine borate buffer, in which it remains stable for 7 days at 4^{o}C. In this study, we have demonstrated that HPLC with fluorescence detection, using NPM as the derivatizing agent, is a very suitable method for

analyzing and detecting cysteamine in biological samples. The method is rapid, simple, and sensitive, and could be used in health institutions for pharmacokinetic studies.

AKNOWLEDGEMENTS

We thank Rong Shi, a graduate student at the University of Missouri – Rolla, for feeding and keeping the rats that were used in this investigation, and for her help in sacrificing the rats and harvesting their organs, and Linu Abraham, for her help with the protein assay. We also thank Barbara Harris for editing the manuscript.

ABBREVIATIONS USED

CSH, cysteamine; GSH, glutathione; CYS, cysteine; HCYS, homocysteine; HPLC, high performance liquid chromatography; NPM, N-(1-pyrenyl) maleimide; mBB, monobromobymane; NAC, N-acetyl-L-cysteine; SBB, serine borate buffer; BHT, butylated hydroxytoluene; DETAPAC, diethylenetriaminepentaacetic aced.

REFERENCES

[1] W.A. Gahl, Eur. J. Pediatr. 162 (2003) 38-41.

[2] W.A. Gahl, N. Bashan, F. Tietze, I. Bernadini. J.D. Schulman, Science. 217 (1982) 1263 -1265.

[3] W.A. Gahl, J.G. Thoene, J.A. Schneider, C.R. Scriver, A.L. Beaudet, W.S. Sly, D. Valle (Eds), The metabolic and molecular basis of inherited disease. McGraw-Hill, New York (2001); 8th edn pp 3763-3797.

[4] J.G, Thoene, R. Oshima, J. Crawhall, D. Olson, J.A. Schneider, J. Clin. Invest. 58 (1976) 180-189.

[5] L.A. Smolin, K.F. Clark, J.G. Thoene, W.A. Gahl, J.A. Schneider, Pediatr. Res. 23 (6) (1988) 616-620.

[6] W.A. Gahl, F. Tietze, J.D.B. Butler, J.D. Schulman, Biochem. J. 228 (1985) 545-550.

[7] G. Ricci, M. Nardini, R. Chiaraluce, S. Dupre, D. Cavallini, J. app. Biochem. 5 (1983) 320-329.

[8] M. Stachowicz, B. Lehmann, A. Tibi, P. Prognon, V. Daurat, D. Pradeau, J.pharm. Biomed. Anal. 17 (1998) 767-773.

[9] P. Lochman, T. Adam, D. Fredecky, E. Hlidkova, Z. Stopover, Electrophoresis. 24 (2003) 1200-1207.

[10] N. Ercal, S. Oztezcan, T.C. Hammond, R.H. Mathews, D.R Spitz, J. Chromatogr. B, Biomed. Appl 685 (1996) 329-334.

[11] M. Hsiung, Y.Y. Yeo, K. Itiaba, J.C. Crawhall, Biochem. Med. 19 (1978) 305-317.

[12] A.J. Jonas, J.A. Schneider, Anal. Biochem. 114 (1981) 429-432.

[13] L.A. Smolin, J.A. Schneider, Anal. Biochem. 168 (1988) 374- 379.

[14] R.A. Garcia, L.L. Hirschberger, M.H. Stipanuk. Anal. Biochem. 170 (1988) 432-440.

[15] H. Kataoka, H. Tanaka, M. Makita, J Chromatogr. B, Biomed. Appl 657 (1994) 9-13.

[16] M. Bradford, Anal. Biochem. 72 (1976) 248-254.

[17] L.A. Rinour, R.A. Winters, N. Ercal, D.R. Spitz, Meth. Enzymol. 299 (1999) 258-67.

[18] K. Kusmierek, R. Glowacki, E. Bald, Anal. Biochem. 382 (2005) 231-233.

[19] M. Cappiello, A. Del Corso, M. Camici, U. Mura, J. Biochem. Biophys. Methods. 26 (1993) 335-341.

[20] P. Lochman, T. Adam, D. Fredecky, E Hlidkova, Z. Skopkova, J. Electrophoresis. 24 (2003) 1200-1207.

[21] A. Wang, Y. Fang, J. Electrophoresis. 21 (2000) 1281-1290.

[22] H. Kataoka, Y. Imamura, H. Tanaka, M. Makita, J. Pharm. Biochem. An. 11 (10) (1993) 963-969.

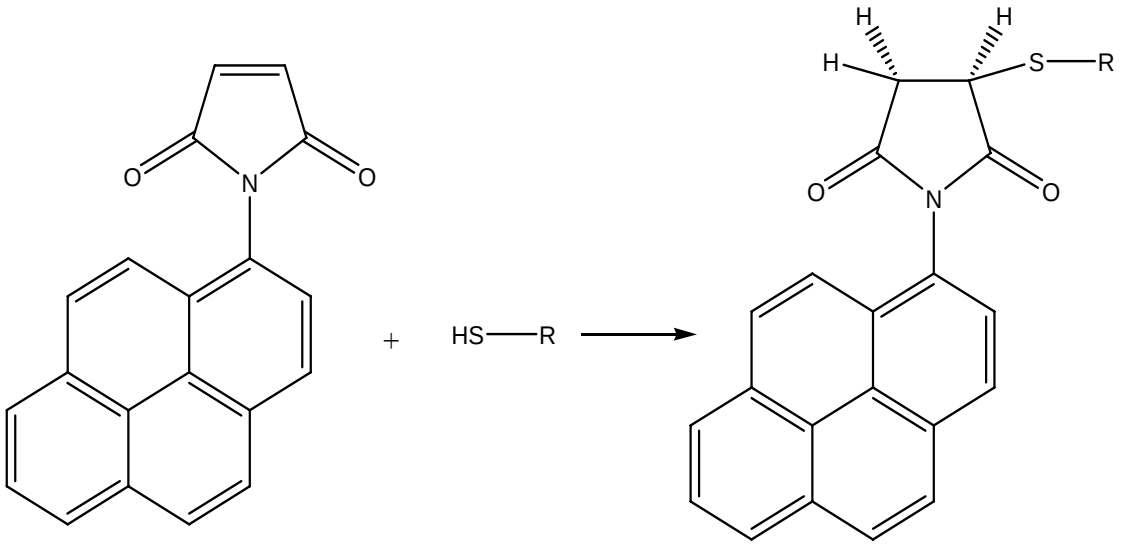

NPM Thiol NPM-Thiol adduct

Figure 1. Reaction of NPM with thiols to form fluorescent adducts.

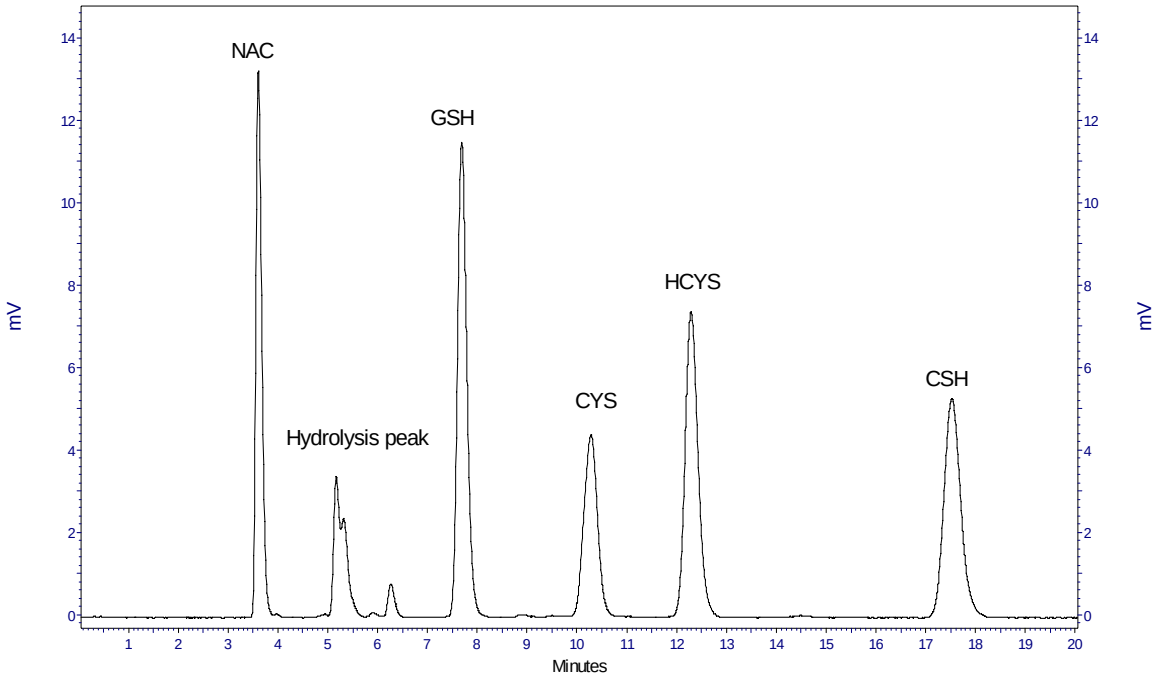

Figure 2. Chromatogram of derivatized standard mixed thiols (600 nM): NAC, GSH, CYS, HCYS, and CSH in a plasma matrix. Separation conditions: an ODS-1 C_{18} Column (5 µm packing material) with 250 x 4.6 mm (i.d) was used for the separation. The NPM derivatives were measured by a fluorescence detector (λ_{ex} = 330 nm and λ_{em} = 376 nm). Flow rate was 1ml/min. The mobile phase was 70% acetonitrile and 30% HPLC water and was adjusted to a pH of about 2 through the addition of 1 mL of both acetic acid and o-phosphoric acid in 1 liter of mobile phase.

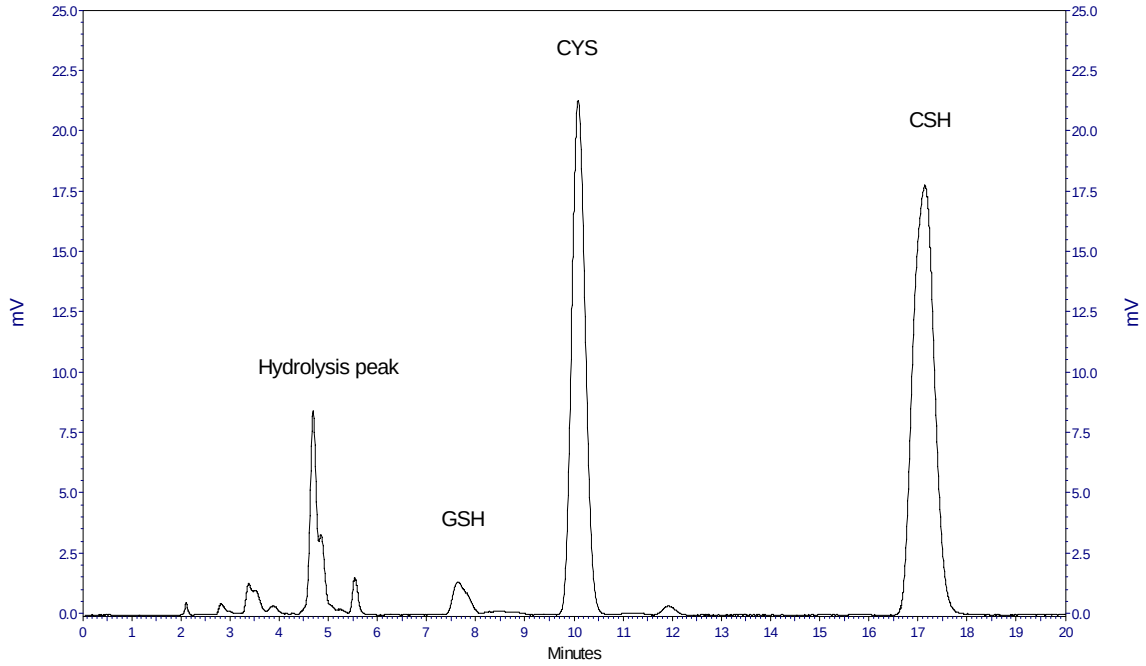

Figure 3. Chromatogram of a kidney sample obtained from an animal sacrificed 30 min after the administration of 300 mg/kg body weight of CSH. The concentrations of GSH, CYS, and CSH were 3.3 ± 1.2, 34.5 ± 6.3, and 24.5 ± 1.2 nmol/mg protein respectively. The separation conditions are the same as mentioned under Figure 2.

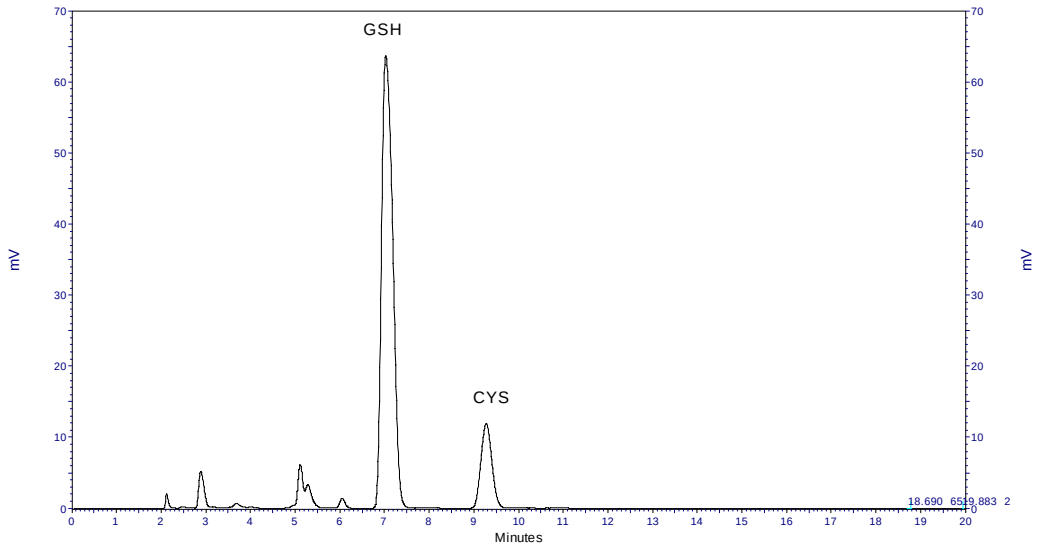

(a)

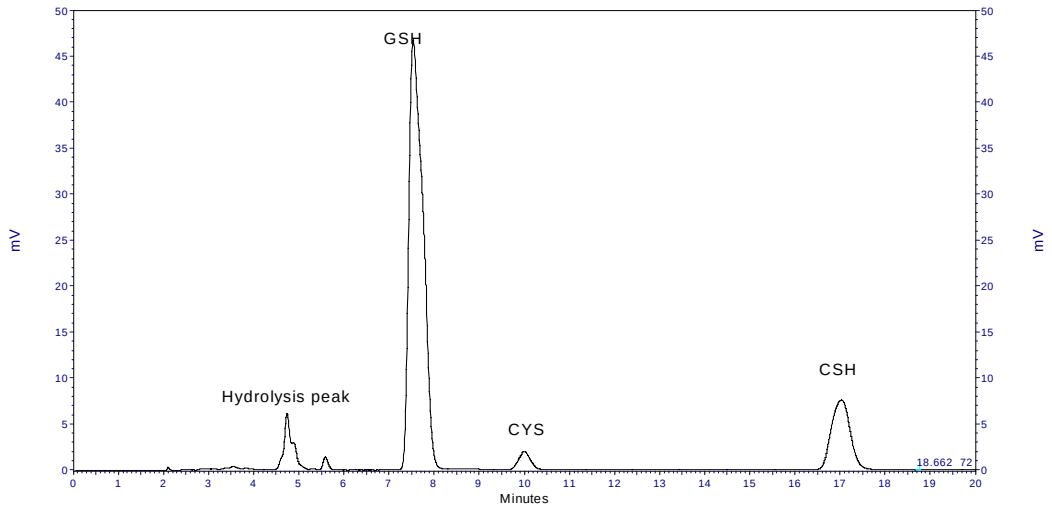

(b)

Figure 4. (a) Chromatogram of a control liver sample obtained from an animal administered phosphate buffered saline solution only. **(b)** Chromatogram of a liver sample obtained from an animal sacrificed 30 min after the administration of 300 mg/kg body weight of CSH. The separation conditions are the same as mentioned under Figure 2.

Table 1. Between-run and within-run precisions, accuracy, and relative recovery of replicate samples spiked with CSH (50, 100, 600, and 1000 nM) in plasma and tissue sample matrices, and standards.

Sample matrix	Brain	Kidney	Liver	Plasma	Standard
Between-run precision (n=6)	0.73-3.19%	0.63-1.83%	1.42-3.32%	1.15-4.17%	1.38-1.99%
Within-run precision (n=6)	1.82-9.20%	1.55-4.04%	0.78-5.82%	2.91-4.49%	0.68-9.90%
Accuracy (n=6)	0.03-6.90%	3.05-5.01%	4.90-4.98%	3.95-5.88%	1.50-3.60%
Relative recovery (n=3)	94.1 ± 7.0%	94.9 ± 6.9%	94.7 ± 2.8%	98.6 ± 5.0%	N/A

(Percentage relative recovery is reported as the average relative recovery ± standard deviation. N/A= not applicable)

Table 2. Thiol levels in biological samples 30 min after oral administration of 300 mg/kg body weight.

Samples (n=3)		CSH	GSH	CYS
Brain	Control	ND	13.6 ± 1.1	1.6 ± 0.3
	CSH-treated	21.8 ± 1.7	15.8 ± 2.4	1.9 ± 0.5
Kidney	Control	ND	2.1 ± 0.5	28.2 ± 3.1
	CSH-treated	24.5 ± 1.2	3.3 ± 1.2	34.5 ± 6.3
Liver	Control	ND	19.2 ± 3.7	3.4 ± 0.2
	CSH-treated	9.5 ± 1.6	21.3 ± 4.2	2.7± 0.4
Plasma	Control	ND	6.2 ± 1.1	15.6 ± 1.8
	CSH-treated	22.4 ± 2.8	7.3 ± 1.4	18.4 ± 2.9

Plasma sample units were in μM, units for tissue samples are in nmol/mg protein. The values are mean ± standard deviation. ND: not detectable.

BIBLIOGRAPHY

1. van der Gaag, M.S., van Tol A., Vermunt, S.H.F., Hendriks, H.F.J. Alcohol consumption stimulates early steps in reverse cholesterol transport. J. Lip. Res. **42**: 2077-2083 (2001).

2. Diane, L.L, Brown, R.A., Wassef, M., Giles, T.D,. Alcohol and the cardiovascular system. *JACC.* **45**: 1916-1924 (2005).

3. Lieber, C.S., Alcoholic fatty liver: its pathogenesis and mechanism of progression to inflammation and fibrosis. *Alcohol.* **34**: 9-19 (2004).

4. National institute of alcohol abuse and alcoholism. *Alcohol Health & Research world*. **17**, 133 (1993).

5. McGinnis, J., Foege, W. Actual course of death in the Unites states. *J AM MED ASS.* **270** : 2208 (1993).

6. Reinke, L.A., Rau, J.M., McCay, P.B. Possible roles of free in alcoholic tissue damage. *Free. Rad. Res*. **9**: 205-211 (1990).

7. Lieber, C.S. Metabolic effects of acetaldehyde. *Biochem Soc Trans*. **16**: 241-247 (1988).

8. Halliwell, B., Gutteridge, J. Free radicals in biology and medicine. *Oxford New York*: oxford University press: 573-575 (1999).

9. Nanji, A.A., Griniuviene, B., Sadrzadeh, S.M.G, Levitsky, S., McCull, J.D. Free radical production during ethanol metabolism. *J. Lipid Res*. **36**: 736-744 (1995).

10. Knecht, K.T., Bradford, B., Thurman, U. Free radical adducts in the bile of rats reated chronicallyvwith intragastric alcohol:inhibition by destruction of Kupffer cells.*Mol. Pharmacol***. 47**(5): 1028-1034 (1995**)**.

11. Bondy, S.C., Guo, S.X. *European journal of pharmacology*, Environmental toxicology and pharmacology section. **270**: 349-355 (1994).

12. Albano, E., Tamosi, A., Ingelman-Sundberg, M. Spin trapping of alcohol-derives radicals in microsomes and reconstituted systems by electron spin resonance. *Meth Enzymol*. **233**: 117-127 (1994).

13. Seitz ,H.K., Poschl, G. Alcohol and the liver. *Ther Umsch*. **57**(4): 227-231 (2000).

14. Moore, D.R., Reinke, L.A., McCay, P.B. Metabolism of ethanol to 1-hydroxyethyl radicals in vivo: detection with the intravenous administration of alpha-(4-pyridyl-1-oxide)-N-t-butylnitrone. Mol. Pharmacol. **47** (6): 1224-1230 (1995).

15. Welch, K.D., Davis, Z., Aust, S.D. *Arch. Biochem. Biophys.*; **397**:360-369 (2002).

16. Kessova, I., Cederbaum, A.I. CYP2E1: Biochemistry, toxicology, regulation and function in ethanol-induced liver injury. *Current molecular medicine*. **3**:509-518 (2003).

17. Sougioultzis, S., Dalakas, E., Hayes, P.C., Plevris, J.N. Alcoholic hepatitis: from pathogenesis to treatment. *Current medical research and opinion*. **21**: 1337-1346 (2005).

18. Reimers, M.J., Flockton, A.R., Tanguay, R.L. Ethanol and acetaldehyde-mediated developmental toxicity in zebrafish. *Neurotoxicology and Teratology.* **26**: 769-781 (2004).

19. Gohlke, J.M., Griffith, W.C., Faustman, E.M. A system based computational model for dose-response comparisons of two mode of action hypotheses for ethanol-induced neurodevelopmental toxicity. *J Toxicological Science*. **86**(2): 470-484 (2005).

20. Sakuta, H., Suzuki, T., Katayama, Y., Yasuda, H., Ito, T. Heavy alcohol intake and type 2 diabetes. *Diabetic Medicine*. **22**(10): 1359-1363 (2005).

21. Carrasco-Pozo, C., Alvarez-Lueje, A., Olea-Azar, C., Lopez-Alarcon, C., Speisky, H,. In vitro interaction between homocysteine and copper ions: potential redox implications. *Expl. Biol. Med*. **231**(9): 1569-1575 (2006).

22. Jones, A.W., Holmgren, P. Comparison of blood ethanol concentration in deaths attributed to acute alcohol poisoning and chronic alcoholism. *J forensic Sci.* **48**(4): 874- 879 (2003).

23. Szuster-Ciesielska, A., Daniluk, J., Bojarska-Januk. Apoptosis of blood mononuclear cells in alcoholic liver cirrhosis. *J Toxicology*. **212**: 124-134 (2005).

24. Neuman, M. G., Shear, N. H., Bellentani, S., Tiribelli, C. Role of cytokines in ethanol-induced cytotoxicity *in vitro* in HepG2 cells. *Gastroenterology*. **115**: 157-166 (1998).

25. Hall, E.J. Radiobiology for the radiobiologist, Fifth edition, J. B. Lippincott company (2000).

26. Vijayalaxmi, Reiter, R.J., Tan, D.X., Herman, T.S., Thomas, J.R.C.R. Melatonin as a radioprotective agent: A review. *Int. J. Radiation Oncology Biol. Phys*. **56**: 639-653 (2004).

27. Zhou, G., Kawata, T., Furusawa, Y., Aoki., M, Hirayama, R., Ando, K., Ito, H. Protective effects of melatonin against low and high-LET irradiation. *J. Radiat. Res*. **47**: 175-181 (2006).

28. Shirazi, A., Ghobadi, G., Ghazi-Khansari, M. Radiobiological review on melatonin: a novel radioprotector. *J. Radiat. Res*. **48**: 263-272 (2007).

29. Karbownik, M., Reiter, R.J. Antioxidative effects of melatonin in protection against cellular damage caused by ionizing radiation. *Proceedings of the Society for Experimental Biology and Medicine*. **225**: 9-22 (2000).

30. Gajewski, E., Rao, G., Nackerdien, Z., Dizdaroglu, M. Modification of DNA bases in mammalian chromatin by radiation-generated free radical. Biochemistry. 29: 7876-7882 (1990).

31. Kasai, H., Crain, P.F., Kuchino, Y., Nishimura, S.A., Ootsuyama, Tanooka, H. Formation of 8-hydroxyguaninemoiety in cellular DNA by agents producing radicalsand evidence for its repair. Carcinogenesis. **7**: 1849-1851 (1986).

32. Edwards, J., Chapman, D., Cramp, W.A., Yatvin, M.B. The effects of ionizing radiation on biomembrane structure and function. *Prog. Biophys. Mol. Biol*. **43**: 71-93 (1984).

33. Verma, S.P., Sonwalker, N. Structural changes in plasma membranes prepared from irradiated Chinese hamster V79 cells are revealed by Raman spectroscopy. *Radiat. Res*. **126**: 27-35 (1991).

34. Aust, A.E., Eveleigh, J.F. Mechanisms of DNA oxidation. *Proceedings of the Society for Experimental Biology and Medicine.* **222**: 246-252 (1999).

35. Steenken, S. Addition-elimination paths in electron-transfer reactions between radicals and molecules. *J. Chem. Soc, Faraday Trans I*. **83**: 113-124 (1987).

36. O'Neill, P. Pulse radiolytic study of the interaction of thiols and ascorbatewith OH-adducts of dGMP and dG: Implications for DNA repair process. *Radiat Ress*. **96**: 198-210 (1983).

37. Vieira, A.J.S.C., Steenken, S. Pattern of OH radical reactions with adenineand its nucleosides and nucleotides: Characterization of two typesof isomeric OH adduct and their unimolecular transformation reactions. *J. Am. Chem Soc*. **112**: 6986-6994 (1990).

38. Dizdaroglu, M. Chemical determination of free radical damage to DNA. *Free. Radic. Biol. Med*. **10**: 225-242 (1992).

39. von Sonntag, C. The chemical basis of radiation biology. London: Taylor & Francic, pp 167-193 (1987).

40. Beesk, F., Dizdaroglu, M., Schulte-Frohlinde, D., von Sonntag, C. Radiation-induced strand breaks in deoxygenatedaqueous solutions: The formation of altered sugars as end groups. *Int. J. Radiat. Biol*. **36**: 565-576 (1979).

41. Dizdaroglu, M., Schulte-Frohlinde, D., von Sonntag, C. Isolation of 2-deoxy-D-erythro-pentonic acidfrom an alkali-labile site in γ-irradiated DNA. *Int. J. Radiat. Biol.* **32**: 481-483 (1977).

42. Elia, M.C., DeLuca, J.G., Bradley, M.O. Significance and measurement of DNA double strand breaks in mammalian cells. *Pharmacol. Ther*. **51**: 291-327 (1991).

43. Peak, G.J., Peak, M.J., Sikorski, R.S., Jones, C.A. Induction of DNA-protein crosslinking in human cells by ultraviolet and visible radiations: Action spectrum. *Photochem. Photobiol.* **41**: 295-302 (1985).

44. Halliwell, B., Chirico, S. Lipid peroxidation: its mechanism, measurement, and significance. *Am. J. Clin. Nutr*. **57** (suppl)715S-725S (1993).

45. Stark, G. The effect of ionizing radiation on lipid membranes. Biochem. *Biophys. Acta*. **1071**: 103-122 (1991).

46. Aust, S.D, Morehouse, L.A., Thomas, C.D. Role of metals in oxygen radical reactions. *J. Free. Radic. Biol. Med.* **1**: 3-25 (1985).

47. Kim, E.H., Sevanian, A. Hematin and peroxide-catalyzed peroxidation of phospholipid liposomes. *Arch. Biochem. Biophys*. **288**: 324-330 (1991).

48. Esterbauer, H. Cytotoxicity and genotoxicity of lipid-oxidation products. *Am. J. Clin. Nutr*. **57** (suppl): 779S-780S (1993).

49. Shacter, E. Quatification and significance of protein oxidation in biological samples. *Drug Metabolism Reviews*. **32** (3&4) 307-326 (2000).

50. Hawkins, C.L., Davies, M.J. Generation and propagation of radical reactions on proteins. *Biochem. Biophys. Acta*. **1504**(2-3): 196-219 (2001).

51. Stadman, E. R. Protein oxidation and aging. *Free. Radic Res*. **40** (12): 1250-1258 (2006).

52. Davies, M.J. Protein oxidation: concepts, mechanisms and new insights. SFRBM annual meeting, (2003).

53. Davies, M.J., Fu, S., Wang, H., Dean, R.T. Stable markers of oxidant damage to proteins and their application in the study of human disease. *Free. Radic Biol. Med*. **27** (11/12): 1151-1163 (1999).

54. Halliwell, B. Reactive species and antioxidants. Redox biology is a fundamental theme of aerobic life. *Plant Physiology*. **141**: 312-322 (2006).

55. Fridovich, I. Superoxide radical and SOD. *Annu. Rev. Biochem*. **64**: 97-112 (1995)

56. Brigelius-Flohe, R. Tissue specific functions of individual glutathione peroxidases. *Free. Radic. Biol. Med*. **27**: 951-965 (1999).

57. Halliwell, B. Establishing the significance and optimal intake of dietary antioxidants: the biomarker concept. *Nutr. Rev*. **57**: 104-113 (1999).

58. Burkart, W. Combined effect of radiation and other agents: Is there a synergism trap? *J. Environ. Pathol. Toxicol. Oncol.* **20** (1): 53-58 (2001).

59. Geard, C.R., Shea, C.M., Georgsson, M.A. Paraquat and radiation effects on mouse C3H10T1/2 cells. *Int. J. Radiat. Oncol. Biol. Phys*. **10** (8): 1407-1410 (1984).

60. Anisimov, V.N., Osipova, G.Y. Carcinogenesis induced by combined neonatal exposure to 5-bromo-2'-deoxyuridine and subsequent total-body X-ray irradiation in rats. *Cancer Lett*. **70** (1-2): 81-90 (1993).

61. Inskip, P.D, Boice Jr., J.D. Radiotherapy-induced lung cancer among women who smoke. *Cancer*., **73** (6): 1541-1543 (1994).

62. Bailey, S.M. and Cunningham CC. Contribution of mitochondria to oxidative stress associated with alcoholic liver disease. *Free Radic Biol Med*. **32**: 11-16 (2002).

63. Anni, H. and Israel, Y. Characterization of adducts of ethanol metabolites with cytochrome c. *Alcohol Clin Exp Res*. **23** (1): 26-37 (1999).

64. Borek, C. Antioxidants and radiation therapy. *J. Nutr*. **134:** 3207S-3209S (2004).

65. Chi, C., Tanaka, R., Okuda, Y., Ikota, N., Yamamoto, H., Urano, S., Ozawa, T., and Anzai, K. Quantitative measurements of oxidative stress in mouse skin induced by x-ray irradiation. *Chem. Pharm. Bull*. **53**(11): 1411-1415 (2005).

66. Jianlin, L., Jiliang, H., Lifen, J., Wei, Z., Baohong, W., and Hongping, D. Measuring the genetic damage in cancer patients during radiotherapy with three genetic end-points. *Mutagenesis*. **19**(6): 457-464 (2004).

67. Kurose, I., Higuchi, H., Kato, S., Miura, S., and Ishii, H. Ethanol-induced oxidative stress in the liver. *Alcohol Clin Exp Res*. **20**(1): 77A-85A (1996).

68. Navasumrit, P., Ward, T.H., Dodd, N.J.F., and O'Connor, P.J. Ethanol-induced free radicals and hepatic DNA strand breaks are prevented in vivo by antioxidants: effects of acute and chronic ethanol exposure. *Carcinogenesis*. **21**(1): 93-99 (2000).

69. Halliwel, B. Mechanisms involved in the generation of free radical. *Pathol Biol*. **44**: 6-13 (1996).

70. Sun, J., Chen, Y., Li, M., and Ge, Z. Role of antioxidant enzymes on ionizing radiation resistance. *Free Radic Biol Med.* **24**: 586-593 (1998).

71. Kim, J.M., Araki, S., Kim, D.J., Park, C.B., Takasuka, N., and Baba-Toriyama, H. Chemopreventive effect of carotenoids and curcumins on mouse colon carcinogenesis after a 1,2-dimethylhydrazine initiation. *Carcinogenesis.* **19**: 81-85(1998).

72. Coia, L.R., and Moyland, D.J. *Introduction to Clinical Radiation Oncology*. Medical Physics Publishing, Madison, WI, (1998).

73. Burkart, W. Combined effect of radiation and other agents: Is there a synergism trap? *Journal of Environmental Pathology, Toxicology and Oncology.* **20**(1): 53-58 (2001).

74. Geard, C.R., Shea, C.M., and Georgsson, M.A. Paraquat and radiation effects on mouse C3H10T1/2 cells. *Int. J. Radiat. Oncol. Biol. Phys*. **10**(8): 1407-1410 (1984).

75. Inskip, P.D., and Boice Jr., J.D. Radiotherapy-induced lung cancer among women who smoke. *Cancer*. **73**(6): 1541-1543 (1994).

76. Bradford, M. Rapid and sensitive method for the quantitation of microgram quantities of protein utilizing the principle of protein-dye binding. *Anal. Biochem.* **72:** 248-256 (1976).

77. Winters, R, Zukowski, J., Ercal, N., Matthews, R.H., and Spitz, D.R. Analysis of glutathione, glutathione disulfide, cysteine, homocysteine, and other biological thiols by high-performance liquid chromatography following derivatization with N-(pyrenyl) maleimide. *Anal Biochem.* **227**: 14-21 (1995).

78. Gutteridge, J. The use of standards for malondialdehyde. *Anal. Biochem*. **69:** 121-126 (1975).

79. Cory, A.H., Owen, T.C., Barltrop, J.A., and Cory, J.G. The use of an aqueous soluble tetrazolium/formazan assay for cell growth assays in culture. *Cancer commun.* **3**(7): 207-212 (1991).

80. Riss, T.L., and Moravec, R.A. Comparison of MTT, XTT, and a novel tetrazolium compound for MTS for in vitro proliferation and chemosensitivity assays. *Mol. Bio. Cell (suppl.)*. **3:** 184a (1992).

81. Aebi, H. Catalase in vitro. Methods Enzymol. **105**: 121-126 (1984).

82. Committee on the biological effects of ionizing radiation (BEIR VI). The health effects of exposure to indoor radon. United States National Academy of Sciences, National Research Council. National Academy Press, Washington, (1998).

83. Anisimov, V.N., and Osipova, G.Y. Carcinogenesis induced by combined neonatal exposure to 5-bromo-2'-deoxyuridine and subsequent total-body X-ray irradiation in rats. *Cancer Lett*. **70** (1-2): 81-90 (1993).

84. Benson, J.M., Barr, E.B., and Lundgren, D.L. Pulmonary retention and tissue distribution of ^{239}Pu nitrate in F344 rats and Syrian hamsters inhaling carbon tetrachloride. p. 146-148 in: Annual Report 1993-1994, Inhalation Toxicology Research Institute (S. A. Belinsky et al., eds.). ITRI-144 (1994).

85. Broerse, J.J., Hennen, L.A., and Klapwijk, W.M. Mammary carcinogenesis in different rat strains after irradiation and hormone administration. *Int. J. Radiat. Biol. Relat. Stud. Phys. Chem. Med.* **51**(6): 1091-1100 (1987).

86. Meister, A. Glutathione metabolism. *Methods Enzymol*. **251**: 3-7 (1995).

87. Neuman, M.G, Shear, N.H., Bellentani, S., and Tiribelli, C. Role of cytokines in ethanol-induced cytotoxicity *in vitro* in HepG2 cells. *Gastroenterology*. **115**: 157-166 (1998).

88. Hirano, T., Kaplowitz, N., and Tsukamoto, H. Hepatic mitochondrial glutathione and progression of experimental alcohol liver disease in rats. *Hepatology*. **16**: 1423-1427 (1992).

89. Devi, B.G., Henderson, G.I., Frosto, T.A., and Schenker, S. Effect of ethanol on rat fetal hepatocytes: studies on cell replication, lipid peroxidation and glutathione. *Hepatology*. **18**: 648-659 (1993).

90. DeLeve, L., and Kaplowitz, N. Glutathione metabolism and its role in hepatotoxicity. *Pharmacol. Ther*. **52**: 287-305 (1991).

91. Bakan, E., Taysi, S., Polat, M.F., Dalga, S., Umudum, Z., Bakan, N., and Gumus, M. Nitric oxide levels and lipid peroxidation in plasma of patients with gastric cancer. Japanese Journal of Clinical Oncology. **32**: 162-166 (2002).

92. Sergent, O., Pereira, M., Belhomme, C., Chevanne, M., Huc, L., and Lagadic-Gossmann, D. Role of membrane fluidity in ethanol-induced oxidative stress of primary rat hepatocytes. *JPET.* **313**: 104-111 (2005).

93. Ingelman-Sundberg, M., Johansson, I., Yin, H., Terelius, Y., Eliasson, E., Clot, P., and Albino, E. Ethanol-inducible cytochrome P4502E2: genetic polymorphism, regulation and possible role in the etiology of alcohol-induced liver disease. *Alcohol*. **10**: 447-452 (1993).

94. Koc, M., Taysi, S., Emin, M., Buyukokuroglu, and Baka, N. Melatonin protects rat liver against irradiation induced oxidative injury. *J. Radiat. Res.* **44**: 211-215 (2003).

95. Manda, K., Ueno, M., Moritake, T., and Anzai, K. α-Lipoic acid attenuates x-irradiation-induced oxidative stress in mice. *Cell Biol Toxicol*. **23**: 129-137 (2007).

96. Bouzouf, M., Martinez-cruz, F., Molinero, P., Guerero, J.M., and Osuna, C. Melatonin prevents hyperhomocysteinemia and neural lipid peroxidation induced by methionine intake. *Current Neurovascular Research*. **2**: 175-178 (2005).

97. Wu, D., and Cederbaum, A.I. Ethanol-induced apoptosis to stable HepG2 cell lines expressing human cytochrome P-4502E1. *Alcohol Clin Exp Res.* **23**(1): 67-76 (1999).

98. Jian-Jun, L., Ji-Yao, W., Erik, H., Cheng, Y., Ake, N., and Rui-Dong, D. Activation of neutral sphingomyelinase participates in ethanol-induced apoptosis in HepG2 cells. *Alcohol alcohol*. **35**(6): 569-573 (2000).

99. Newton, K., and Strasser, A. Ionizing radiation and chemotherapeutic drugs induce apoptosis in lymphocytes in the absence of fas or FADD/MORTI signaling: Implications for cancer therapy. *J. Exp. Med*. **191**(1): 195-200 (2000).

100. Bravard, A., Luccioni, C., Moustacchi, E., and Rigaud, O. Contribution of antioxidant enzymes to the adaptive response to ionizing radiation of human lymphoblasts. *Int. J. Radiat. Biol*. **75**(5): 639-645 (1999).

101. Schmidt-Ullrich, R.K., Dent, P., Grant, S., Mikkelsen, R.B., and Valarie, K. Signal transduction and cellular radiation responses. *Radiat. Res.* **153**: 245-257 (2000).

102. Ribere, C., Sinaceur, J., Nordmann, J., and Nordmann, R. Discrepancy between the different subcellular activities of rat liver catalase and superoxide dismutases in response to acute ethanol administration. *Alcohol Alcohol*. **20**: 13-18 (1985).

103. Komov, V.P., Srelkova, M.A., and Makeeva, A.L. Effect of ionizing radiation on the turnover of catalase-degrading proteinase in rat hepatocytes. *Radiobiologiia.* **27**(3): 390-392 (1987).

104. Shindo, Y., Witt, E., Han, D., and Packer, L. Dose-response effects of acute ultraviolet irradiation on antioxidants and molecular markers of oxidation in Murine epidermis and dermis. *J. Invest. Dermatol*. **102**: 470-475 (1994).

105. Schisler, N.J., and Singh, S.M. Effect of ethanol in vivo on enzymes which detoxify oxygen free radicals. *Free Radic Biol Med*. **7**: 117-123 (1989).

106. Kono, Y., and Fridovich, I. Superoxide inhibits catalase. *J Biol Chem*. **257**: 5751-5754 (1982).

107. Neuman, M.G., Koren, G., and Tribelli, C. In vitro assessment of the ethanol-induced hepatotoxicity on HepG2 cell line. *Biochem. Biophys. Res. Commun*. **197**(2): 932-941 (1993).

108. Neuman, M.G., Cameron, R.G., Shear, N.H., Bellentani, S., and Tiribelli, C. *Gastroenterology*. **109**: 555-563 (1995).

109. Wright, J.A., Keegan, K.S., Herendeen, D.R., Bentley, N.J., Carr, A.M., Hoekstra, M.F., and Concannon, P. Protein kinase mutants of human ATR increase sensitivity to UV and ionizing radiation and abrogate cell cycle checkpoint control. *Proc. Natl. Acad. Sci*. USA. **95**: 7445-7450 (1998).

110. Meister, A. Glutathione. In *The liver: Biology and Pathology, Second Edition* (Aria, I. M., Jakoby, W. B., Popper, H., Schachter, D., and Shafritz, D. A., eds). 401-417 , Raven Press, New York (1988).

111. Fernandez-Checha, J., Lu, S.C., Ookhtens, M., DeLeve, L., Runnegar, M., Yoshida, H., Saiki, H., Kannan, R., Garcia-Ruiz, C., and Kaplowitz, N. The regulation of hepatic glutathione. In *Hepatic Anion Transport and Bile Secretion: Physiology and Pathophysiology* (Trovoloni, N and Berk P. D., eds). 363-395, Marcel Dekker, New York (1992).

112. Ribble, D., Goldstein, N.B., Norris, D.A., and Shellman, Y.G. A simple technique for quantifying apoptosis in 96-well plates. *BMC Biotechnology*. **5**: 12 (2005).

113. Li, J., Chen, W., Zhang, P., and Li, N. Topoisomerase II trapping agent teniposide induces apoptosis and G2/M or S phase arrest of oral squamous cell carcinoma. *World Journal of Surgical Oncology*. **4**: 41 (2006).

114. Neuman, M.G. Cytokines – central factors in alcoholic liver disease. *Alcohol Res Health.* **27**(4): 307-316 (2003).

115. Navder, K.P., and Lieber, C.S. Dilineoylphosphatidylcholine is responsible for beneficial effects of PPC on ethanol-induced mitochondrial injury in rats. *Biochemical and Biophysical Research Communications*. **291**: 1109-1112 (2002).

116. Ogony, J., Matthews, R., Anni, H., Shannon, K., and Ercal, N. The mechanism of elevated toxicity in HepG2 cells due to combined exposure to ethanol and ionizing radiation. *J. Appl. Toxicol*. **27.**(in press); (www.interscience.wiley.com) DOI: 10.1002/jat.1285 (2007).

117. Nordmann, R., Ribiere, C., and Rouach, H. Implication of free radical mechanisms in ethanol-induced cellular injury. *Free. Radic. Biol. Med*. **12**(3): 219-240 (1992).

118. Kukielka, E., Dicker, E., and Cederbaum, A.I. Increased production of reactive oxygen species by rat liver mitochondria after chronic ethanol treatment. *Arch Biochem Biophys*. **309**: 377-386 (1994).

119. Bailey, S.M., and Cunningham, C.C. Contribution of mitochondria to oxidative stress associated with alcoholic liver disease. *Free. Radic. Biol. Med.* **32**(1):11-16 (2002).

120. French, S.W., Wong, K., Jui, L., Albano, E., Hagbjork, A.L., and Ingelman-Sundberg, M. Effect of ethanol on cytochrome P_{450} 2E1 (CYP 2E1), lipid peroxidation, and serum protein adduct formation in relation to liver pathology pathogenesis. *Exp. Mol. Pathol*. **58**: 61-75 (1993).

121. Lee, J.H., and Park, J. Protective role of α-phenyl-*N*-*t*-butylnitrone against ionizing radiation in U937 cells and mice. *Can. Res*. **63**: 6885-6893 (2003).

122. Katiyar, S.K., and Meeran, S.M. Obesity increases the risk of UV radiation-induced oxidative stress and activation of MAPK and NF-$_K$B signaling. *Free. Radic. Biol. Med*. **42**(2):299-310 (2007).

123. Bhosle, S.M., Huilgol, N.G., and Mishra, K.P. Enhancement of radiation-induced oxidative stress and cytotoxicity in tumor cells by ellagic acid. *Clinica Chimica Acta*. **359**: 89-100 (2005).

124. Gorsky, L.D., Koop, D.R., and Coon, M.J. The stoichiometry of oxidase and momooxygenase reactions catalyzed by liver microsomal cytochrome P_{450}. *J Biol Chem*. **259**: 6812-6817 (1984).

125. Ekstrom, G., and Ingelman-Sundberg, M. Rat liver micrtosomal NADPH-supported oxidase activity and lipid peroxidation dependent on ethanol-inducible cytochrome P450 (P-450IIE1). *Biochem Pharmacol*. **38**:1313-1318 (1989).

126. Ekstrom, G., Cronholm, T., Ingelman-Sundberg, M. Hydroxyl-radical production and ethanol oxidation by liver microsomes isolated from ethanol-treated rats. *Biochem J*. **233**: 1532-1535 (1986).

127. Lieber, C.S, and Decarli, L.M. Hepatic microsomal ethanol-oxidizing system. In vitro characteristics and adaptive properties in vivo. *J Biol Chem*. **245**: 2505-2512 (1970).

128. Marimoto, M., Zem, M.A., Hagbjork, A.L., Ingelman-Sundberg, M., and French, S.W. Fish oil, alcohol and liver pathology: Role of cytochrome P450 2E1. *Proc. Soc. Exp. Biol. Med*. **207**: 197-205 (1994).

129. Tsukamoto, H., Horne, W., Kamimura, S., Niemela, O., Parkkila, S., Yla-Herttuala, S., and Brittenham, G.M. Experimental Liver cirrhosis induced by alcohol and iron. *J. Clin. Invest*. **96**: 620-630 (1995).

130. Gouillon, Z., Lucas, D., Li, J., Hagbjork, A.L., French, B.A., Fu, P., Fang, C., Ingelman-Sundberg, M., Donohue, T.M., and French, S.W. Inhibition of ethanol-induced liver disease in the intragastric feeding rat model by chlormethiazole. *Proc. Soc. Exp. Biol. Med.* **224**: 302-308 (2000).

131. Engerson, T.D., Mckelvey, T.G., Rhyne, D.B., Boggio, E.B., Snyder, S.J., and Jones, H.P. Conversion of xanthine dehydrogenase to oxidase in ischemic rat tissue. *J Cin Invest*. **79**: 1564-1570 (1987).

132. Esterbauer, H., Schaur, R.J., and Zollner, H. Chemistry and biochemistry of 4-hydroxynonenal, malondialdehyde and related aldehydes. *Free. Radic. Biol. Med.* **11**:81-128 (1991).

133. Sharma, S., and Haldar, C. Melatonin prevents X-ray irradiation induced oxidative damage in peripheral blood and spleen of the seasonally breeding rodent, *Funambulus pennanti* during reproductively active phase. *Int. J.Radiat. Biol*. **82**(6): 411-419 (2006).

134. Von, S.C. *The chemical basis of radiation biology*. London. Taylor and Francis. (1987).

135. Halliwell, B., and Gutterridge, J.M.C. *Free Radicals in Biology and Medicine*. 2nd edn, Oxford Clarendon Press (1989).

136. Herold, D., Hanlon, A., and Hanks, G.E. Diadetes mellitus: an independent predictor of significant late complications after external beam radiotherapy. *Int J Radiat Oncol Biol Phys*. **42**(1): 311 (1998).

137. Hall, E.J. Radiobiology for the Radiologist, 4th ed.(1994) Lipincott, Philadwlphia, 246.

138. Mathews, R.H. Collagen vascular disease and irradiation. *Int J Radiat Oncol Biol Phys*. **17**: 1123-1124 (1989).

139. Pilepich, M.V., Perez, C.A., Walz, B.J., and Zivnuska, F.R. Complications of definitive radiotherapy for carcinoma of the prostate. *Int J Radiat Oncol Biol Phys.* **7**: 1341-1348 (1981).

140. Dalle-Donne, I., Rossi, R., Colombo, R., Giustarini, D., and Milzani, A. Biomarkers of oxidative damage in human disease. *Clin. Chem*. **52**: 601-623 (2006).

141. Dhalla, N.S., Temsah, R.M., and Netticadan, T. Role of oxidative stress in cardiovascular disease. *J. Hypertens*. **18**: 655-673 (2000).

142. Jenner, P. Oxidative stress in Parkinson's disease. *Ann. Neurol*. **53**: S26-S36 (2003).

143. Sayre, L.M., Smith, M.A., and Perry, G. Chemistry and biochemistry of oxidative stress in neurodegenerative disease. *Curr. Med. Chem*. **8**: 721-738 (2001).

144. Weeks, J., Watson, R., and Dunn, M.J. Murine retrovirus infection and the effects of chronic alcohol consumption: Proteomic analysis of cardiac protein expression. *Alcohol. Alcohol*. **38**(2): 103-108 (2003).

145. Wu, D., and Cederbaum, A. Glutathione depletion in CYP2E1-Expressing liver cells induces toxicity due to he activation of p38 mitogen-activated protein kinase and reduction of nuclear factor-*k*B DNA binding activity. *Mol Pharmacol*. **66**: 749-760 (2004).

146. Vile, G.F., andTyrrel, R.M. UV A radiation-induced oxidative damage to lipids and proteins in vitro and in human skin fibroblasts is dependent on iron and singlet oxygen. . *Free. Radic. Biol. Med.* **18**(4): 721-730 (1995).

147. Burkart, W., and Jung, T. Health risks from combined exposures: Mechanistic considerations on deviations from additivity. *Mutat. Res*. **411**: 119-128 (1998).

148. Ishikawa, Y.T., Mori, Y., Kato, et al. Lung cancers associated with thorotrast exposure: high incidence of small-cell carcinoma and implications for estimation of radon risk. *Int. J. Cancer*. **52**(4): 570-574 (1992).

149. Ehling, U.H., and Neuhauser-Klaus, A. Induction of specific-locus and dominant-lethal mutations by cyclophosphamide and combined cyclophosphamide-radiation treatment in male mice. *Mutat. Res*. **199**: 21-30 (1988).

150. Montour, J.L., Dutz, W., and Harris, L.S. Modification of radiation carcinogenesis by marihuana. *Cancer*. **47**(6): 1279-1285 (1981).

151. Maisin, J.R., Saint-Georges, L.D., Janowski, M. et al. Effects of X-ray alone or combined with diethylnitrosamine on cancer induction in mouse liver. *Int. J. Radiat. Biol. Relat Stud. Phys. Chem. Med*. **51**(6): 1049-1057 (1987).

152. Tsukamoto, H., and Lu, S.C. Current concepts in the pathogenesis of alcoholic liver injury. *FASEB J.* **15**: 1335-1349 (2001).

153. Hoek, J.B., and Pastorino, J.G. Cellular signaling mechanisms in alcohol-induced liver damage. *Semin. Liver Dis*. **24**: 257-272 (2004).

154. Lieber, C.S. Alcohol and the liver: 1994 update. Gastroenterology. **106**: 1085-1105 (1994).

155. Borisenko, S.A., Kiianmaa, K., Lekhtosalo, I., Mannisto, P., and Burov, I.V. Effect of chronic administration of ethanol on the blood-brain barrier permeability of 14C-tyrosine and horseradish peroxidase in rats. *Biull Eksp Biol Med.* **102**(9):313-315 (1986).

156. Singh, A.K., Jiang, Y., Gupta, S., and Benlhabib. E**.** Effects of chronic ethanol drinking on the blood**–**brain barrier and ensuing neuronal toxicity in alcohol-preferring rats subjected to intraperitoneal LPS injection. *Alcohol. Alcohol*. doi:10.1093/alcalc/agl120.

157. Fromenty, B., and Pessayre, D. Inhibition of mitochondrial beta-oxidation as a mechanism of hepatotoxicity. *Pharmacol Ther*. **67**: 101-154 (1995).

158. Kurose, I., Higuchi, H., Kato, S., Miura, S., and Ishii, H. Ethanol-induced oxidative stress in the liver. *Alcohol Clin Exp Res*. **20**(1): 77A-85A (1996).

159. Calabrese, V., Renis, M., Calderone, A., Russo, A., Reale, S., Barcellona, M.L., and Rizza, V. Stress proteins and SH-group in oxidant-induced cellular injury after chronic ethanol administration in rat. *Free Radic Biol Med*. **24**: 1159-1167 (1998).

160. Lieber, C.S. Role of oxidative stress and antioxidant therapy in alcoholic and nonalcoholic liver disease. *Adv Pharmacol*. **38**: 601-628 (1997).

161. Borek, C. Antioxidants and radiation therapy. *J. Nutr*. **134**: 3207S- 3209S (2004).

162. Zentella de Pina, M., Corona, S., Rocha-Hernandez, A.E., Saladana, B.Y., Cabrera, G., and Pina, E. Restoration by piroxicam of liver glutathione levels decreased by acute ethanol intoxication. *Life Sci*. **54**: 1433-1439 (1994).

163. DeLeve, L., and Kaplowitz, N. Glutathione metabolism and its role in hepatotoxicity. *Pharmacol Ther*. **52**: 287-305 (1991).

164. Meister, A. (1988). Glutathione. In *The liver: Biology and Pathology, Second Edition* (Aria, I. M., Jakoby, W. B., Popper, H., Schachter, D., and Shafritz, D. A., eds, Raven Press, New York). 401-417.

165. Suthanthiran, M., Anderson, M.E., Sharma, V.K., and Meister, A. Glutathione regulates activation-dependent DNA synthesis in highly purified normal human T lymphocytes stimulated via the CD2 and CD3 antigens. *Proc. Natl. Acad. Sci. USA*. **87**: 3343-3347 (1990).

166. Hutter, D.E., Till, B.G., and Greene, J.J. Redox state changes in density-dependent regulation of proliferation. *Exp. Cell. Res*. **232**: 435-438 (1997).

167. Zhong, W., Oberley, L.W., Oberley, T.D., Yan, T., Domann, F.E., and St. Clair, D.K. Inhibition of cell growth and sensitization to oxidative damage by overexpression of manganese superoxide dismutase in rat glioma cells. *Cell Growth Differ*. **7**: 1175-1186 (1996).

168. Lu, S.C. Regulation of hepatic glutathione synthesis: current concepts and controversies. *FASEB J*. **13**: 1169-1183 (1999).

169. Escobar, J.A., Rubio, M.A., and Lissi, E.A. SOD and catalase inactivation by singlet oxygen and peroxyl radicals. *Free Radic Biol Med*. **20**(3): 285-290 (1996).

170. Ribière, C., Sinaceur, J., Nordmann, J., and Nordmann, R. Discrepancy between the different subcellular activities of rat liver catalase and superoxide dismutases in response to acute ethanol administration. *Alcohol Alcohol*. **20**(1):13-8 (1985).

171. Potier, M., Villemure, J., and Thauvette, L. Radiation inactivation of proteins: temperature- dependent inter-protomeric energy transfer in ox liver catalase. *Biochem J*. **298**: 571-574 (1994).

172. Torbenko, V.P., Bogdanova, I.A., and Gerasimov, A.M. Effect of a combined radiation lesion on the enzyme activity of the glutathione redox system of the rat liver. *Biull Eksp Biol Med*. **95**(2):48-50 (1983).

173. Oh, S.I., Kim, C.I., Chun, H.J., and Park, S.C. Chronic Ethanol Consumption Affects Glutathione Status in Rat Liver. *J Nutr*. **128**(4): 758-763 (1998).

174. Wlodek, L., and Rommelspacher, H. Ethanol-induced changes in the content of thiol compounds and lipid peroxidation in the livers and brains from mice: protection by thiazolidene derivatives. *Alcohol Alcohol*. **29**(6): 649-657 (1994).

175. Dewey, D.L., and Beecher, J. Interconversion of cystine and cysteine induced by x-rays. *Nature*. **206**(991):1369-70 (1965).

176. Mansouri, A., Demeilliers, C., Amsellem, S. Pessayre, D., and Fromenty, B. Acute ethanol administration oxidatively damages and depletes mitochondrial DNA in mouse liver, brain, heart, and skeletal muscles: protective effects of antioxidants. *J. Pharmacol. Exp. Ther*. **298**: 737-743 (2001).

177. Chevion, S., Or, R., and Berry, E.M. The antioxidant status of patients subjected to total body irradiation. *Biochem. Mol. Biol. Int*. **47**: 1019-1027 (1999).

178. Varsney, R., and Kale, R.K. The effects of calmodulin antagonists on radiation induced lipid peroxidation in microsomes. *Int. J. Radiat. Biol*. **58**. 733-743 (1990).

179. Taysi, S., Koc, M., Buyukokuroglu, M.E., Altinkaynak, K., and Sahin, Y.N. Melatonin reduces lipid peroxidation and nitric oxide during irradiation-induced oxidative injury in the rat liver. *J. Pineal Res*. **34**: 173-177 (2003).

180. Sener, G., Jahovic, N., Tosun, O., Atasoy, B.M., and Yegen, BC. Melatonin ameliorates ionizing radiation-induced oxidative organ damage in rats. *Life Sci*. **74**: 563-572 (2003).

VITA

Joshua Were Ogony was born on April 21, 1966, at Kisumu, Kenya. He obtained his primary and high school education in Kisumu, Kenya, and received a Diploma in Education (Science) (Chemistry/Biology) from Kenya Science Teachers' College, Nairobi, Kenya in November, 1990. From 1991 to 1998, he was employed by the Teachers Service Commision (TSC) of Kenya, and worked as a High School Chemistry and Biology Teacher. In 1997 Joshua was selected by the Kenya National Examinations Council (KNEC) to be a national examiner of chemistry. He joined Kenyatta University, Nairobi, Kenya in 1998 and received a Bachelor of Education (Science) (Chemistry/Zoology) Degree in October, 2002. From the fall of 2003 to the summer 2004, he was enrolled as a Master of Science student in the Chemistry Department at the University of Missouri-Rolla, Rolla, Missouri, USA and worked toward a Master's Degree while also pursuing a Ph.D. degree. He received a Master of Science Degree in Chemistry from the University of Missouri-Rolla in May 2007. Since the fall of 2004, Joshua has been enrolled as a Ph.D. candidate in the Chemistry Department at the University of Missouri – Rolla. He received a Ph.D. in Chemistry in December 2007.